DEVELOPMENT OF NEAR INFRARED SPECTROSCOPIC METHODS TO PREDICT AND UNDERSTAND DISSOLUTION OF SOLID ORAL DOSAGE FORMS

By
Eduardo Hernández Torres

A dissertation submitted in partial fulfillment of the requirements for the degree of
DOCTOR OF PHILOSOPHY
In
APPLIED CHEMISTRY
UNIVERSITY OF PUERTO RICO
MAYAGÜEZ CAMPUS
2019

Approved by:

_____	_____
Rodolfo J. Romañach, PhD President, Graduate Committee	Date
_____	_____
Jessica Torres Candelaria, PhD Member, Graduate Committee	Date
_____	_____
Rafael Méndez Roman, PhD Member, Graduate Committee	Date
_____	_____
Martha Laura Lopez Moreno, PhD Member, Graduate Committee	Date
_____	_____
Miguel F. Canals, PhD. Representative of Graduate Studies	Date
_____	_____
Enrique Melendez, PhD Chairperson of the Department	Date

ABSTRACT

Shear stress is created in a system by moving one surface over another to cause displacements in the direction of the moving surface. Shearing of powder is essential to break down agglomerates in cohesive powders, promoting micro-mixing, and thus uniform blends. During material processing, particles rub against each other, leading to development of shear forces. In solid dosage manufacturing, powder is subjected to different unit operations, and thus to different levels of normal and abrasive stresses and strain. This mechanical shear also affects the hydrophobicity of pharmaceutical powder blends and its impact on drug release from tablets during dissolution testing.

The dissolution test is required in the development, registration, approval and quality control of a solid oral dosage form except where the label says that they are to be chewed. The dissolution test is required by over 500 tablet and capsule products described in the United States Pharmacopeia (USP), and is the only test performed in manufacturing with the objective of monitoring whether the product will perform adequately throughout its shelf life.

Drug concentration in the dissolution medium is currently determined with High Performance Liquid Chromatography (HPLC) or Ultraviolet/Visible Spectroscopy (UV/VIS) using solvents with high cost and leading to significant solvent wastes generated in the analysis. USP establishes in chapter <711> four different systems to perform dissolution test. USP Apparatus 1 (Basket) and 2 (Paddle) consist in a fixed volume of dissolution medium. USP apparatus 3 (Reciprocating Cylinder) and 4 (Flow-Through Cell) when the USP Apparatus 1 and 2 are not suitable for the analysis (e.g. polymeric thin films). This type of testing destroys the tablets leaving nothing to

investigate if the test fails. Based on that information, a nondestructive method for dissolution analysis of tablets id needed. Near infrared spectroscopy is a non-destructive fast technique suitable for these purposes. NIR is an analytical method capable of monitoring critical quality parameters that are valuable in the improvement of pharmaceutical processes. Near infrared spectroscopy has become one of the most used analytical techniques to monitor pharmaceutical processes since the spectra provides information on the physical and chemical properties, and can obtain a high signal to noise ratio spectrum in one minute without sample preparation.

This dissertation describes three studies to enhance the understanding of near infrared spectroscopy and chemometrics and to advance their adoption within pharmaceutical manufacturing. The first study was based on the changes observed in the near infrared diffuse reflectance spectra of pharmaceutical tablets after these tablets were subjected to different levels of strain (exposure to shear) during the mixing process. These changes in the near infrared spectra (NIR) could affect results obtained from NIR calibration models. Shear was applied using a Couette cell and tablets were produced using a tablet press emulator. Tablets with different shear levels were measured using near infrared spectroscopy in the diffuse reflectance mode. The NIR spectra were baseline corrected to maintain the scattering effect associated with the physical properties of the tablet surface. Principal Component Analysis was used to establish the principal sources of variation within the samples. The angular dependence of elastic light scattering shows that the shear treatment reduces the size of particles and produces their uniform and highly isotropic distribution. Tablet compaction further reduces the diffuse component of scattering due to realignment of particles. The aim of the study was to understand changes in the near infrared

diffuse reflectance spectra that can be associated with different levels of shear developed during blend shearing of laboratory samples.

A second study describes how the shear applied to the formulation affects the dissolution, and how near infrared spectroscopy can be used to predict dissolution. This stress affects the dissolution of oral solid dosages forms. However, dissolution testing destroys the entire tablet, making it impossible to evaluate tablet properties when an out of specification result is obtained. Thus, a nondestructive technique such as near infrared spectroscopy is desirable to predict dissolution. The aim of this study was to predict dissolution on tablets with different levels of shear using near infrared spectroscopy in combination with multivariate data analysis. Dissolution profiles were obtained using United States Pharmacopeia (USP) Apparatus 2 as a reference method. Principal component analysis was used to study the sources of variation in the spectra obtained. Partial least squares 2 was used to predict dissolution on tablets with different levels of shear.

The third set of studies consisted in two collaborative studies using near infrared chemical imaging (NIRCI). The first study consisted in the investigation of Active Pharmaceutical Ingredient (API) distribution in a pharmaceutical blend using a Resonant Acoustic Mixer. The resonant acoustic mixer promotes macro and micromixing without providing mechanical force to the blend. the qualitative and quantitative results correlates the acceleration force and total mixing time with aggregate surface are on the samples. Overall, the resonant acoustic mixing performance increased with increasing acceleration force and mixing time promoting agglomeration of the API on the samples.

The use NIRCI was also investigated to evaluate the possible correlation between the variability of gelatin and chitosan with his mechanical properties of the edible films. Edible films are used in the food industry to extend the shelf life of products. Near infrared chemical Imaging was used to determine the abundance of films containing Chitosan and gelatin with different combination of plasticizer. The chemical images were obtained, and preprocess with standard normal variate and second derivative to enhance the signal of chitosan and gelatin on the films. Abundance results shows proper distribution of chitosan and gelatin on films with different plasticizers. Statistical results shows a correlation between the abundance and the tensile strength of the films.

RESUMEN

El “Shear” se crea en un sistema al mover una superficie sobre otra para causar desplazamientos en la dirección de la superficie en movimiento. El “shearing” es esencial para romper los aglomerados en polvos cohesivos, promoviendo el micro-mezclado, y por lo tanto mezclas uniformes. Durante el procesamiento del material, las partículas se frotan unas contra otras, lo que lleva al desarrollo de “Shear”. En la manufactura de dosificaciones sólidas, el polvo se somete a diferentes operaciones unitarias y, por lo tanto, a diferentes niveles tensiones normales y abrasivas. Estas fuerzas mecánicas también afectan la hidrofobicidad de las mezclas de polvos farmacéuticos y esto tiene como impacto la liberación de droga de las tabletas durante las pruebas de disolución.

La prueba de disolución se requiere en el desarrollo, registro, aprobación y control de calidad de dosificaciones orales sólida, excepto cuando la etiqueta indique que deben ser masticadas. La prueba de disolución es requerida por más de 500 productos de tabletas y cápsulas descritos en la Farmacopea de los Estados Unidos (USP), y es la única prueba realizada en manufactura con el objetivo de controlar si el producto funcionará adecuadamente durante su vida útil.

La concentración de drogaen el medio de disolución se determina actualmente con cromatografía líquida de alto rendimiento (HPLC) o espectroscopía ultravioleta / visible (UV / VIS) utilizando solventes con un alto costo y que generan importantes desechos de solventes generados en el análisis. USP establece en el capítulo <711> cuatro sistemas diferentes para realizar la prueba de disolución. El aparato USP 1 (cesta) y 2 (aspas) consisten en un volumen fijo de medio de disolución. Aparato USP 3 (Cilindro reciprocate) y 4 (Celda de flujo continuo) cuando el Aparato

USP 1 y 2 no son adecuados para el análisis (por ejemplo, películas finas poliméricas). Este tipo de prueba destruye la muestra y no deja nada para investigar si la prueba falla. Basado en esa información, se necesita un método no destructivo para el análisis de disolución de las tabletas. La espectroscopia de infrarrojo cercano es una técnica rápida no destructiva adecuada para estos fines. NIR es un método analítico capaz de monitorear parámetros de críticos de calidad que son importantes en la optimización de procesos farmacéuticos. La espectroscopia de infrarrojo cercano se ha convertido en una de las técnicas analíticas más utilizadas para monitorear procesos farmacéuticos, ya que los espectros proporcionan información sobre las propiedades físicas y químicas, y pueden obtener un alto espectro de alta relación señal-ruido en un minuto sin preparación de muestra.

Este estudio se describen los cambios observados en los espectros de infrarojo cercano en modo de reflectancia difusa de tabletas farmacéuticas después de que se sometieran a diferentes niveles de deformación (exposición a “shear”) durante el proceso de mezclado. Estos cambios en los espectros de (NIR) podrían afectar los resultados obtenidos a partir de modelos de calibración NIR. El “shear” se aplicó utilizando una celda modificada y las tabletas se crearon a partir de una tabletera simuladora. Las tabletas con diferentes niveles de “shear” se midió utilizando espectroscopia de infrarrojo cercano en el modo de reflectancia difusa. Los espectros se corrigieron solo usando corrección de línea base para mantener el efecto de dispersión asociado con las propiedades físicas de la superficie de las tabletas. Análisis de Componentes Principales se utilizó para establecer las principales fuentes de variación dentro de las muestras. La dependencia angular de la dispersión elástica de la luz muestra que el tratamiento de “shear” reduce el tamaño de las partículas y produce una distribución uniforme y altamente isotrópica. La compactación de la

tableta reduce aún más el componente difuso de dispersión debido a la realineación de las partículas. El objetivo del estudio era entender los cambios en los espectros de reflectancia difusa de infrarrojo cercano que pueden estar asociados con diferentes niveles de “shear” desarrollada durante el mezclado de muestras de laboratorio.

Un segundo estudio describe cómo el “shear” afecta los componentes de la formulación en la disolución y cómo la espectroscopia de infrarrojo cercano se puede utilizar para predecir la disolución. Este estrés afecta la disolución de dosis sólidas orales. Sin embargo, las pruebas de disolución destruyen toda la tableta, por lo que es imposible evaluar adicionalmente las propiedades de la tableta cuando se obtiene un resultado fuera de especificación. Por lo tanto, una técnica no destructiva, tales como la espectroscopia de infrarrojo cercano es deseable para predecir la disolución. El objetivo de este estudio fue predecir la disolución de las tabletas con diferentes niveles de deformación (“shear”) mediante espectroscopia de infrarrojo cercano en combinación con el análisis de datos multivariados. Los perfiles de disolución se obtuvieron usando un Aparato USP 2 como método de referencia. Se utilizó el análisis de componentes principales para estudiar las fuentes de variación en los espectros obtenidos. Mínimos cuadrados parciales, variación 2 se utilizó para predecir la disolución de las tabletas con diferentes niveles de “shear”.

El tercer conjunto de estudios consistió en dos estudios de colaboración que utilizan imágenes químicas infrarrojas cercanas (NIRCI). El primer estudio consistió en la investigación de la distribución de Ingrediente Farmacéutico Activo (API) en una mezcla farmacéutica utilizando un Mezclador de resonancia acústica. El mezclador de resonancia acústica promueve el macro y micromezclado sin proporcionar fuerza mecánica a la mezcla. Los resultados cualitativos y

cuantitativos se correlacionan con la fuerza de aceleración y el tiempo total de mezcla con la aglomeración en la superficie en las muestras. En general, el rendimiento del mezclador de resonancia acústica se incrementó al aumentar la fuerza de aceleración y el tiempo de mezclado, lo que favorece la reducción de aglomeración del ingrediente activo en las muestras.

El uso de NIRCI también se investigó para evaluar la posible correlación entre la variabilidad de la gelatina y el quitosano con sus propiedades mecánicas de las películas comestibles. Las películas comestibles se utilizan en la industria alimentaria para prolongar la vida útil de los productos. Se usaron imágenes químicas en el infrarrojo cercano para determinar la abundancia de películas que contienen quitosano y gelatina con una combinación diferente de plastificante. Se obtuvieron las imágenes químicas y se preproceso con una variable normal estándar y una segunda derivada para mejorar la señal de quitosano y gelatina en las películas. Los resultados de abundancia muestran una distribución adecuada de quitosán y gelatina en películas con diferentes plastificantes. Los resultados estadísticos muestran una correlación entre la abundancia y la resistencia a la tensil de las películas.

DEDICATION

To my family that believe in me in this adventure, but especially to my wife Dayra Rodriguez and my daughter Alanis Sofia that teaches me the true meaning of love.

ACKNOWLEDGEMENTS

I want to acknowledge my parents Eduardo Hernández Bermudez (Din) and Norma I. Torres Valentin, who believed and encourage me during all these years of study. To my friends and colleagues that support me in all the decisions I made during graduate school. To my wife Dayra Rodriguez that believe in me at every moment and still supporting me at all time.

Thanks to the University of Puerto Rico at Mayaguez to give the opportunity to do my graduates studies, but specially to Dr. Rodolfo J. Romañach and the Analytical and Pharmaceutical Lab for all his guidance and support during these eight years. To the graduate committee that support with me with recommendations to focus my research. Also to Dr. Juan Osorio and Dr. Francisco Palma to letting me work with them in their research projects. Also to Lilly del Caribe, Inc. that allow me to do my practicum and gave me the opportunity to apply my PAT knowledge in a real life situation.

This work was funded by the National Science Foundation through the NSF-AIR Program grant no. 1237873 and National Science Foundation Engineering Research Center on Structured Organic Particulate Systems, through Grant NSF-ECC 0540855. I also received the support of the Sloan Minority Ph.D. Program.

TABLE OF CONTENTS

LIST OF FIGURES

LIST OF TABLES

LIST OF ABBREVIATIONS AND SYMBOLS

Abbreviation	Definition
°C	Celsius Degree
µm	micrometers
A	Absorbance
ANOVA	Analysis of Variance
APAP	Acetyl-Para-Amino-Phenol
BRDF	bidirectional reflectance distribution function
BSDF	bidirectional scatter distribution function
BTDF	bidirectional transmittance distribution function
cm	centimeter
cm^{-1}	reciprocal centimeter
cps	centipoise
f	frequency
f_2	similarity factor
FDA	Food and Drug Administration
EMA	European Medicine Agency
FoV	Field of View
FPA	Focal Plane Array
g	grams
He–Ne	Helium,-Neon
HPLC	High Performance Liquid Chromatography
IVIVC	In-Vivo/In-Vitro Correlation
kN	kilo Newton
L	liter
MCC	Microcrystalline Cellulose
MgSt	Magnesium Stearate
min	minutes
mm	millimeters
MPA	Multipurpose Analyzer
MPa	Megapasclas
mW	milliwatt
NIR	Near Infrared
NIRCI	Near Infrared Chemical Imaging
NIRS	Near Infrared Spectroscopy
nm	nanometers

Abbreviation	Definition
PAT	Process Analytical Technology
PC	Principal Component
PCA	Principal Component Analysis
PCR	Principal Component Regression
pH	numeric scale used to specify the acidity or basicity of an aqueous solution
PLS	Partial Least Square
PLS-DA	Partial Least Square Discriminant Analysis
QbD	Quality by Design
R	Reflectance
R^2	Correlation Coefficient
rpm	revolutions per minutes
RSEcv	Relative Standard Error of Cross Validation
RSEP	Relative Standard Error of Prediction
SNV	Standard Normal Variate
USP	United States Pharmacopeia
UV/VIS	Ultraviolet/Visible
λ	Wavelength

CHAPTER 1

Theoretical Background and Literature Review

1. INTRODUCTION

In vitro dissolution is a critical parameter for the manufacturing of pharmaceutical oral dosages. Over the past three decades the Food and Drug Administration (FDA) has emphasized the importance of dissolution to compare batch to batch performance and the bioequivalence of pharmaceutical oral dosages[1]. The dissolution test is critical to determine whether recently manufactured batches are similar to those originally manufactured and approved by FDA.

The United States Pharmacopeia (USP) describes the general dissolution testing and the type of instrumentation to perform this test. However, the dissolution test as currently described in the Pharmacopeia destroys the tablet. Difficulties in having suitable USP calibration tablets, physical-chemical (temperature, particle size, solubility, and polymorphism) and mechanical (position of the aliquot, vibrations, paddle or vessel position) factors can contribute to dissolution variability[2]. Drug concentration in the dissolution medium is determined by High Performance Liquid Chromatography (HPLC) or Ultraviolet/Visible Spectroscopy (UV/VIS) using solvents with high cost and leading to significant solvent wastes generated in the analysis. Near infrared spectroscopy (NIRS) provides information on the physical and chemical properties, obtaining a high signal to noise ratio spectrum in one minute.

1.1. MOTIVATION AND JUSTIFICATION

The purpose of this investigation was to understand physical characteristics that can affect the dissolution and provide a new analytical method to predict dissolution behavior without destroying the tablets. The dissolution test is required in the development, registration, approval and quality control of a solid oral dosage form except where the label says that they are to be chewed and is required by over 500 tablet and capsule products described in the USP. Dissolution test is the only test performed in manufacturing with the objective of monitoring whether the product will perform adequately throughout its shelf life. FDA may grant a waiver for in vivo bioequivalence study based dissolution results[3]. In Vitro/In Vivo correlation (IVIVC) is not always achieved[1]. However, even in cases where IVIVC is not obtained the dissolution test is still valuable for batch-to-batch comparison. In 2004 the FDA started encouraging manufacturers to implement Process Analytical Technology (PAT) in the pharmaceutical industry to facilitate scientific and risk based decisions based on Quality by Design (QbD)[4]. PAT seeks the implementation of new process instrumentation and tools to extract information on critical process parameters and quality attributes from the process in a faster and more reliable way. For this NIRS was used to provide real time information of dissolution.

In this dissertation, the understanding on how a process parameter affect NIR spectra and dissolution behavior and prediction of the tablets was evaluated. Chapter 2 shows how the shear affects the near infrared (NIR) spectra during a mixing process and the scattering on the surface of the tablets. This information was used to study the dissolution behavior of the core tablets and

predict dissolution using a chemometric model that includes all the related variability of the process in Chapter 3.

Chapter 4 and 5 describe collaborative studies using the Near Infrared Chemical Imaging (NIRCI) system on food and pharmaceutical sciences applications. NIRCI gives spatial and spectral information on a 3D matrix and relates the distribution of the analyte of interest through the entire sample.

1.2. FUNDAMENTAL BACKGROUND

1.2.1. Near Infrared Spectroscopy

2. NIR spectroscopy is a non-destructive analytical technique as it does not require sample preparation and. However, extracting information from NIR spectra is very difficult due to overlapping of vibrational modes. The information obtained in NIR spectroscopy is based on the overtones of the fundamental vibrations of C-H, O-H, and N-H. This do not follow the Hooke's law represented by the energy of a system consisting in two masses bonded by a spring is given by equation 1:

$$E = \frac{h}{2\pi}\sqrt{\frac{k}{\mu}} \quad (1)$$

Where: k corresponds to the force constant of the spring, *h* is the Planck's constant and μ is the reduced mass (equation 2):

$$\mu = \frac{m_1 m_2}{m_1 + m_2} \quad (2)$$

The quantum model is required to define the possible vibrational energy levels as seen in equation 3[5]:

$$E_\upsilon = \left(\upsilon + \frac{1}{2}\right) h\nu \quad (3)$$

Where: υ corresponds to the quantum number of the vibrational transition and, ν is the fundamental frequency of the vibration.

The potential energy curve is parabolic and symmetrical as seen in Figure 1. In the harmonic oscillator the energy levels are equidistant and transitions are only allowed between neighboring energy levels with Δn = ± 1. However, the NIR overtones bands cannot be explained using the harmonic oscillator model due to repulsive forces between vibrating atoms and dissociation when the vibrating atom is strongly extended.

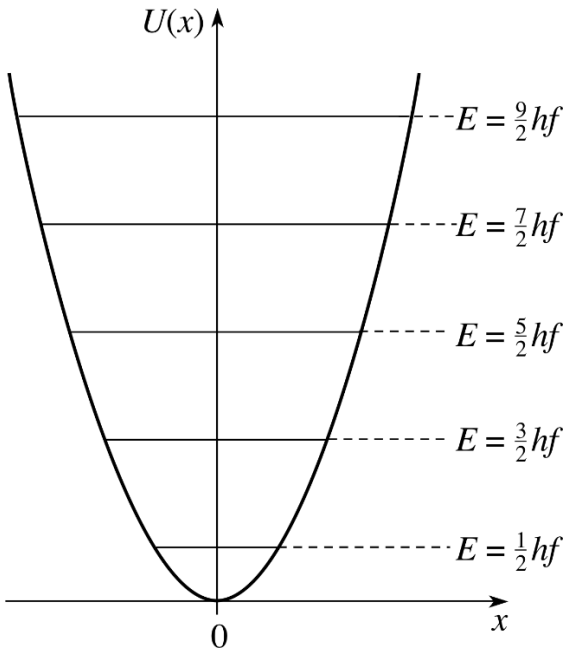

Figure 1. Harmonic oscillator representation

A modification to the harmonic oscillator model was made to explain the overtone transition. Anharmonicity makes possible overtones transitions involving an increase in the quantum vibrational number higher than one[6]. The combination bands corresponding to a simultaneous increase in the quantum vibrational number in two or more vibrations ($\Delta n = \pm 2, \pm 3$) with the same photon (figure 2). In addition, the energy gap between the vibrational states are not equal and as consequence the anharmonicity constant is required x_m. Equation 4 represents the calculation of the energy levels for the anharmonic oscillator model.

$$E = \left(v + \frac{1}{2}\right) h\nu - x_m h\nu \left(v + \frac{1}{2}\right)^2 \quad (4)$$

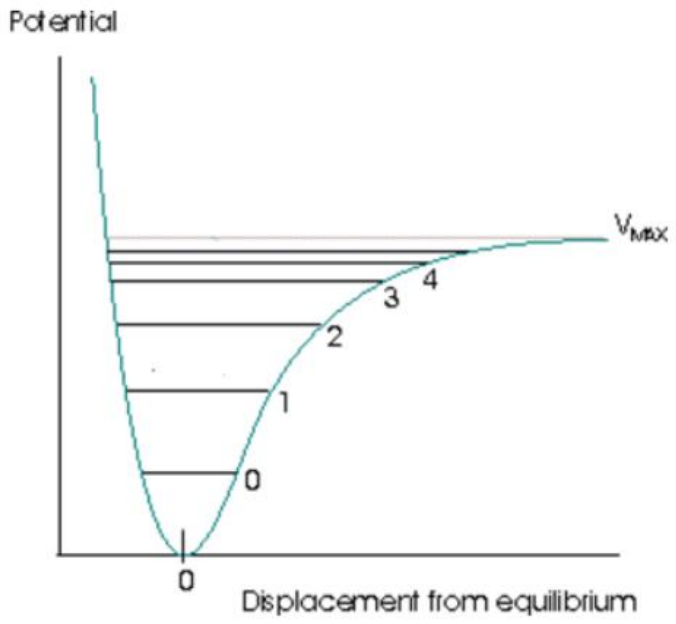

Figure 2. Harmonic oscillator representation

2.1.1. Chemometrics

2.1.1.1.Baseline Correction

Baseline correction is a pre-treatment that can correct spectral offset due to additive effects and light scattering effects. This procedure may be performed by subtracting the offset in all spectral wavelengths, or in a lower number of wavelengths[7].

$$Baseline\ Correction = X_1 - X_1,\ X_2 - X_1,\ X_3 - X_1 \ldots X_{n+1} - X_1 \quad (5)$$

When X_1 = Intensity of first spectral point

2.1.1.2.Standard Normal Variate

Standard normal variate (SNV) is a spectral pretreatment that reduces the multiplicative effects that scales the entire spectrum by a given factor and additive effects, which is observed as a baseline off set on NIR spectra[8]. SNV subtract the mean of each spectral point and divide each spectral point by the standard deviation. Each spectrum standard deviation is different, and all centralized to zero. The SNV attenuates additive and multiplicative effects on the spectra data set. Equation 6 describes the calculation of SNV:

$$SNV = \frac{X_i - x_{ave}}{s} \quad (6)$$

When x_i = Intensity of first spectral point, x_{ave} = to spectrum average and s = standard deviation of the spectrum.

2.1.1.3.Derivatives

Derivatives are often used to removes nonzero bias and partially compensate for baseline offset. Derivatives removes offset and slope variation related to background interferences and scattering. The most important enhance additional information from the spectrum. But derivatives cannot correct for multiplicative effects and only removes general baseline drift related to particle size.[5].

2.1.1.4.Modeling

2.1.1.4.1. Principal Component Analysis

PCA is a multivariate technique used in the studies in this dissertation to highlight differences through a decomposition process. Each spectrum was decomposed mathematically into scores. This algorithm present information in a new set of axis called principal components that are used to explain the variation obtained in the calibration set. Each principal component is orthogonal. This means that the variation contained for each principal component is not contained in the others principal components[8].

2.1.1.4.2. Partial Least Square Regression

PLS incorporates the reference values in the decomposition process. As result, the eigenvector and scores from PLS are different than the PCA. PLS maximizes the covariance that already exists between the spectral variation and the reference values. Spectra and reference values are expressed as projections and maximize the linear fit in the regression. A regression vector is then calculated for each factor[9].

2.1.2. Dissolution Testing

Dissolution testing is required in the pharmaceutical industry in the development of new products, quality control, and to assist bioequivalence. This test consists in monitoring the release of drug during time extracting samples from the dissolution bath manually or automatically. The FDA has emphasized the importance of dissolution test and reviews the USP monograph for consistency in product approval of New Drug Applications[10].

The United States Pharmacopeia (USP) establishes in chapter <711> four different systems to perform dissolution test. USP Apparatus 1 (Basket) and 2 (Paddle) consist in a fixed volume of dissolution medium. These methods provide a steady stirring motion in a large vessel[11]. The dissolution medium is at 37°C (body temperature). USP Apparatus1 and 2 are commonly used for immediate release forms. USP apparatus 3 (Reciprocating Cylinder) and 4 (Flow-Through Cell) when the USP Apparatus 1 and 2 are not suitable for the analysis.

CHAPTER 2

The Effect of Shear Applied During a Pharmaceutical Process on Near Infrared Spectra

Based on work Published in: *Applied Spectroscopy 2016, Vol. 70(3) 455–466.*

2.1. LITERATURE REVIEW

Process Analytical Technology (PAT) is based on the development and application of analytical methods capable of monitoring critical quality parameters that are essential for the improvement of pharmaceutical processes. Near infrared spectroscopy (NIRS) has become one of the most used analytical techniques to monitor pharmaceutical processes since it does not require sample preparation, is capable of obtaining spectra in seconds and is also a non-invasive technique[12]. NIRS applications have been developed to determine the drug and excipient concentration during mixing[13-16], and moisture content during drying[17]. NIR spectra depend on the chemical composition of the materials analyzed and on their physical properties such as particle size. Thus, the development of NIR methods to determine chemical composition usually requires mathematical transformations (called spectral pretreatments) to remove multiplicative and additive effects observed in NIR spectra that often occur due to particle size differences. The larger surface area to volume ratio from smaller particles leads to more light remitted to the detector and a diffuse reflectance spectrum with reduced absorbance[7]. NIR spectra obtained from pharmaceutical processes also show significant differences in their baseline. Without spectral pretreatments, the

changes in the NIR spectra related to the physical properties of materials would be confused with chemical changes and could lead to errors in the determination of chemical composition.

This study showed that shear also affects NIR spectra. Powder shearing is important in mixing of cohesive powders. Shear stress is created in a system by moving one surface over another to cause displacements in the direction of the moving surface[18]. In solid dosage manufacturing, powder is subjected to different unit operations and thus to different levels of normal and abrasive stresses and shear. Lacey et al reviewed the fundamental mechanisms (convective and diffusive) in powder mixing and indicated that agitation and shear help both in convective (macro-mixing) and dispersive (micro-mixing) mixing[19, 20]. Shearing of powder is essential to break down agglomerates in cohesive powders, promoting micro-mixing and thus uniform blends[21]. Most drug particles like acetaminophen and ibuprofen are intended to be of smaller size to allow a larger surface area for dissolution. However, decreasing the particle size also increases their cohesive nature. Mechanical shear also affects the hydrophobicity of pharmaceutical powder blends and its impact on drug release from tablets[22]. Typically, dissolution[23] and hardness[24] are adversely affected by excessive shear. This phenomenon is known as over-lubrication[25, 26]. The work in this manuscript was done with acetaminophen, which is a cohesive material and widely sold active pharmaceutical ingredient.

The effect of shear on NIR spectra is investigated in this study. Several studies describe the effect of compaction on NIR spectra[27-32]. However, the authors understand that this is the first studies on the effect of shear on NIR spectra. The observation of differences in NIR spectra due of the effect of shear is important, as it could be a source of error in NIR methods developed to determine chemical composition. The effect of shear on NIR spectra could also be important for gaining

better understanding of pharmaceutical processes and could serve as a process signature to evaluate the authenticity of a commercial product. In this work, the effect of shear has been studied by comparison of NIR spectra obtained after subjecting blends to different shear conditions. In addition to the near infrared spectroscopy studies, NIR chemical imaging, and angle-resolved elastic light scattering were used to study and explain these observed spectral differences. The work in this chapter investigates the effect of shear on the NIR spectra for two different formulations. These formulations will be addressed herein as Case II and Case III.

2.2. MATERIALS AND METHODS

2.2.1. Materials and Sample preparation

Case II Formulation: Powder blends were prepared by mixing microcrystalline cellulose (Avicel PH102, FMC biopolymer, Newark, DE mean particle size 100 μm), and lactose monohydrate NF (Foremost farms, Rothschild, Wisconsin, mean particle size 90 μm) as excipients, semi-fine acetaminophen (Mallinckrodt Inc. Raleigh, NC, lot 008111H411) as an active ingredient (mean particle size 42 μm), and magnesium stearate NF (Mallinckrodt, St. Louis, Missouri, lot: P09247 mean particle size: 38 μm) as a lubricant. Each of these materials were passed through different sieves. Sieve no. 18 was used for acetaminophen (resulting mean particle size of 45 μm), and sieve no. 30 each for lactose (resulting particle size of 70 μm) and magnesium stearate (8 μm). Sieving was done to break agglomerates, if any. *Case III Formulation:* Powder blends were prepared with lactose monohydrate NF (Foremost farms, Rothschild, Wisconsin, mean particle size 90 μm) as excipient material, semi-fine acetaminophen (Mallinckrodt Inc. Raleigh, NC, lot 008111H411) as an active ingredient (mean particle size 42 μm), and magnesium stearate NF (Mallinckrodt, St.

Louis, Missouri, lot: P09247 mean particle size: 38 μm) as a lubricant. Each of these materials were subjected to sieving to break agglomerates in the Case II Formulation. Table 1 provides the composition of the formulations known as Case II and Case III.

Case Study	Component	Concentration % (w/w)	Total % (w/w)
II	Acetaminophen	9	100
	Lactose	45	
	Micro Crystalline Cellulose	45	
	Magnesium Stearate	1	
III	Acetaminophen	9	100
	Lactose	90	
	Magnesium Stearate	1	

Table 1. Tablet composition description for Case II and Case III.

2.2.2. Blending and shearing procedure

Case II: The blending was done in a 1.87L V –blender (Patterson-Kelley). One kilogram of the blend was made wherein the major ingredients: lactose, acetaminophen and microcrystalline cellulose were layered in a top-bottom fashion and rotated at 15 rpm for 15min. a total of 10 g of the lubricant, magnesium stearate was added to this premix and mixed for 25 revolutions. This step was undertaken so that sufficient macro-mixing and de-agglomeration was attained. Further micro-mixing was achieved in the Couette Cell (Measurement Control Corporation, East Hanover, N.J.) (Figure 3). The mixing time of lubricant in the blender was kept low and the intensifier bar of blender was not operated to have minimum exposure to uncontrolled shear in the blender prior to exposing it to controlled shear in the shearing device (Couette Cell)[33]. The blended powder was then removed from the V-blender and was split into three sets of 300g each. For Case III a similar

procedure was followed and an additional shear level of 2560 revolutions was introduced where the blend was sheared at 80 rpm for 32 minutes.

Figure 3. Modified couette cell instrument

The Case II and III blends were subjected to controlled and uniform shear environment in a modified Couette cell equipped with equidistant baffles. The Couette cylindrical cell consists of two concentric cylinders, which rotate relative to each other and 300g of the blend is filled in the annular region of the cylinder. The equidistant pins are uniformly spaced and the entire setup creates a uniform shear environment on the powder[33]. The shear rate was kept constant at 80 rpm for all the sets. The first set was subjected to a no shear level, the second sample was subjected to a shear level of 160 revolutions (sheared for 2 min), a third sample was subjected to a shear of 640 revolutions (8 min), and a fourth sample was subjected to a shear of 2560 revolutions (32 min) respectively. The 2560 revolutions samples were only with the Case III formulation. Samples within the range of 160 to 640 revolutions are considered representative of a continuous mixing process based on the authors' previous experience, while the 2560 revolutions samples are considered an extreme case. However, the shear applied to these formulations is more uniform than the shear in industrial processes, because of the use of the Couette cell, which was necessary to perform reproducible experiments and promote micro-mixing of the ingredients by dispersion.

2.2.3. Tableting procedure

Sheared powder samples were compressed into tablets at Rutgers University using a Presster, a tablet press emulator (The Presster, Measurement Control Corporation, East Hanover, NJ) designed to match compaction force and dwell time of any tablet press. The simulated press is a Kikusui Libra 2 with both pre-compaction and compaction rolls of 250 mm in diameter. The speed was kept constant at 20 rpm. Flat-faced punches and round dies were used to make round tablets of 10 mm diameter. The dosing position was adjusted and fixed to give tablets of 350 mg weight. Tablets were made at an average force of 8 kN, 12 kN and 16 kN respectively by changing the compaction gap between the punches. For Case III all tablets had a constant compaction force of 24 kN. To avoid tablet weight variance, tablets at the start of the batch were discarded until the stable average pressure and weight was obtained. Finished tablets were kept inside a sealed bag to prevent exposure to moisture. A total of 54 tablets were made. Table 2 describes the tablets prepared.

Shear level	**Compaction Force (kN)**	**Weight**	**Thickness**
		(mg)	**(mm)**
0 revs	8.5	350	3.45
	12	360	3.40
	16	350	3.33
160 revs	8.3	350	3.14
	11.7	350	3.34
	15.8	350	3.28
640 revs	7.8	350	3.58
	11.2	350	2.34
	15.7	340	3.16

Table 2. Conditions and description of case II tablets used in study.

2.2.4. NIR Spectral Acquisition Parameters and Data Analysis.

All spectra were obtained with a Multipurpose Analyzer (MPA) with a high intensity source from Bruker Optics (Billerica, MA). The diffuse reflectance spectra were obtained with a resolution of 32 cm^{-1}. A total of 256 background scans was obtained and 128 sample scans. The resolution for the transmission measurements was also 32 cm^{-1}. A total of 256 background scans was obtained and 256 sample scans. NIR data analysis was performed using The Unscrambler X v10.3. All spectra were pretreated using baseline correction at the first spectral point.

2.2.5. NIR Chemical Imaging Instrument set up

Near Infrared Chemical Imaging (NIR-CI) was used to investigate the slope of the NIR spectra obtained across the tablet surface. A previously developed method to create an image based on the slope of the NIR spectra was used[29]. A Malvern Spectral Dimensions SyNIRgi chemical imaging spectrometer with a focal plane array detector was used. All samples were analyzed with a 40-µm objective with a field of view (FoV) of 12.8 x 10.2 mm. Spectra were obtained in reflectance mode by placing the tablets over a white ceramic disk with a diameter of 28 mm. The reflectance spectra were converted to absorbance, log (1/R), followed by pixel correction to remove areas of non-uniform illumination and the effect of unresponsive pixels. The images consist of 320 x 256 pixels, with a spectral range of 1200 to 2400 nm, forming the spectral hypercube. This disk was used as a reference for the acquisition system. Image analysis was performed with the Malvern ISys 5.0 and MATLAB 2013A.

2.2.6. Scattering Measurements

Angle resolved elastic light scattering measurements were used to analyze how the light scatters from the tablets. These measurements were obtained by the scatterometer shown in Figure 4. In this experiment a 15 mW He–Ne linearly polarized laser with wavelength λ=632.8 nm was used to illuminate samples. The beam was focused on the sample surface into a spot of ~300 μm at normal incidence. The scattered light within the hemisphere was collected by an elliptical mirror of 20-cm diameter and projected onto charge-coupled device (CCD, SBIG ST-7MXEI-Camera, Santa Barbara, CA). The CCD exposure time for each measurement was 300 ms. Integral light scattering was measured by a calibrated Si photodiode.

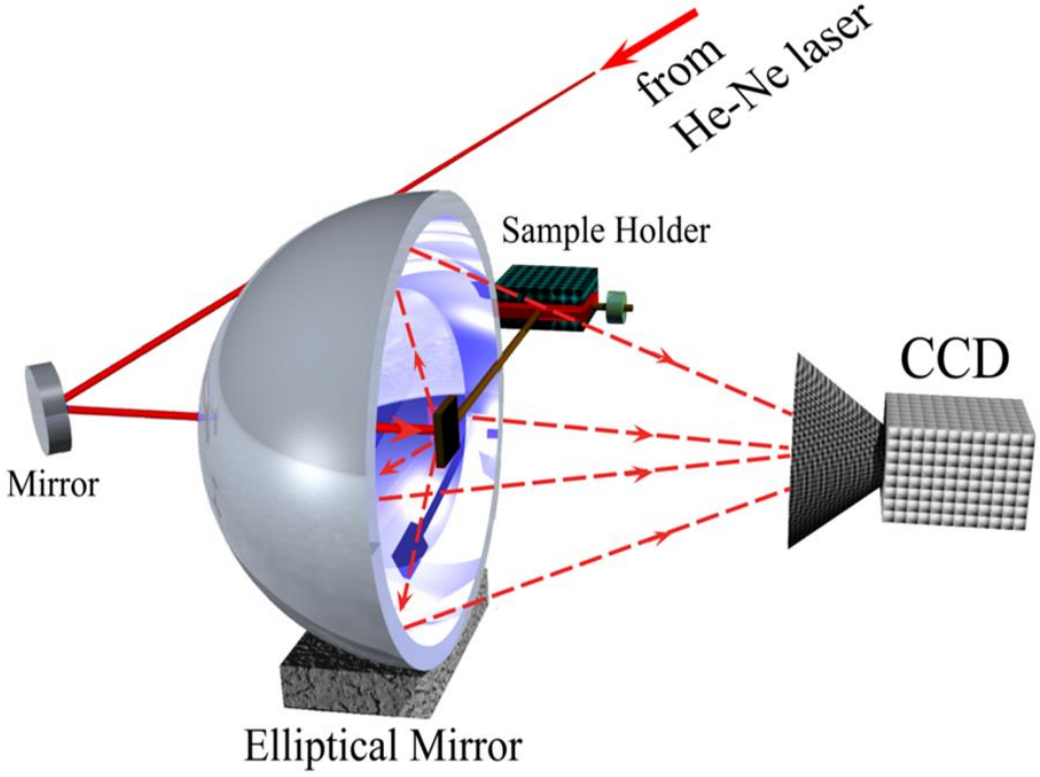

Figure 4. Scatterometer used to measure the angle-resolved elastic light scattering the scattering from tablets[34] (courtesy of Sergiy Lysenko)

The scattering indicatrix images were analyzed using the bidirectional scatter distribution function BSDF. The BSDF is a mathematical distribution, which describes the way the light is scattered from a surface (equation 6). The BSDF is a superset of bidirectional transmittance distribution function (BTDF) and bidirectional reflectance distribution function (BRDF)[35], and is defined as:

$$\mathrm{BSDF}(\theta,\varphi)=\left(\frac{dP_r(\theta,\varphi)}{d\Omega}\right)/P_i \cos\theta \quad (6)$$

θ and φ are the polar and azimuthal angles, dP_r is radiance light differential, $d\Omega$ is a solid angle differential and P_i is the irradiance light. This equation can be applied for rapid evaluation of diffuse component of scattering indicatrix. Since fully diffuse scattering obeys Lambertian cosine law[36, 37], the BSDF in this case will be constant over all scattering angles.

2.3. RESULTS AND DISCUSSION

2.3.1. Near Infrared Spectroscopy

Figures 5 show the pure component spectra used for Case II formulation (a) acetaminophen (APAP), lactose, microcrystalline cellulose (MCC) and magnesium stearate (MgSt)) and figure. 6 shows Case III formulation (APAP, lactose, and MgSt).

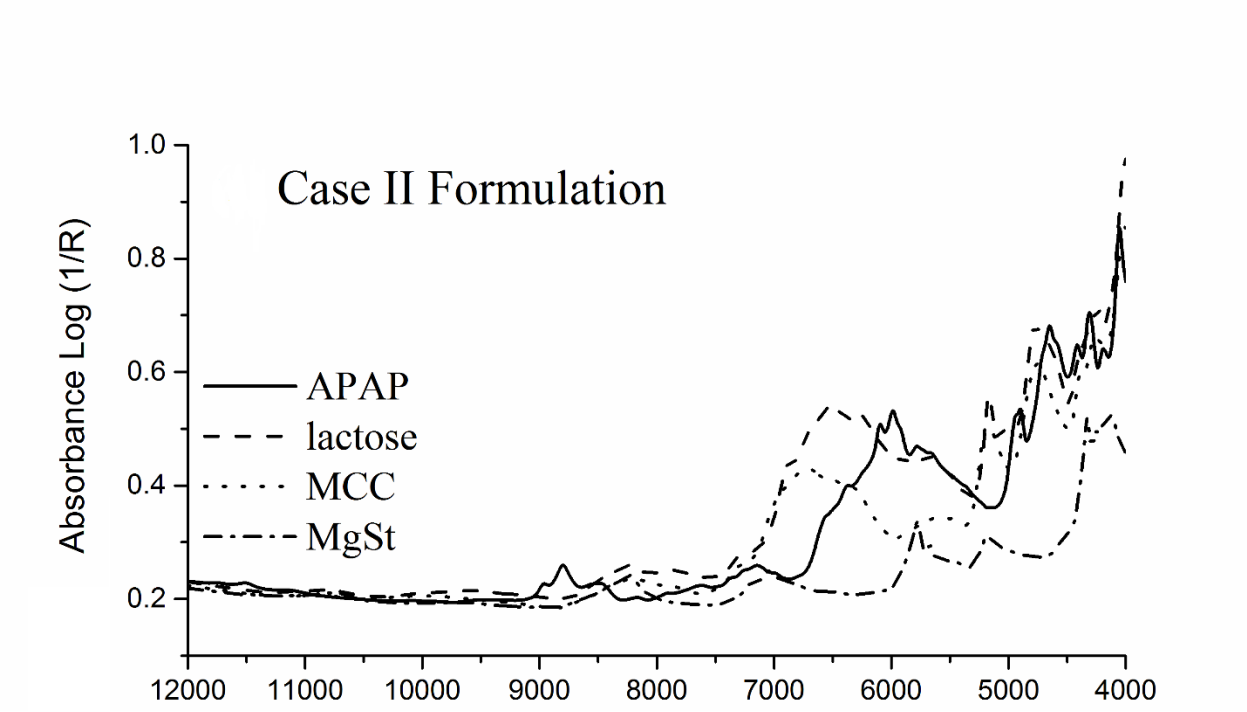

Figure 5. Near infrared pure components spectra used for Case II formulation.

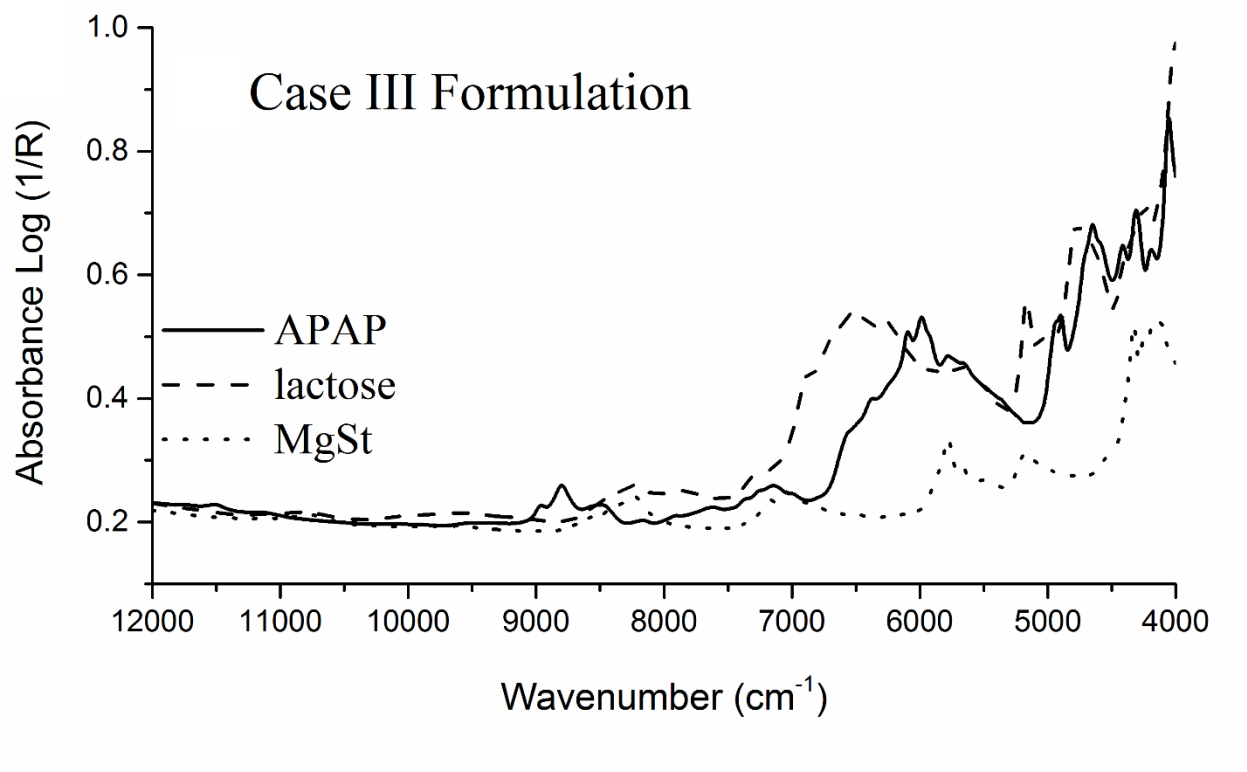

Figure 6 – Near infrared pure components spectra used for Case III formulation.

Figure 7 shows the differences between the diffuse reflectance spectra of tablets obtained after compaction at 8 kN for blends of similar composition subjected to the three shear levels: no shear, 160 revolutions, and 640 revolutions, where strain refers to the duration of exposure to shear rate[38]. Broad bands are obtained at no shear conditions. As the shear is increased, the bands became more defined as observed in figure 7, figure 8 and figure 9. These spectra show significant differences in two spectral regions: 7450 - 7000 cm^{-1}, and 5600 - 5100 cm^{-1}. Figure 8 was obtained for tablets at 12 kN and figure 9 for 16 kN does not show differences between the second and third shear levels (160 and 640 revolutions), but the broad band in the no shear sample was still observed and two clearly defined bands are observed. Maxima are obtained at 7266 cm^{-1} and 7189 cm^{-1}after compaction forces of 12 kN and 16 kN. NIR tablet transmission spectra did not show variation associated with shear. The spectra were baseline corrected to maintain scattering effects on the spectrum that could be related to the differences in porosity (physical differences) between the tablets[7]. However, the spectral differences associated with variation in shear level are still observed after the SNV transformation or the second derivative is applied. The differences observed in terms of compaction force were expected[27-32], but not the differences in the 7450 - 7000 cm^{-1}, and 5600 - 5100 cm^{-1} region. The 7450 - 7000 cm^{-1} bands have been assigned to combinations of the first overtones of the C-H stretching modes and the C-H bending modes of cellulose[39, 40].

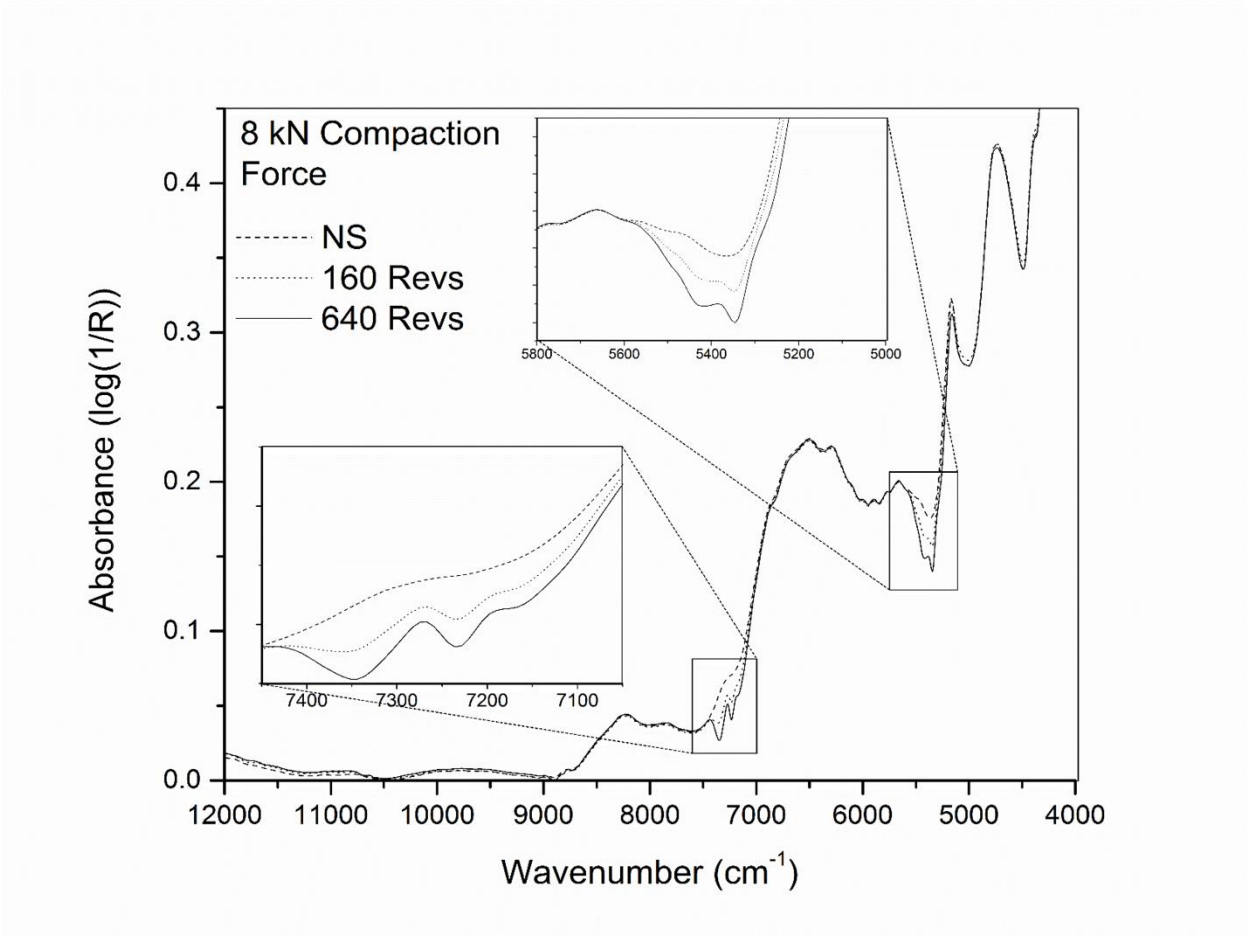

Figure 7 - Baseline corrected DR FT-NIR Spectra of tablets with 8 kN compaction forces with three different shear levels: no shear, 160 revolutions and 640 revolutions.

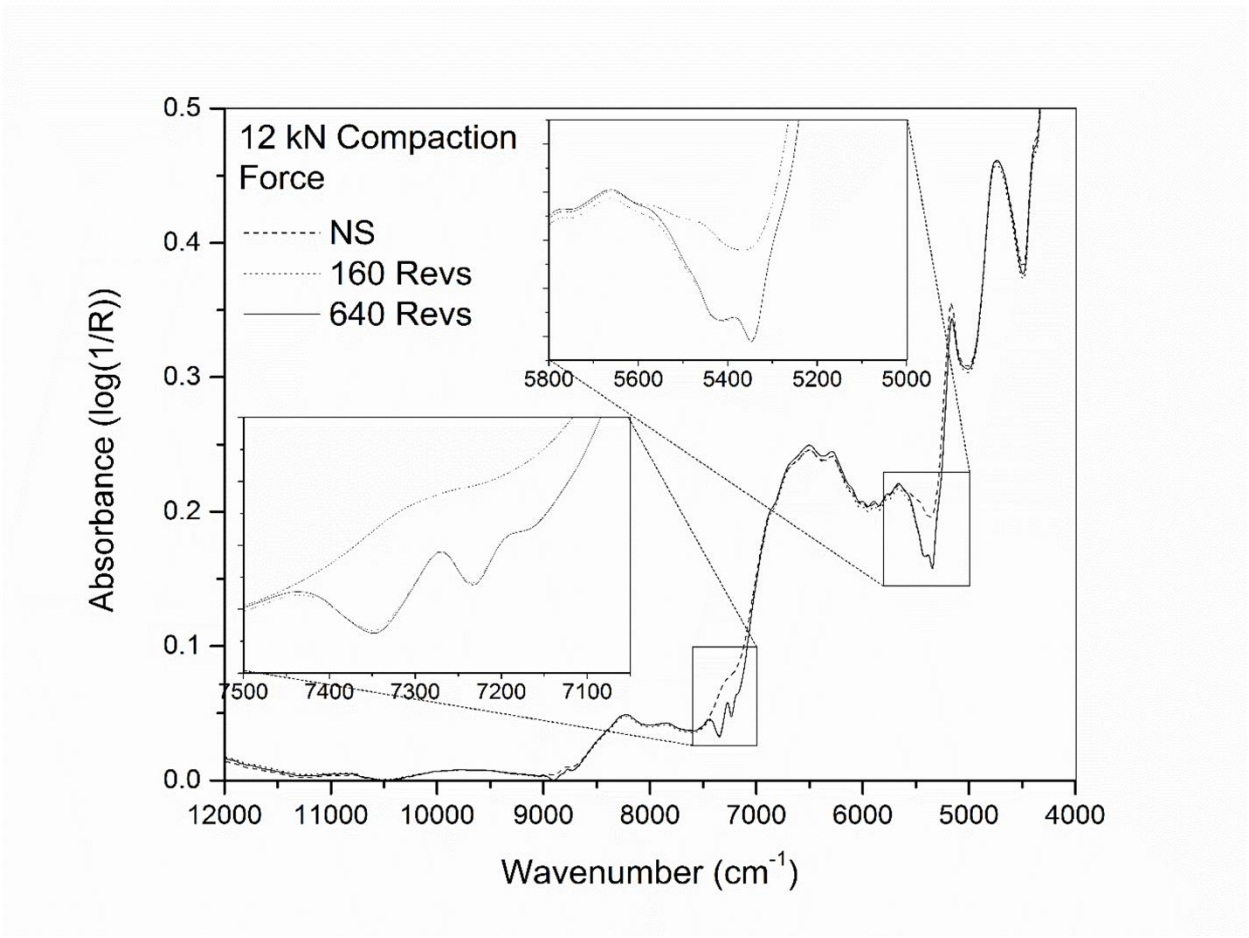

Figure 8 - Baseline corrected DR FT-NIR Spectra of tablets with 12 kN compaction forces with three different shear levels: no shear, 160 revolutions and 640 revolutions.

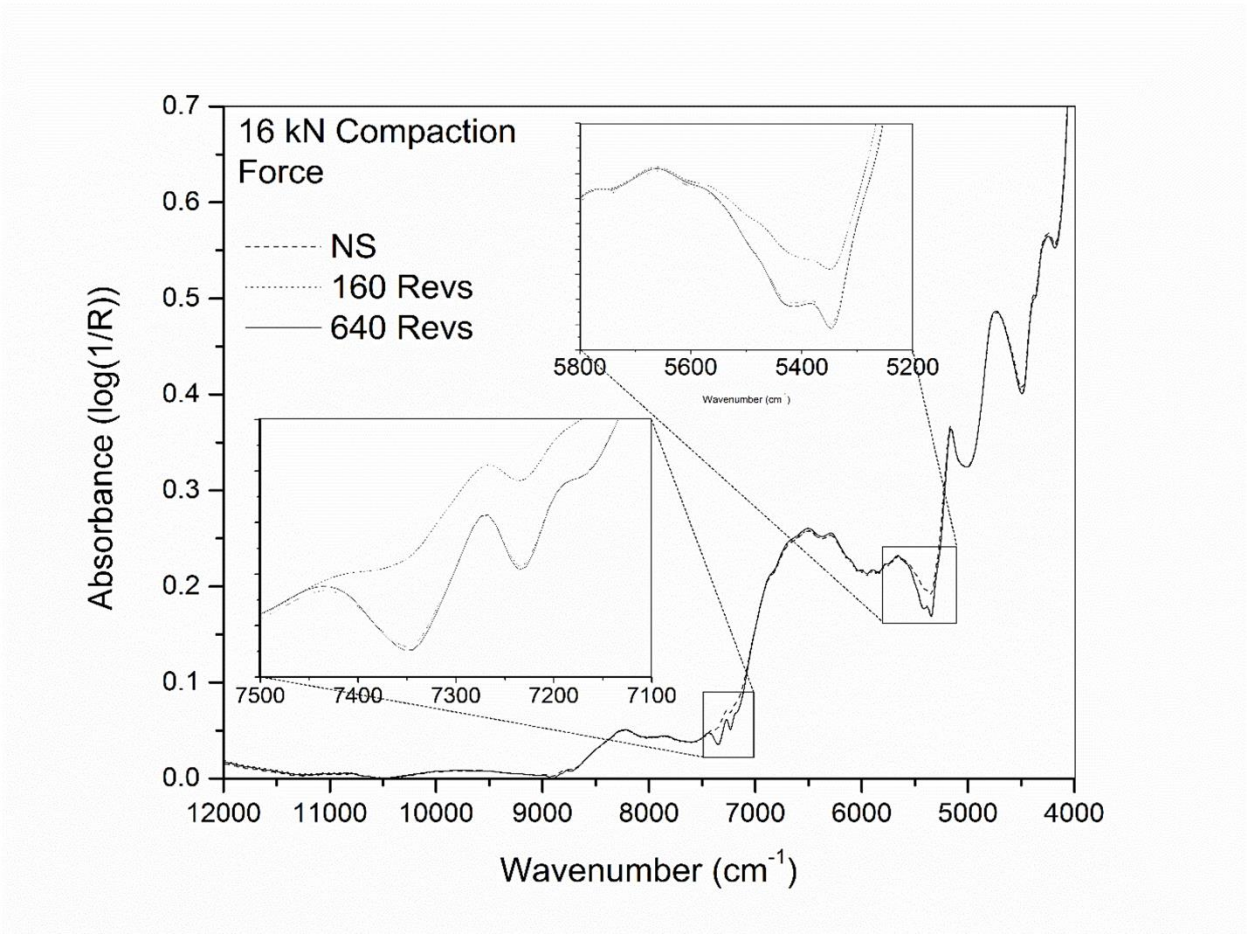

Figure 9. Baseline corrected DR FT-NIR Spectra of tablets with 16 kN compaction forces with three different shear levels: no shear, 160 revolutions and 640 revolutions

Previous studies have shown that at lower compaction forces the irregular surface of the particles combined with their random orientation results in the radiation becoming diffuse. At higher compaction forces, the surface area is reduced and the transmission of radiation increases with higher compaction force[27, 28]. Thus, higher compaction results in higher absorbance results in the diffuse reflectance spectrum and lower absorbance in the transmission spectra. However, in this study the transmission spectra did not indicate significant differences between the tablets analyzed. The changes that occur in the NIR spectra because of differences in compaction were observed

throughout the entire NIR spectrum, and cause changes in both spectral baseline and slope. Thus, the changes in compaction do not fully explain the spectral changes observed in this study.

Figure 10 shows a Principal Component Analysis (PCA) scores plot of the spectra obtained with the entire set of 54 tablets. The PCA scores plot shows that spectra are grouped by compaction force and by the level of shear applied to the blends. The compaction force is the principal source of variation as indicated by PC1. The differences in compaction force were expected since several studies have also shown that compaction pressure affects NIR spectra[27-32]. However, the effect of shear is a new observation discussed in this study. At 8 kN the spectra from the three shear levels are clearly separated confirming the results shown in Fig. 7. At 12 and 16 kN the scores from the 160 and 640 revolutions are very similar, but they are separated from those obtained for no shear tablets.

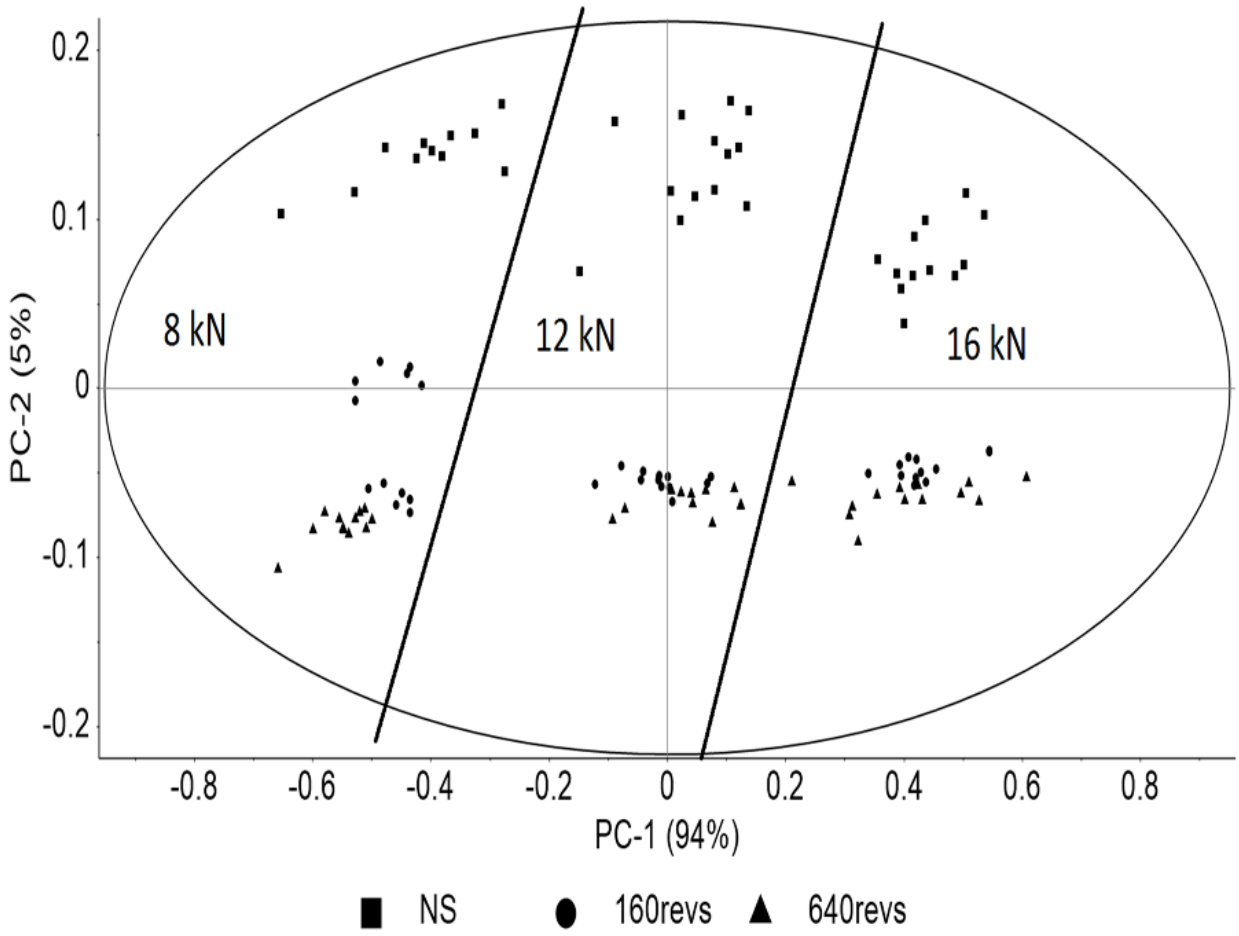

Figure 10. PCA Score plot with the entire set of 54 tablets where compression force and shear were varied.

The PC1 loading represents the compaction force as first source of variation. This loading has a correlation coefficient with the NIR spectra of 0.9954 for 8 kN, 0.9962 for 12 kN and 0.9967 for 16 kN tablets describing that the spectra are changing with respect to the compaction force. The PC2 loading shows that shear is a second source of variation. This loading presents two bands at 7450 - 7000 cm^{-1}, and 5600 - 5100 cm^{-1} region describing the change in the spectra related to the shear shown in figure 11 and does not correlate with any of the pure component in the formulation. Table 3 shows the correlation coefficients of PC1 and PC2 with the pure components and tablets with different compaction forces. The spectra discussed were all obtained from tablets prepared

under the conditions described in Table I for Case II. NIR spectra of blends for Case II were also obtained. These blends did not reveal the spectral variation observed in the 7450 - 7000 cm^{-1}, and 5600 - 5100 cm^{-1} region.

Principal component	Pure Components				Tablets		
	APAP	lactose	MCC	MgSt	8kN	12kN	16kN
1	0.9387	0.9834	0.9805	0.8536	0.9954	0.9962	0.9967
2	-0.0828	-0.0975	-0.0642	-0.0393	-0.0620	-0.0578	-0.0684

Table 3. PC loadings correlation coefficient results for pure components and tablets with different compaction forces.

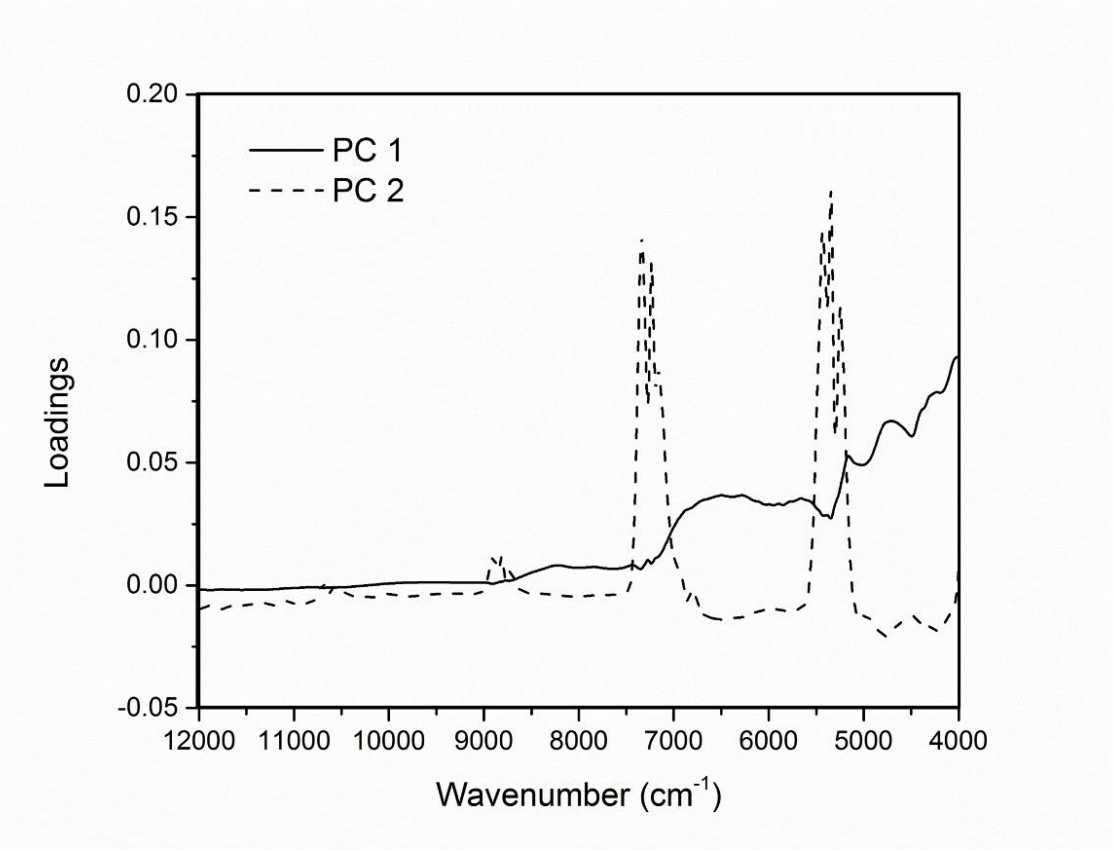

Figure 11. Loadings for Case II tablets. PC1 represent changes associated with compaction force and PC2 represent changes in shear effect

The effect of a number of pretreatment methods on the NIR spectra was also evaluated for Case II. Spectral pretreatments are often used to remove or reduce the effects of light scattering on NIR spectra[32]. The different spectral pretreatments removed the effect of tablet compaction forces, but did not remove the effect of shear level from the NIR spectrum. Table 4 shows the results obtained for several spectral pretreatments.

Pretreatment (All Spectral Region)	**1st PC**		**2nd PC**	
	Property	**Explained Variance**	**Property**	**Explained Variance**
Baseline Corrected	Compaction	94%	Shear	5%
SNV	Shear	79%	No clear grouping	12%
SNV+1st Der. (15 points)	Shear	91%	Compaction	6%
SNV+2nd Der. (15 points)	Shear	96%	Compaction	2%

Table 4. Different spectral pretreatment evaluated with PCA.

The effect of shear was also evaluated in the Case III formulation. In this case the differences observed in the 7500 - 7000 cm^{-1} and 5600 - 5100 cm^{-1} regions were not observed as shown in figure 12. However, subtle differences were observed in the diffuse reflectance region of 7000 to 5000 cm^{-1} and PCA showed four distinct groups of scores associated to the level of shear. Once again, transmittance spectra were very similar and did not reveal spectral differences as the level of shear varied.

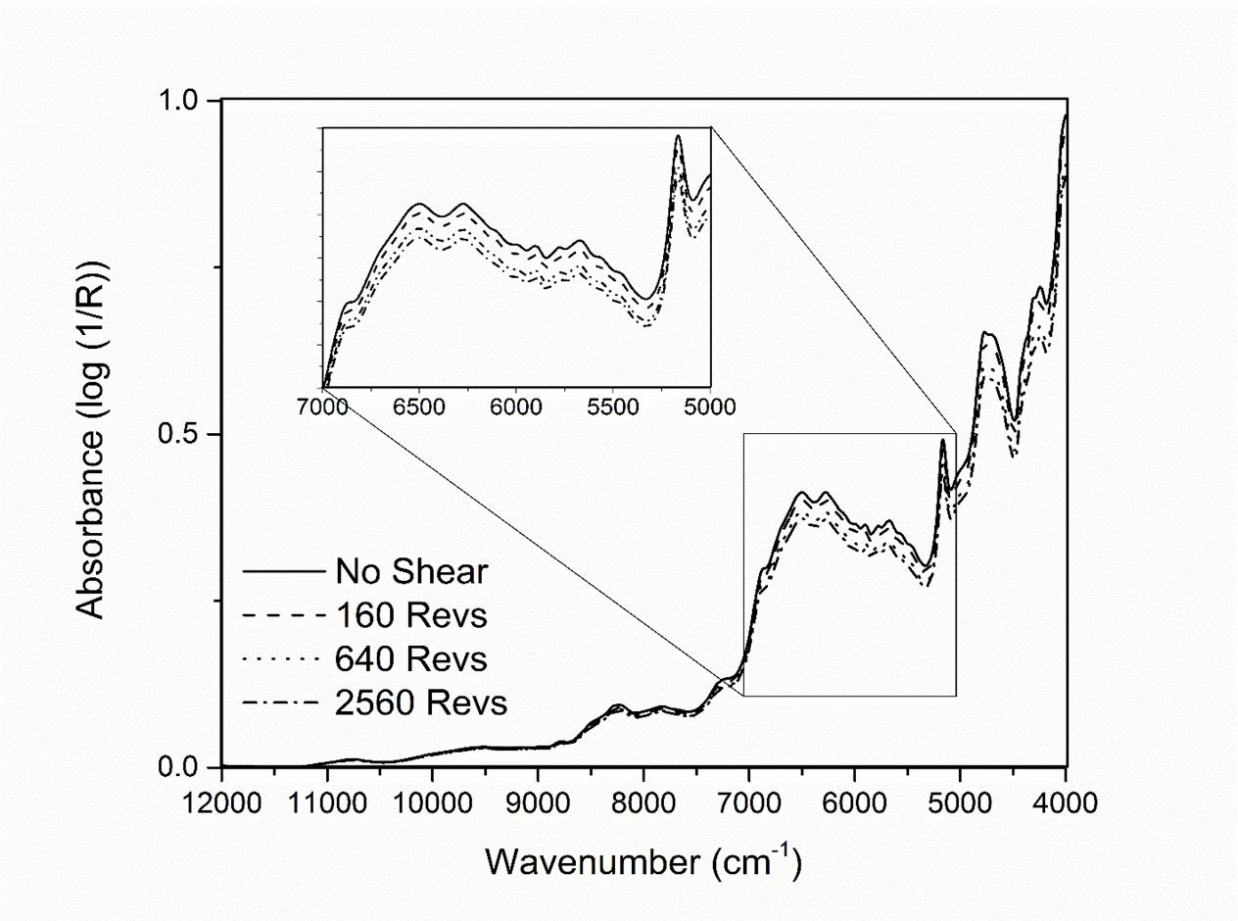

Figure 12. Baseline corrected DR FT-NIR spectra for Case III tablet with 24 kN compaction force and four different shear levels: no shear, 160 revolutions, 640 revolutions and 2560 revolutions.

Figure 13 shows the PCA scores plot for the spectra from the Case III tablets. The PC1 loading shows the variation for changes in shear. This loading has a correlation with the tablet spectra of 0.9943 describing the spectra is changing with respect to shear. This second formulation was only compacted at 24 kN and an additional shear level was introduced (2560 revolutions). However, the effect of shear is clearly observed in the NIR spectra. The spectral differences between Case II and Case III are obviously related to the chemical differences since Case III does not have MCC incorporated in the formulation. Hydrogen bonding affects NIR spectra[39] and a recent study indicates that MCC has a shear rate sensitivity as a viscoelastic excipient increasing the elastic

effect at high speed direct compression[41]. This critical material attribute of MCC was observed in a mechanical process and now observed using NIR spectroscopy. MCC appears to be a material that is affected by the shearing process and these effects are observed in the NIR spectra.

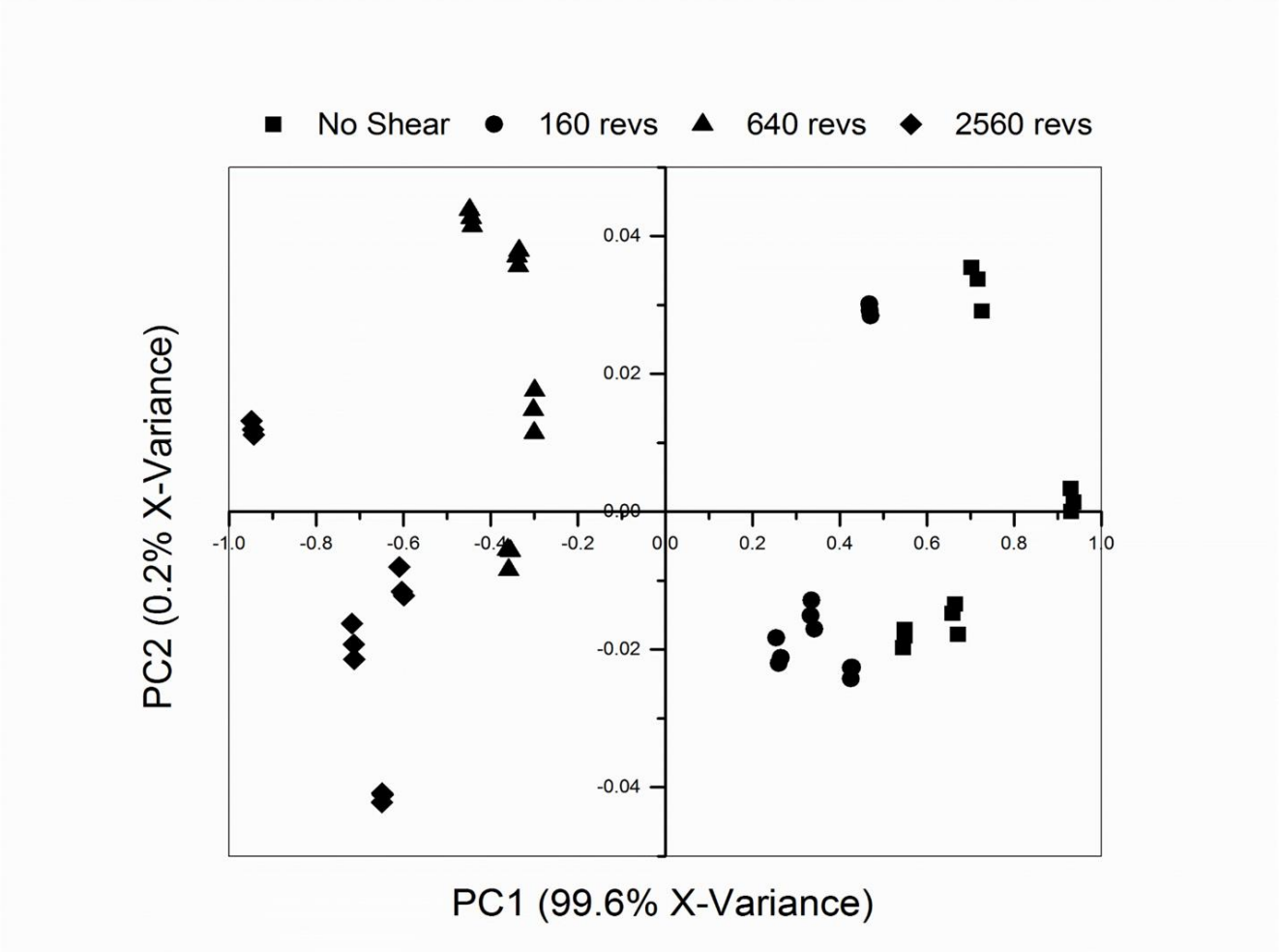

Figure 13. PCA Score Plot for Case III formulation. Compaction force are constant and shear effect are varied.

2.3.2. Near Infrared Chemical Imaging

NIR-CI was used to investigate whether changes in the slope of the spectra are related to the shear effect in the tablets. The slope image was calculated using the first image plane of the spectral hypercube and the correspondent absorbance intensity with the last image plane and correspondent

intensity. The slope calculation was used to determine the slope value with Eq. 7 and image statistics are summarized in Table 5.

$$m = \frac{A_2 - A_1}{\lambda_2 - \lambda_1} \quad (7)$$

When A_1 = intensity of first image plane, A_2 = intensity of last image plane and λ_1= First wavelength, (1340 nm), λ_2 = last wavelength (2220 nm). In this way, differences in baseline do not affect the calculations.

Shear (Revs)	Compaction Force (kN)	Mean Slope (10^{-3})	Std. Dev (10^{-4})	Skew	Kurtosis
0	8	2.47	2.63	0.43	6.19
0	12	2.79	2.95	0.44	6.11
0	16	3.07	2.95	0.01	6.88
160	8	2.45	3.29	0.62	5.17
160	12	2.74	3.36	0.61	5.51
160	16	3.03	3.35	0.58	5.9
640	8	2.4	3.27	0.67	5.3
640	12	2.77	3.33	0.49	7.04
640	16	3.01	3.14	0.17	5.69

Table 5. Results of calculation of the slope for three shear levels and three different compaction forces.

A two-factor analysis of variance (ANOVA) was performed to evaluate the variation in the slope obtained throughout the tablet surface. Table 6 summarized ANOVA results that show significant differences of the mean slope of the tablets according to the level of compaction[29]. However, the evaluation showed that the spectral changes were not related to changes in slope.

Source of Variation	*SS*	*df*	*MS*	*F*	*P-value*	F_{crit}
Compaction	3.77×10^{-07}	2	1.89×10^{-07}	**22.03**	0.01	**6.94**
Shear	1.36×10^{-08}	2	6.8×10^{-09}	**0.79**	0.51	**6.94**
Error	3.43×10^{-08}	4	8.57×10^{-09}			
Total	4.25×10^{-07}	8				

Table 6. Results of ANOVA Two Factor analysis for three levels of Shear and three different compaction forces.

2.3.3. Angle-resolved elastic light scattering

Hemispherical measurements of scattered light were performed in order to gain knowledge about material morphology. Pharmaceutical tablets are strongly diffuse scatterers with particles of different size. For particles larger than the wavelength of incident light the analysis of scattering pattern is more complex since the phase and amplitude of the scattered light changes as a function of particle geometry and orientation. Nevertheless, the angular distribution of scattered light and its integral intensity are directly related to the size and distribution of particles in the sample. In terms of single scattering approach, the scattering signal can be mapped versus spatial frequency $f = sin\ \theta/\lambda$ of surface relief Fourier decomposition[35, 42]. Here, the surface relief is represented as a sum of diffraction gratings with different periods, amplitudes, phases and orientations. Therefore, statistical information about grain size and local morphology can be obtained from angle-resolved light scattering data. For pharmaceutical tablets, the scattering problem is complicated by multiple scattering processes inside the material, where the correlation between directions of final scattering act and incident light is partly lost.

Figure 14 shows log [BSDF (φ, θ)] scattering indicatrices for the tablets with different compaction force and shear treatment. Here the scattering intensity gradually decreases as shear or

compression is applied. In addition, these treatments noticeably increase the degree of scattering isotropy. Data in Figures 14, 15 indicate that the compaction modifies the sample morphology. The compaction reduces the average distance between particles and aligns each particle in respect to the others. Since the orientation of particles becomes to be strongly dependent on surrounding and on direction of compaction force, a fluctuation of material density decreases. As a result, scattering intensity also decreases due to lower sample heterogeneity. The most significant influence of the compaction force on scattering indicatrix can be observed for the samples without shear treatment. Thus, the cross-section of scattering indicatrix for 8 kN compaction shows nearly constant value of BSDF (θ) up to θ =75˚ as show in figure 15 (a). This fact indicates that the untreated tablet scatters light highly diffusively, almost as Lambertian source[36, 37, 42]. As compaction increases, the scattering signal diminishes with noticeable change at larger polar angles (θ>40˚) due to mutual ordering of smaller particles with spatial frequencies above $f \approx 1 \mu m^{-1}$. We note that for all types of samples (figure 15 (a)-(c)) the tilt of BSDF (θ) gradually increases with compaction force, indicating the suppression of diffuse component of scattering.

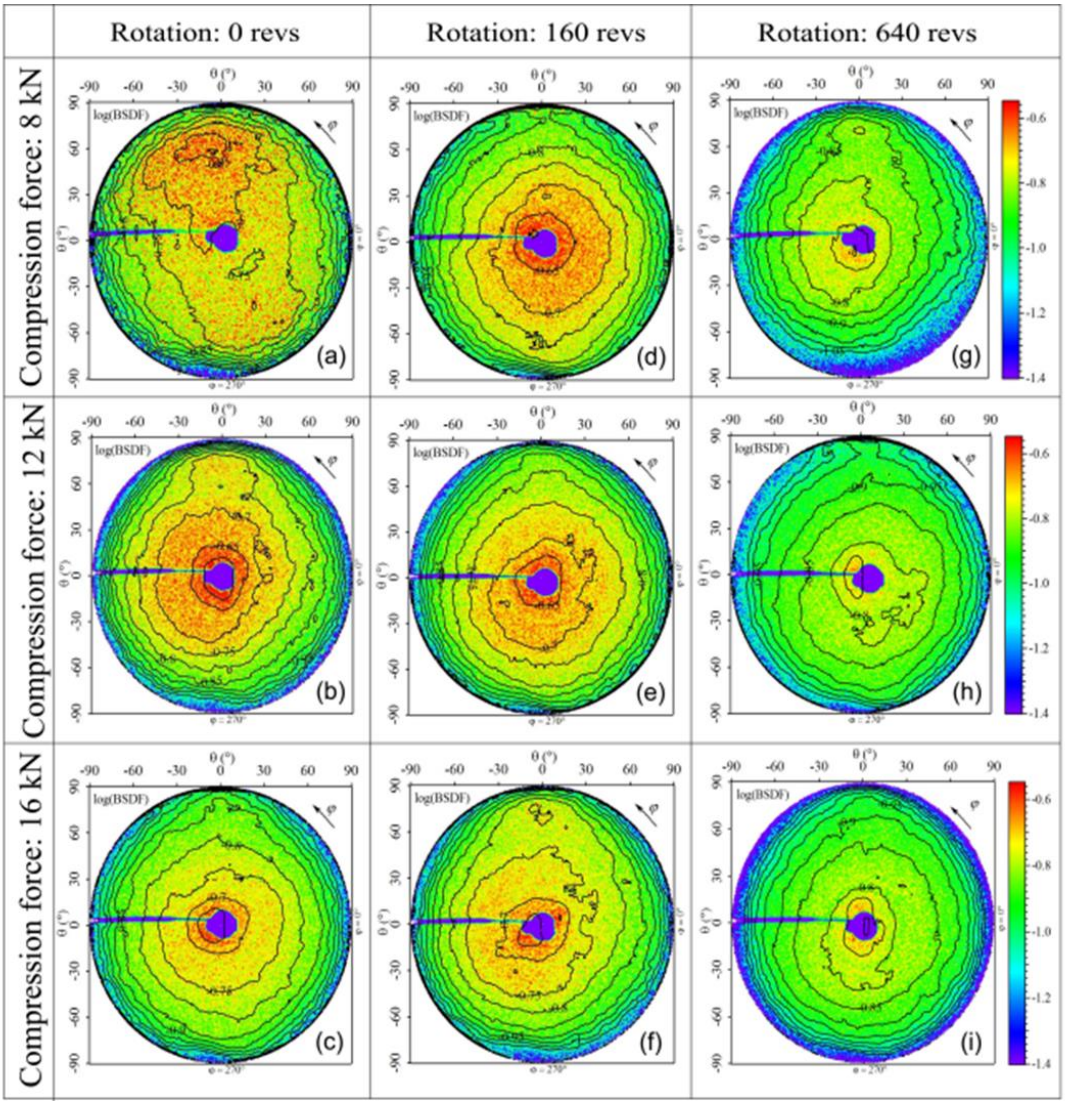

Figure 14. Scattering indicatrix as a function of polar and azimuthal angles for tablets at different compacting forces and revs.

The shear treatment de-agglomerates the constituent powder, reducing the average size of microparticles[38]. As a result, this treatment reduces the scattering intensity. Thus, 160 revolutions (figure 15 (b)) increase the tilt of BSDF (θ), and after 640 revolutions the BSDF (θ) drops to its minimal level (figures 14, 15 (c)). Moreover, the scattering angular isotropy increases with the number of revolutions (figure 14). This indicates that the shear treatment not only reduce the surface roughness but also provides better mixing of constituent powder. The posterior

compaction produces further ordering of the structure, resulting in gradual decrease of scattering intensity.

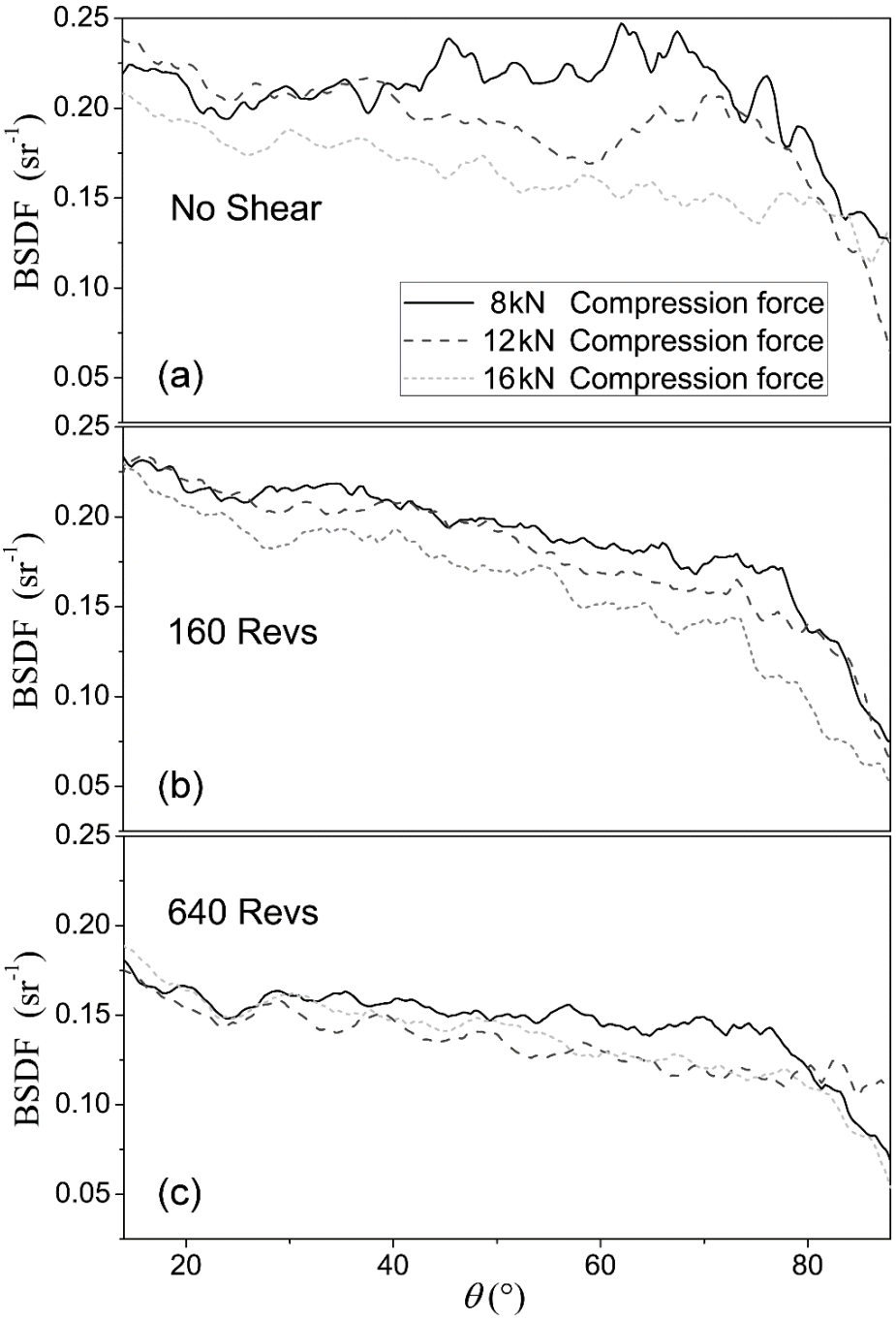

Figure 15. BSDF as a function of polar angle for (a) samples formed without shear and shear treatment (b) samples formed with shear and shear treatment at 160 revs, and (c) samples formed at 640 revs.

2.4. CONCLUSION OF CHAPTER 2

This study shows that shear stress applied on the powder mixtures affects the diffuse reflectance spectra and angle resolved light scattering of tablets. The spectral changes related to shear stress were not expected, unlike spectral changes related to compaction force, which have been observed by several researchers. The NIR diffuse reflectance spectra of blends (prior to compaction) do not show changes associated with shear. However, for tablets the reflectance spectra noticeably change when the shear stress is applied, while the transmission spectra remain the same. In the transmission spectra, the NIR radiation interacts with a greater fraction of the tablet. Therefore, the spectra are less affected by the tablet surface. Thus, the NIR diffuse reflectance spectra indicate differences in the tablet surface, which were then investigated by angle-resolved light scattering.

The angle-resolved light scattering measurements show significant changes in the material morphology after different levels of shear applied. The compaction realigns microparticles and reduces distance between them. As a result, scattering intensity decreases with noticeable change in the scattering indicatrix. The shear stress treatment reduces surface roughness and provides better mixing of constituent powder, which reduces scattering but increases its isotropy. Angle-resolved light scattering confirms the differences in tablet properties first observed by NIR spectroscopy.

CHAPTER 3

Prediction of Dissolution Profiles by Non-Destructive Near Infrared Spectroscopy in Tablets Subjected to Different Levels of Strain

Based on work Published in: *Journal of Pharmaceutical and Biomedical Analysis 117 (2016) 568–576.*

Eduardo Hernandez, Pallavi Pawar, Golshid Keyvan, Yifan Wang, Natasha Velez, Gerardo Callegari, Alberto Cuitino, Bozena Michniak-Kohn, Fernando J. Muzzio, Rodolfo J. Romanach.

3.1. LITERATURE REVIEW

Performance evaluations of a pharmaceutical product are essential and mandatory to assess and confirm the quality of a drug product that will ultimately be delivered to patients. In the pharmaceutical industry, dissolution testing is a key analytical tool in both drug development and quality control. The data obtained from dissolution tests can be used to detect physical changes in an active pharmaceutical ingredient (API) and formulated product, to establish *IVIVC* of drug products, and justify post-approval changes [43, 44]. Furthermore, it is useful in identifying critical manufacturing variables, such as mixing time, compaction speed and pressure, and coating parameters.

The standard-setting body, the USP outlines the use of four industries standard dissolution testing protocols that describe the USP Apparatus 1 (basket) the USP Apparatus 2 (paddle, the USP

Apparatus 3 (Reciprocating Cylinder) and the USP Apparatus 4 (Flow-Through Cell). The choice of the equipment to be used depends on the physico-chemical characteristics of the dosage form. Immediate-release, modified-release, and extended release tablets are usually tested in the USP Apparatus equipped with paddles. In contrast, floating capsules and tablets are generally tested using USP Apparatus 1 equipped with baskets[45].

Despite its simplicity of design and the ease of use the dissolution apparatus lacks reproducibility, and this has become a concern to the FDA as well as to the pharmaceutical industry. The variability observed in dissolution results often stems from uneven mixing within the dissolution vessels. Studies have shown that tablet position in the vessel, USP Apparatus, and operators have also contributed to variability in drug release profiles [1, 46]. Additionally, the most significant challenge has been lack of biorelevance as dissolution methods are often not correlated to *in vivo* performance [47]. Difficulties in having suitable USP calibration tablets, physical-chemical (temperature, particle size, solubility, and polymorphism) and mechanical (position of the aliquot, vibrations, paddle or vessel position) factors can contribute to dissolution variability [2]. Drug release concentration in the dissolution medium is determined with High Performance Liquid Chromatography (HPLC) or Ultraviolet/Visible Spectroscopy (UV/VIS) using solvents with high cost and leading to significant solvent wastes generated in the analysis. However, use of Quality by Design (QbD) has been introduced in the pharmaceutical industry, and efforts have been underway to control the variance observed in the USP Apparatus [10, 48].

Besides formulation parameters, dissolution rate is also affected by process parameters such as tablet press speed and compaction force. One such process parameter that is often neglected is the

total amount of strain that the powder experiences, before it goes into the tablet press. Pingali et al. found that the amount of powder strain becomes all the more important when the formulation contains hydrophobic, low melting lubricant such as magnesium stearate, which often is the case [22]. For batch mixing in a V-Blender, Murthy et al. confirmed that the amount of lubricant and shear experienced by the blend leads to a decrease in the rate of in- vitro dissolution on tablets [49]. Dissolution performance can be affected by the nature of the process stress within the manufacturing steps (batch or continuous). Studies have been carried out to predict the sources and nature of shear that are related to the process stress in such a continuous process. Vanarase et al. explained the effect of number of blade passes (which depend on the residence time and the blade (rpm) and the lubricant feeding point on powder properties for a continuous mixer [50]. Mendez et al. investigated the increase in hydrophobicity of tablets and hence dissolution time, owing to the shear exposure in feed frame of tablet press [51]. NIR can be used to investigate effects of such shear and thus help predict dissolution of oral solid dosage forms. Near Infrared Spectroscopy (NIRS) gives the opportunity to obtain information on the physical and chemical properties, obtaining a high signal to noise ratio spectrum in one minute and without destroying the unit dose.

Near Infrared Spectroscopy (NIRS) is widely used in the pharmaceutical industry as a fast and non-destructive technique for evaluation of quality attribute of solid oral dosage forms. Near infrared (NIR) spectroscopy provides information on the physical properties (compaction force, shear, etc.) and chemical composition (content uniformity, water content, etc.) of the sample [12]. This information can be filtered out or maintained, depending on the quality attribute of interest. This is achieved using multivariate data analysis. Multivariate data analysis provides several

analysis techniques such as principal component analysis (PCA) and partial least square (PLS), and principal component regression (PCR) for extracting this information.

Several researchers have worked with NIR and multivariate data analysis to evaluate the drug release from the final product. Zannikos et al. related the dissolution profiles of carbamazepine tablets exposed to different levels of humidity with NIR spectra [52]. Donoso et al. related the NIR diffuse reflectance spectra using linear regression, nonlinear regression and PLS models to predict drug release of theophylline tablets with different compaction forces at different time points of the dissolution. [53]. Freitas et al. correlated the dissolution profiles with NIR reflectance spectra using a PLS calibration model to predict drug release behavior at different time intervals and for media with different pH [54]. Blanco et al. used a single PLS-2 model to predict the dissolution profiles of tablets made at different compaction forces and consisting of different API concentration[55]. PLS-2 gives the opportunity to predict multiple variables in a single calibration model [56]. Otsuka et al. used transmission and diffuse reflectance spectra using multivariate regression models to predict dissolution properties in tablets containing indomethacin as active pharmaceutical ingredient (API) [28]. Tabasi et al. used PLS to predict dissolution profiles at different time points of tablets with different coating grades [57]. These researchers used several PLS calibration models for the selected time point in the dissolution profile. These methods were developed using multiple PLS calibration models at any given time point in the dissolution profile.

This study describes a non-destructive NIR method to predict dissolution profiles based on how shear affects the drug release of tablets with similar drug concentration and compaction force. The authors understand the importance of characterization of shear in continuous processes and this

paper explains a way to characterize such shear by non-destructive testing and ultimately predict tablet dissolution. The authors understand that this is the first study that takes into consideration the shear forces from continuous mixers to develop a non-destructive NIR method to predict dissolution profiles. The non-destructive method has an advantage over the current dissolution test, where it is impossible to evaluate the unit dose when the test fails. With the non-destructive NIR test, the root of cause of the failing unit may be investigated through multivariate data analysis and by other techniques such as Raman spectroscopy, NIR-Chemical Imaging, Ultrasound or Terahertz [29, 58, 59]. In addition, a dissolution profile that currently takes two hours could be obtained in only two minutes with this non-destructive test. Following the methodology of this study the authors establish an implementation strategy that can be recommended for continuous manufacturing processes in the pharmaceutical industry.

3.2. MATERIALS AND METHODS

3.2.1. Materials and sample preparation

The blend consisted of semi-fine acetaminophen (Mallinckrodt Inc. Raleigh, NC, lot 008111H411) as an active ingredient, lactose monohydrate NF (Foremost Farms, Rothschild, Wisconsin, lot 8513111410) as excipient material, magnesium stearate NF (Mallinckrodt, St. Louis, Missouri, lot: P09247) as lubricant. The individual materials were deagglomerated by passing through 18 mesh sieve for acetaminophen (resulting mean particle size of 45 µm), and 30 mesh sieve each for lactose (resulting particle size of 80µm) and magnesium stearate (8 µm). The particle size was measured post sieving using a LS 13 320 multi wavelength laser diffraction particle size analyzer (Beckman Coulter Inc., Miami, FL).

3.2.2. Blending and shearing process

The formulation consisted of 90% lactose, 9% acetaminophen and 1% magnesium stearate (w/w). One kg of the blend was made in a 1.87 L V-Blender (Patterson Kelley). Lactose monohydrate NF (900g) and semi-fine acetaminophen (90g) were layered in a top-bottom fashion and rotated at 15 rpm for 15 min. Magnesium stearate was added to this pre-blend and mixed further for 25 revolutions. The mixing time was kept short and the intensifier bar was not used to minimize the exposure of the blend to uncontrolled, non- uniform shear. To study the effect of shear, the blend was exposed to a uniform and controlled shear environment. This was achieved in a modified Couette cell which consists of two concentric cylinders that rotate relative to each other creating a shearing action [33]. The equidistant baffle is uniformly spaced and the entire setup creates a uniform shear environment on the powder. Three subsets of 300g each were obtained from the blending procedure and transferred to the annular region of the cylinder one at a time and subjected to different shear levels: no shear level, 160 revolutions (sheared for 2min), 640 revolutions (8 min) and 2560 rev (32 min) respectively. The shear rate was kept constant at 80 rpm for all these tests.

3.2.3. Tableting

A tablet press emulator (Presster [TM], Measurement Control Corporation, East Hanover, NJ), set to emulate Kikusui Libra2 tablet press, was used to compress the sheared powder samples into tablets. The speed was kept constant at 20 rpm. Flat-faced punches were used to obtain cylindrical tablets of 10 mm diameter. The dosing position was adjusted and fixed to give tablets of 350 mg

weight. The compaction gap between the punches was changed to compress tablets at an average targeted pressure of 305 MPa.

3.2.4. Near Infrared Spectroscopy

A Bruker Optics Multipurpose Analyzer (MPA) FT-NIR spectrometer (Billerica, Massachusetts) was used to obtain tablet diffuse reflectance spectra with a resolution of 32 cm^{-1}. The integrating sphere unit was used within the spectral range of 12500 to 3500 cm^{-1}. A total of 256 background and sample scans were averaged. Spectra were obtained from both sides of the tablet.

3.2.5. In-Vitro Dissolution Testing

The drug release studies were performed using the USP paddle method at a rotational speed of 50 rpm in a VK 7010 dissolution apparatus (Varian Inc., Santa Clara, CA). The dissolution medium was composed of 900 ml pH 5.8 phosphate buffer, and the temperature was maintained at 37.0±0.5^{o}C. Six tablets were each placed in chambers in the dissolution apparatus and ejected into the dissolution vessels simultaneously. Aliquots of the dissolution medium were pumped at 3-minute time intervals using a peristaltic pump VK 810 (Varian Inc., Santa Clara, CA). The medium was then filtered through 35 μm full flow filters prior to detection using a UV spectrophotometer. A wavelength of 243 nm was used to analyze the samples using a Cary 50 UV-Visible spectrophotometer (Varian Inc., Santa Clara, CA). Absorbance values for each tablet were converted to the percent of drug released at each analysis time and used for the calibration model[60].

3.2.6. Multivariate data analysis

Multivariate data analysis was performed using The Unscrambler X 10.2 (Camo, Oslo, Norway) for baseline correction of the spectra. Certain process parameters like compaction pressure affect the physical properties of tablets (example: tablet density). This in turn affects the scattering of radiation and thus affects the near infrared spectrum. Baseline correction was performed to maintain the scattering effects related to physical properties in the spectra obtained. This preprocessing step consisted in setting the first point of the spectra to zero. The Unscrambler X was only used for baseline correction.

After baseline correction, the spectra were exported to SIMCA 14 (Umetrics, Umeå, Sweden) to perform principal component analysis (PCA) and partial least square-2 (PLS-2). A total of 40 spectra obtained from the two sides of 20 tablets were used as calibration set. In the calibration set, the compaction pressure remained constant (305 MPa) but the shear applied varied (0, 160, 640, 2560 revolutions). PCA was used for exploratory data analysis to study the spectral differences rising from the differences in shear.

PLS-2 method was used to develop the calibration model for percent drug released in tablets with differences in shear applied. A PLS-2 model was created to predict percent drug released at 40 different time points from 3 to 120 minutes. A total of 40 variables (percent drug released at the specific time points) were used as dependent variable to create the PLS-2 model. Cross-validation (CV) was used for initial method evaluation and as a tool to help in method development. CV groups were established by shear condition to perform a leave-one class-out challenge to the

model. Table 7 summarizes CV groups. CV consists in leaving one group out that is then predicted with the other groups. The preliminary model developed with CV, was further challenged with a validation set consisting of 24 spectra from twelve tablets (Table 1) that were prepared separately from the calibration tablets. The validation set included tablets with the entire range in the shear applied (0, 160, 640, 2560 revolutions). NIR predictions of the validation set were compared with the dissolution profiles of the destructive method (obtained from USP Apparatus 2).

Set	Shear Level (Revolutions)	Number of Tablets	Number of Spectra	Cross Validation Group
Calibration	0	5	10	1
	160	5	10	2
	640	5	10	3
	2560	5	10	4
Validation	0	3	6	
	160	3	6	
	640	3	6	
	2560	3	6	

Table 7. Calibration and Validation set description for the model.

3.3. RESULTS AND DISCUSSION

3.3.1. In-Vitro Dissolution Testing and Effect of Shear

The dissolution test was performed for tablets of 305 MPa and four levels of shear applied. The dissolution profiles showed changes based on the shear applied to the blends used to prepare the tablets. Figure 16 shows the effect of shear on the dissolution profiles. The results show that as shear was increased, the amount and the rate of drug release decreased. This could be an example of overlubrication due to formation of a magnesium stearate hydrophobic film covering the active

ingredient in the formulation [22, 61]. Figure 16 shows that the blend shea affected the drug release, decreasing the dissolution of the tablets in the aqueous medium.

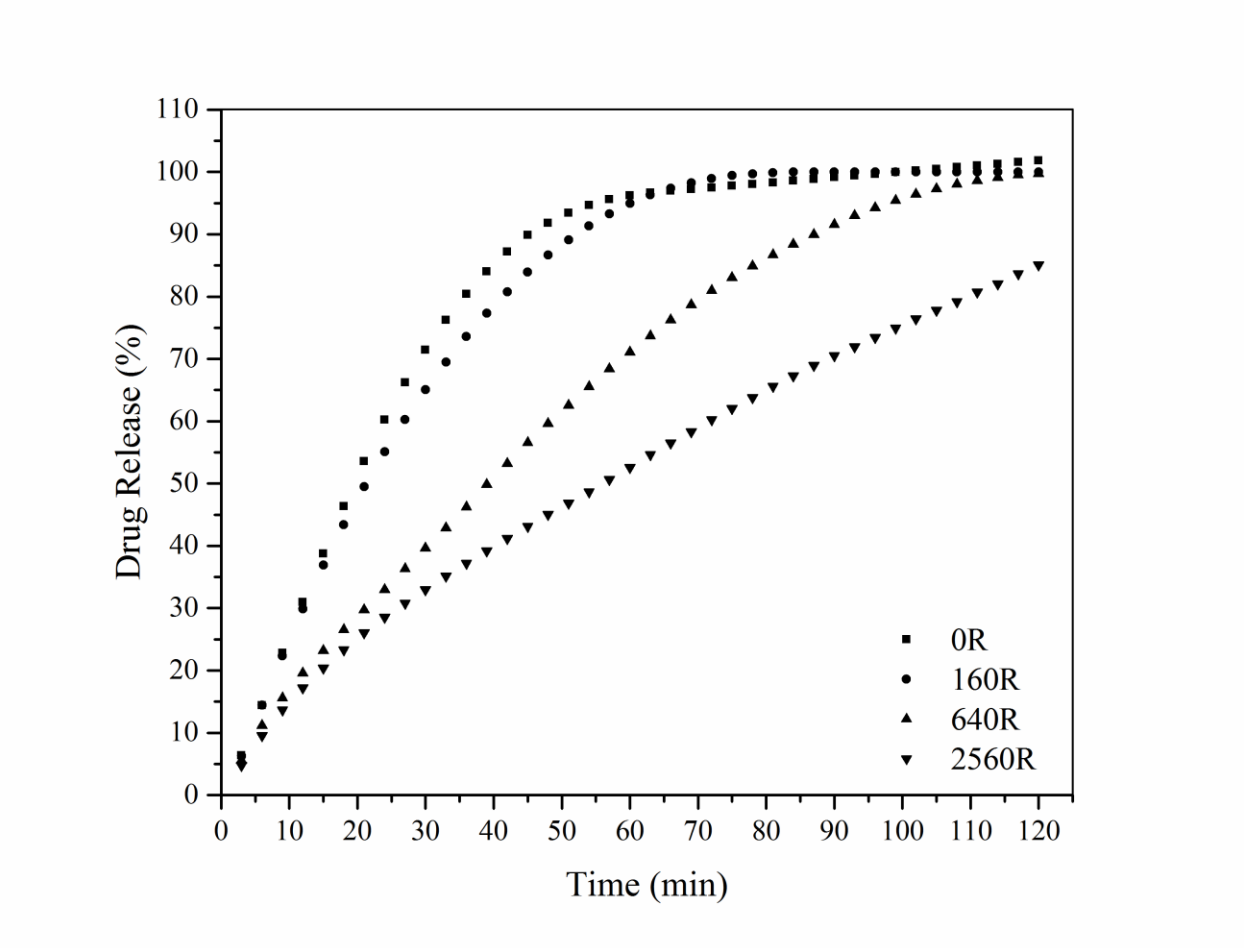

Figure 16. Dissolution profiles obtained from USP Apparatus 2.

3.3.2. Evaluation of NIR Spectra, relationship between spectra and dissolution

NIR diffuse reflectance spectra were acquired for tablets. Baseline correction was used to maintain all scattering effects associated with physical properties of tablets before performing any multivariate data analysis. This was done because physical properties of the tablet can affect the dissolution as demonstrated in previous studies where an increase in compaction force resulted in

increases in the intensity of NIR diffuse reflectance spectra and dissolution was a function of compaction force [28]. Several studies have shown that light scattering is a function of the physical properties of particles [7, 27, 29]. These differences in scattering result in the multiplicative and additive effects observed in the NIR spectra which are usually removed by normalization and derivatives[8]. But baseline correction does not remove multiplicative and additive effects in the spectra, and thus the scattering effects from differences in the physical properties of particles are included in the model. All spectra obtained in this study showed small but significant variations in the spectral slope from 7000 to 5500 cm^{-1}. Figure 17 shows that as shear increased, the spectral slope decreased separating the tablets spectra according to the shear applied. The differences observed in the tablets NIR spectra as the shear was varied indicated the feasibility of developing a calibration model to predict dissolution.

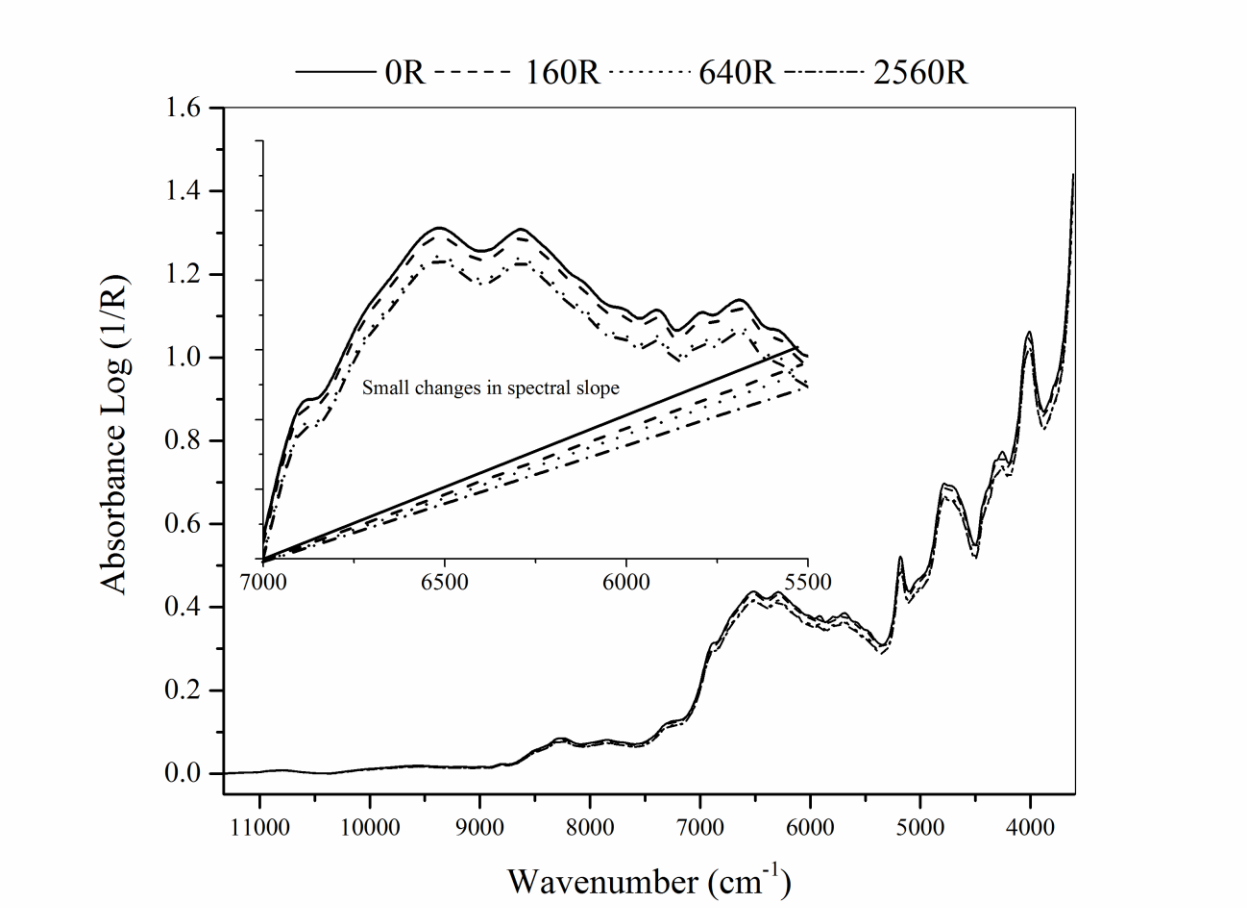

Figure 17. NIR spectra for tablets subjected to different levels of shear. Zoom of the spectral region of 7000-5500 cm^{-1} were slope changes that are observed.

PCA was used to investigate the spectral differences observed. The PCA method shows that the first source of variation associated with the samples was the shear applied since four different groups are observed in Figure 18. PC1 explains the principal source of variation observed in the spectra and this variation is associated with shear as shown in Figure 18. Four groups were separated along the PC1 with 98.7% of the variation explained. PC1 loading plot as displayed in Figure 19 shows that spectra varied through the entire spectral region. PCA computes latent variables that are a linear combination of the original manifest variables[62]. The loading plot describes how the principal component is related to the original variables [8].

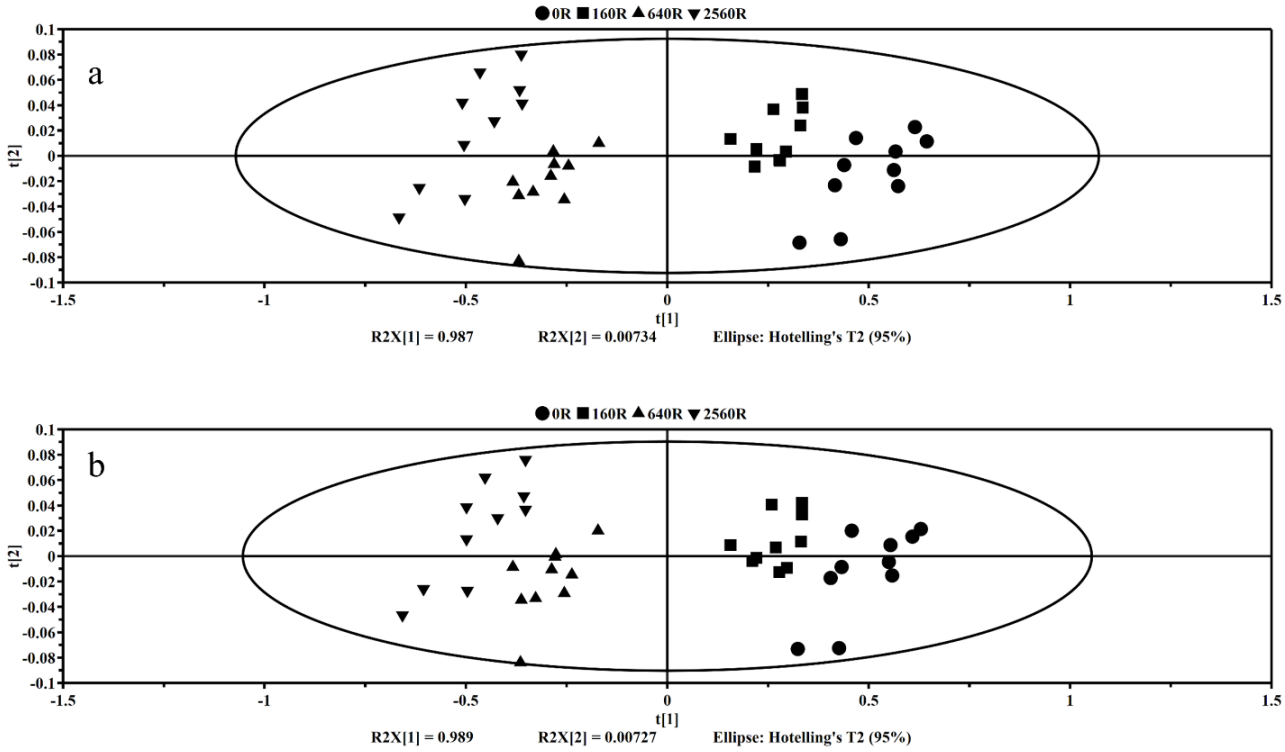

Figure 18. (a) PCA score plot of NIR spectra for the entire spectral region from tablets with different levels of shear. (b) PCA score plot of NIR spectra for the spectral region of 7000 to 5500 cm^{-1} from tablets with different levels of shear.

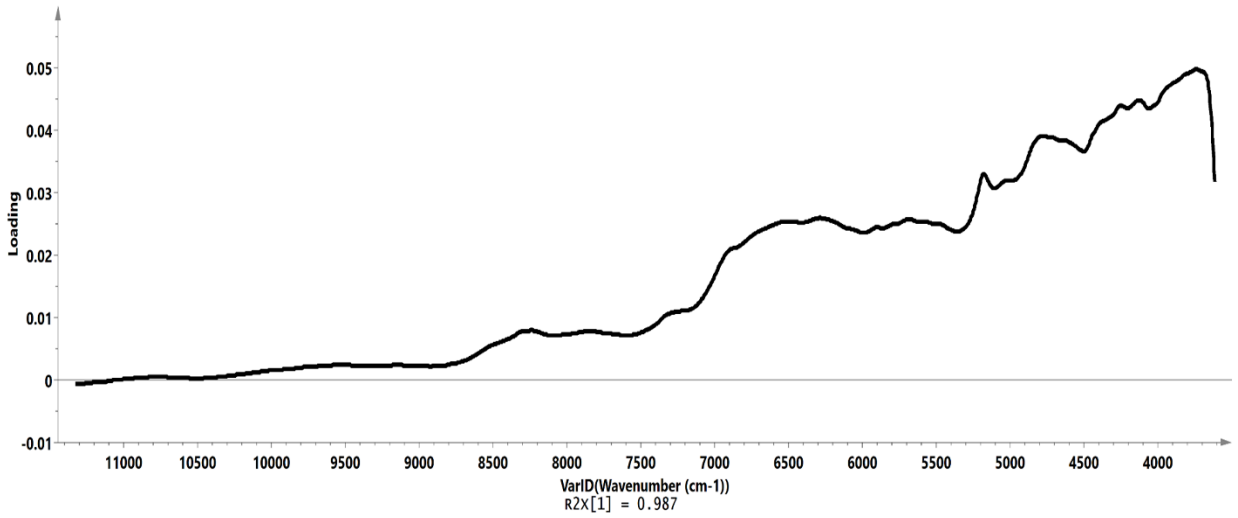

Figure 19. Loading plot of PC1.

3.3.3. PLS model method evaluation

A PLS-2 calibration model for predicting the drug release was developed relating the spectral differences to the percent drug release from the dissolution test. The spectra (independent variables) used for the calibration model consisted of tablets compressed at 305 MPa and four different shear levels and two spectral regions:11328 to 3614 cm^{-1} and 7000 to 5500 cm^{-1}, The dependent variables consisted of percent drug release values obtained with the dissolution test every three minutes for the complete 120-minute dissolution profile. All spectra were mean centered and baseline corrected. Table 8 summarizes the calibration model statistics for 1 to 4 PLS factors for both spectral ranges. The PLS calibration model was developed with two PLS factors. The bias for the leave one class out cross validation results was only 0.59 % for two PLS factors,

and only -0.53 % drug release for the validation set tablets in the entire spectral region. For 7000 to 5500 cm^{-1} the bias for leave one class out cross validation was -0.61% for two PLS factors and 0.70 for the validation s The bias is considered low and indicative of excellent accuracy since percent dissolution increases to almost 100%. The results were also evaluated through relative standard error of cross validation or prediction (RSE) as shown in equation 8:

$$RSE(\%) = 100\ x \sqrt{\frac{\sum_{i=1}^{n}(y_{pred}-y_{obs})^2}{\sum_{i=1}^{n}(y_{obs})^2}} \quad (8)$$

where y_{pred} is the value predicted and y_{obs} is the value for each analysis time in the dissolution profile. Relative Standard Error of cross validation (RSEcv = 8.3%) are based on a leave-one class-out cross validation and Relative Standard Error of Prediction (RSEP = 6.3%) are based on the validation set for the entire spectral range. Results of RSE (%) for 7000 to 5500 cm^{-1} shows an RSEcv of 8.5% for leave one class out cross validation and RSEP of 7.2% for external samples.

Spectral range	PLS Factor	RMSEE	RSEC (%)	BIAS cv	RMSEcv	RSEcv (%)
11328-3614 cm^{-1}	1	5.26	7.25	-0.568	6.14	8.78
	2	4.74	6.23	-0.592	5.97	8.31
	3	4.97	6.36	-0.455	6.26	8.66
	4	4.48	5.67	-0.491	6.25	8.62
7000-5500 cm^{-1}	1	5.34	7.48	-0.57	6.24	9.04
	2	4.82	6.42	-0.61	6.04	8.51
	3	4.61	6.02	-0.58	6.23	8.73
	4	4.49	5.74	-0.59	6.11	8.54

Table 8. Calibration model statistic summary for 1 to 4 PLS factors. (RMSEE = root mean square error of estimation, RSEC (%) = relative standard error of calibration, RMSEcv = root mean square error of cross validation, RSEcv (%) = relative standard error of cross validation.)

3.3.4. PLS model validation

The validation set included 24 spectra (12 Tablets) of 305 MPa compaction force with four levels of shear applied (Table 7). These are completely independent tablets, none of which was included in the calibration set. The PCA model was used to project validation set spectra (marked TS in figure 20) into the score plot space. Figure 20 (a) shows the multivariate 95% confidence interval as marked by the ellipse (Hotelling's T^2 test) and the results obtained for the full NIR region and figure 20 (b) for the spectral region of 7000 to 5500 cm^{-1}. All the spectra were within the 95% confidence interval, except for one spectrum from a tablet subjected to 640 revolutions.

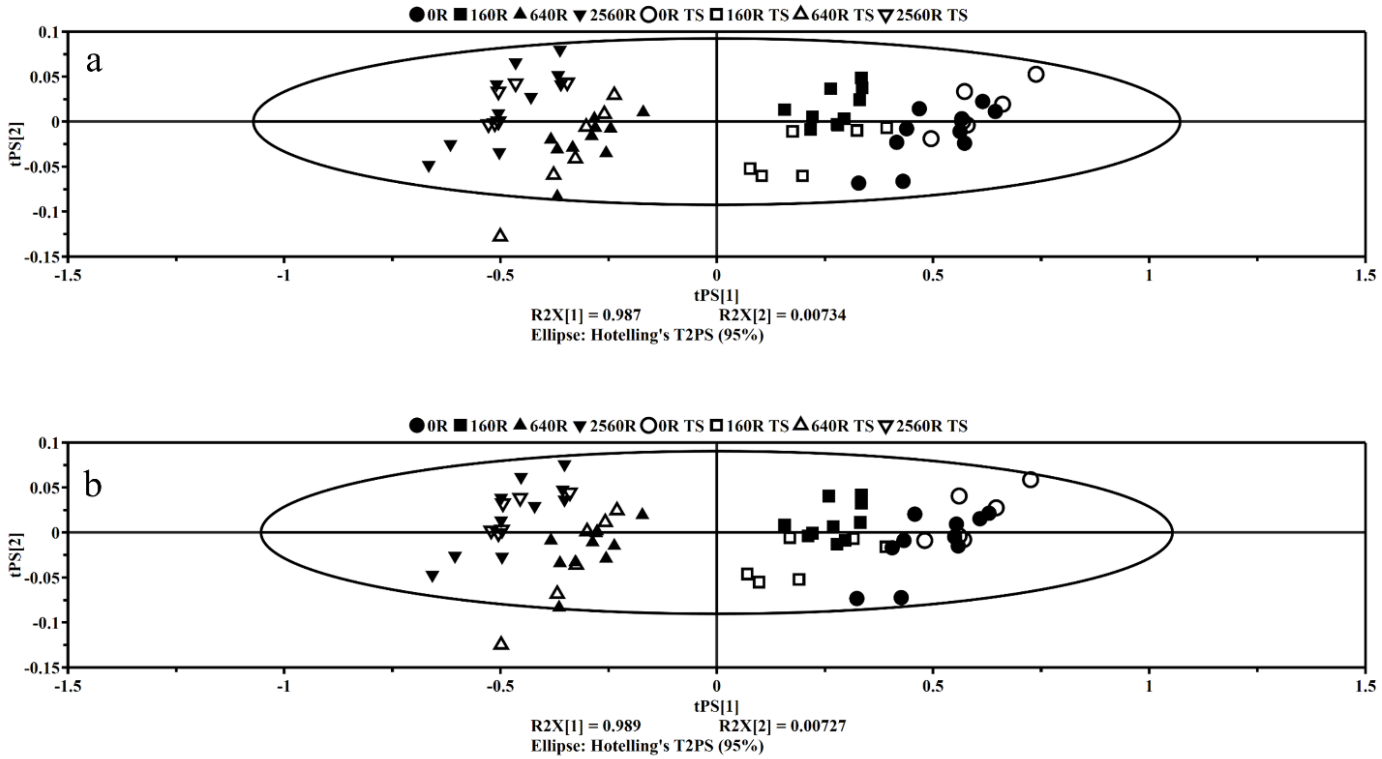

Figure 20. Projection of validation set on the PCA scores plot of NIR spectra. (a) Full NIR region, (b) spectral region of 7000 to 5500 cm^{-1}. Black symbols represent calibration set and white symbols represent validation set.

The PLS-2 calibration model predicted drug release for validation set tablets. Figure 21 and figure 22 presents the predictions correlation comparing both dissolution profiles and NIR predictions for the entire spectral range. Predicted dissolution profiles show a high correlation when compared with the reference method achieving a 0.9992 correlation coefficient for 0 and 160 revolutions, 0.9983 for 640 revolutions and 0.9977 for 2560 revolutions. Using the spectral range of 7000-5500 cm^{-1} a correlation coefficient of 0.9952 for 0 revolutions, 0.9989 for 160 revolutions 0.9997 for 640 revolutions and 0.9985 for 2560 revolutions was obtained. The accuracy of the prediction of dissolution was evaluated through the use of the RSEP. RSEP for 640 and 2560 revolution shows and increase as evaluated individually. However, 640 and 2560 revolutions are an extreme case not typical of a regular manufacturing process. RSEP for the validation set using the entire spectral region was 6.3% and 7.23% for 7000 to 5500 cm^{-1}. Table 9 summarized the validation set evaluation of the model for both spectral ranges. Minor changes in compaction force and concentration are likely contributing to the variation observed.

Spectral range (cm^{-1})	**PLS Factor**	**Shear Level (Revolutions)**	**BIAS TS**	**RMSEP**	**RSEP (%)**	**f_2**	**F**	**R^2**
11328-3614	2	0	-3.077	4.130	4.68	67	0.6222	0.9992
		160	1.532	4.339	5.06	93	0.0359	0.9992
		640	5.815	7.294	9.51	75	0.1484	0.9982
		2560	-2.148	3.525	6.06	69	0.3157	0.9977
		Global Results	0.531	4.822	6.33			
7000-5500	2	0	-2.936	4.039	4.60	65	0.5688	0.9952
		160	1.636	4.601	5.39	88	0.0389	0.9989
		640	5.964	7.344	9.66	79	0.1399	0.9997
		2560	-1.860	5.181	9.26	67	0.3219	0.9985
		Global Results	0.701	5.291	7.23			

Table 9. Validation set results for 2 PLS factors (shear level results and global results) (RMSEP = root mean square error of prediction, RSEP (%) = relative standard error of prediction, f_2 = similarity factor, R^2 = correlation coefficient).

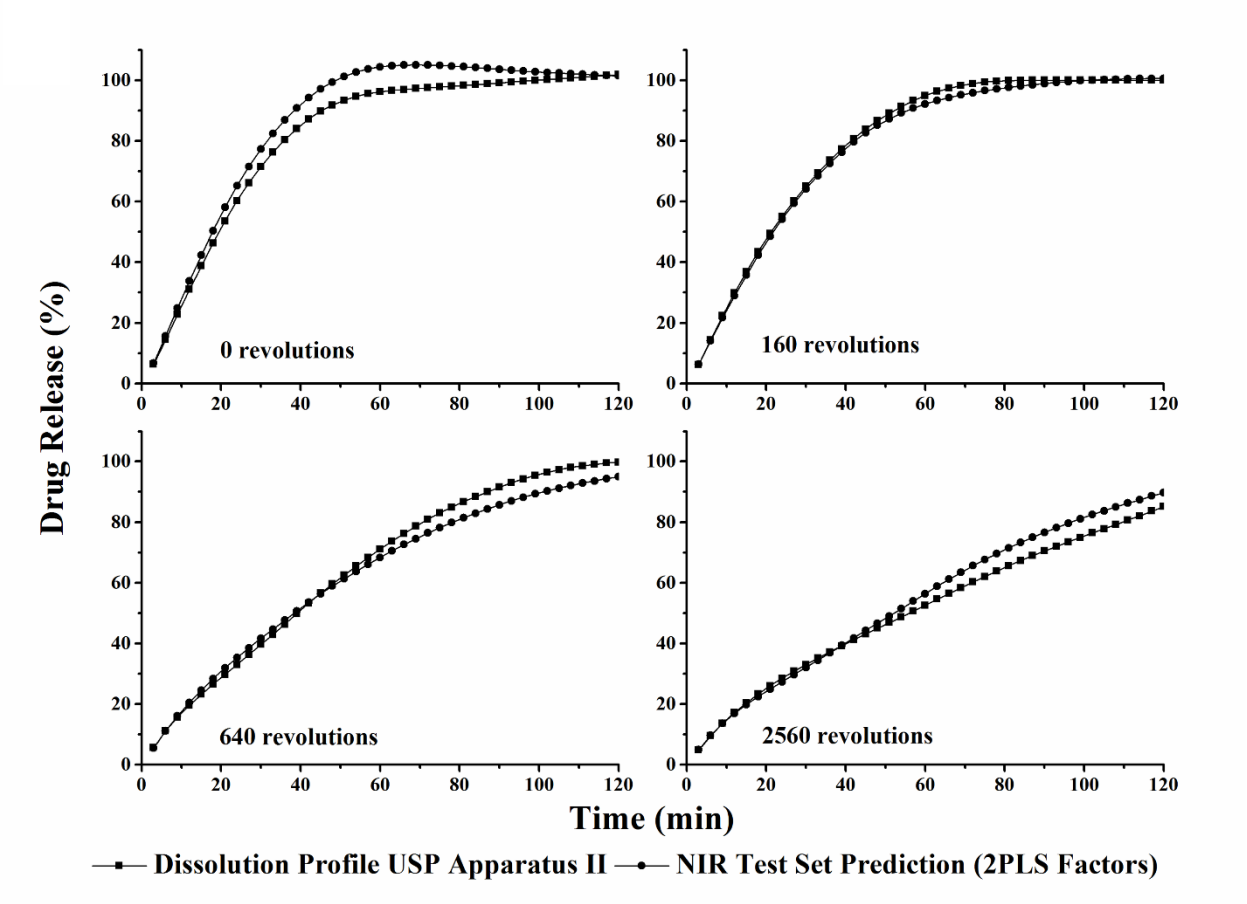

Figure 21. a) Full NIR region PLS prediction comparison of USP Apparatus 2 dissolution profile and NIR dissolution profiles predicted with 2 PLS factors

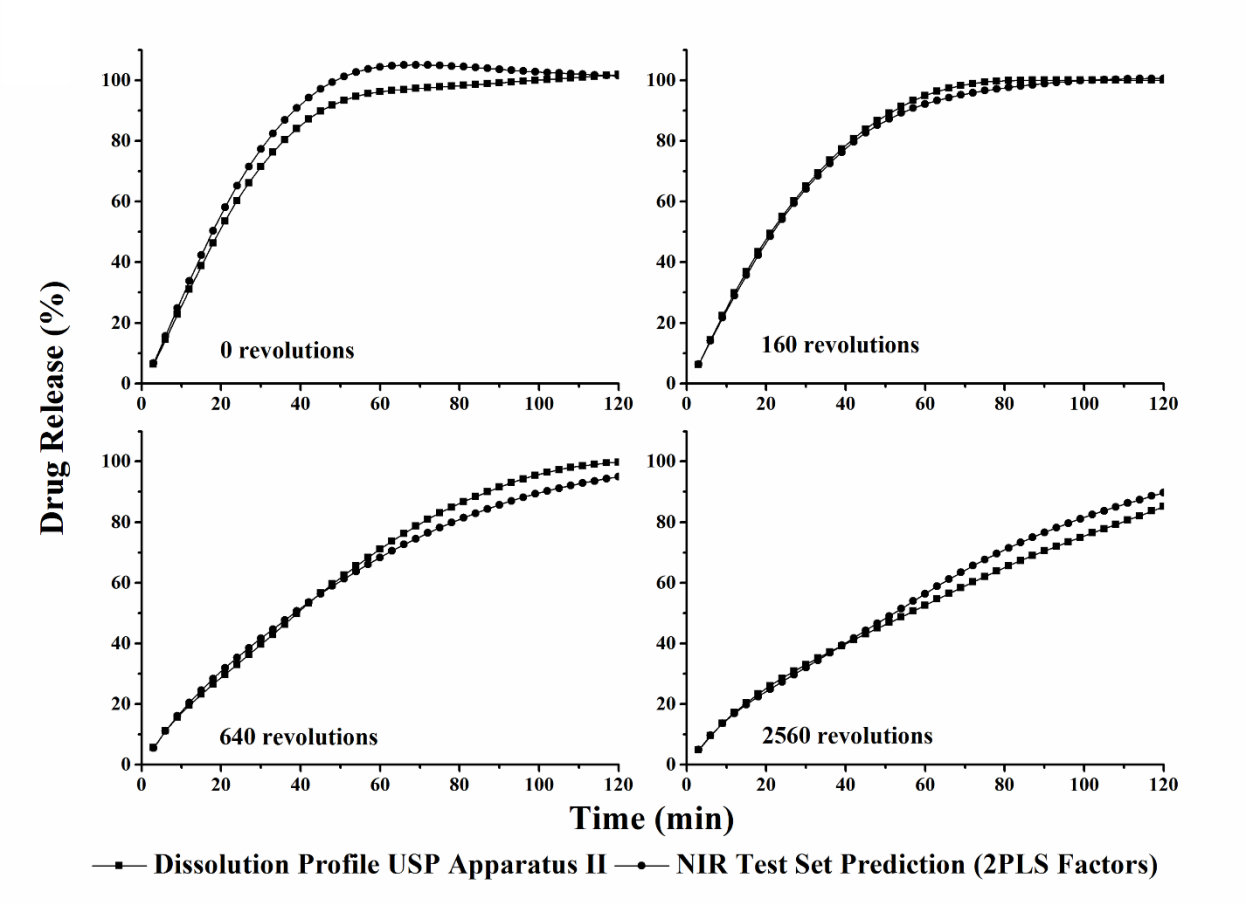

Figure 22 - Spectral region of 7000 to 5500 cm^{-1} PLS predictions comparison of USP Apparatus 2 dissolution profile and NIR dissolution profiles predicted with 2 PLS factors.

3.3.5. Evaluation of dissolution profiles

PCA was also used to compare the dissolution profiles predicted by the NIR method [63, 64]. The independent variables matrix consisted of dissolution values. The PCA scores plot shows four separate groups shown in Figure 23 related to shear level for USP Apparatus 2 values and NIR predictions are shown in Figure 23. PC1 explained 94.5% of the variation from the dissolution values for the entire spectral range model that corresponded to the variation in Shear level. For 7000 to 5500 cm^{-1} the variation explained by the model in the PC1 was 98.9%, and again four separate groups related to shear levels are observed. Samples with 0 revolutions and 160

revolutions are close together as expected due to the short time that the sample was exposed to the shear cell. The profiles predicted by NIR are also aligned with the corresponding shear level. Figure 23 shows PCA score plot and the projections of the validation set onto the model. The PCA evaluation shows that dissolution profiles predicted by NIR are similar to the dissolution values obtained with the USP Apparatus 2 within the 95% confidence interval.

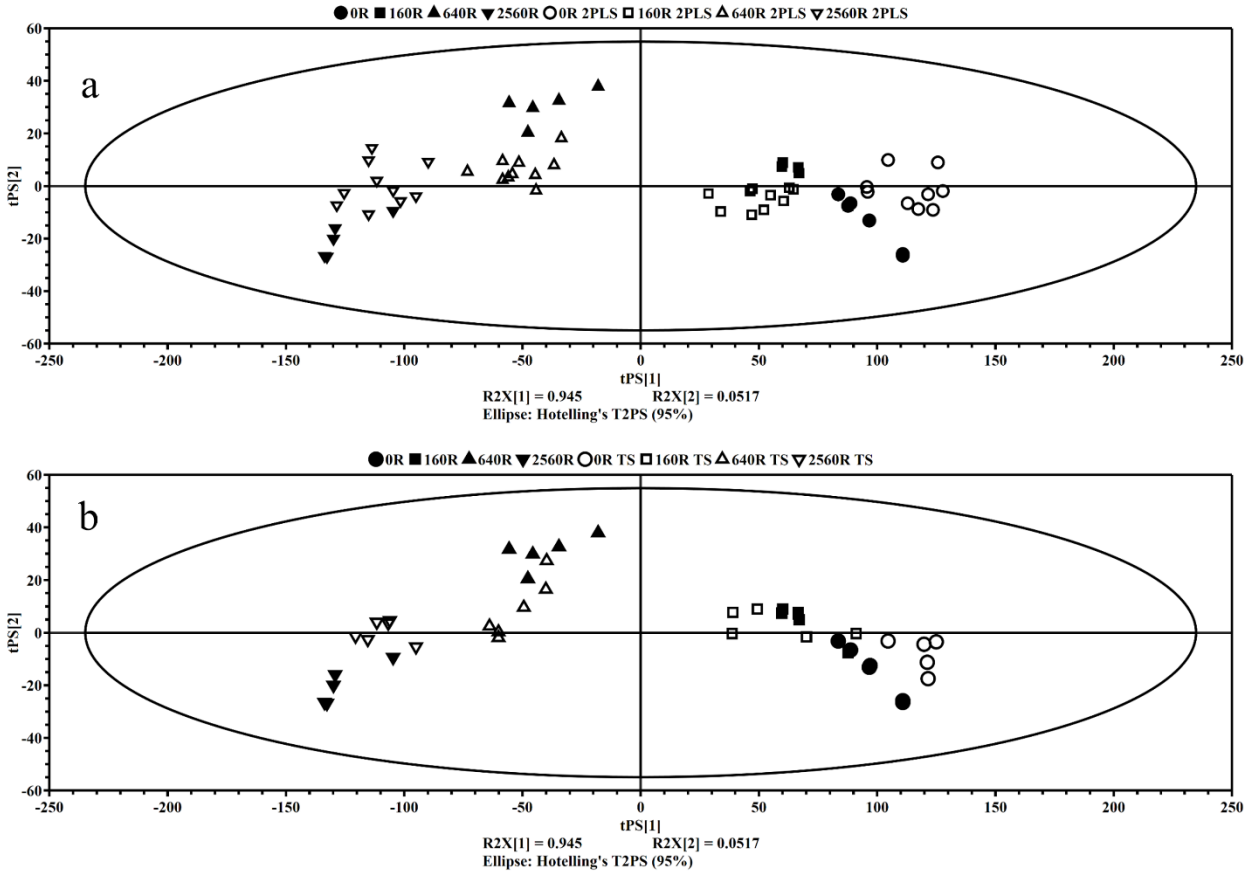

Figure 23. (a) Full NIR region comparison between USP Apparatus 2 dissolution profile and NIR dissolution profiles predicted with 2 PLS factors. (b) Spectral region of 7000 to 5500 cm^{-1} comparison between USP Apparatus 2 dissolution profile and NIR dissolution profiles predicted with 2 PLS factors. Black symbols USP Apparatus 2 dissolution profiles and white symbols represent NIR prediction with 2 PLS factors.

The similarity factor calculation (f_2) was used to evaluate the similarity between dissolution profiles obtained from the USP Apparatus 2 profiles and NIR prediction profiles. Equation 9 describes how the similarity factor was calculated.

$$f_2 = 50 \bullet \log \{[1 + (1/n) \sum_{t=1}^{n} (R_t - T_t)^2]^{-0.5} \bullet 100\} \quad (9)$$

when n is the number of points when both profiles are ≥ 85 % drug released, R_t is the dissolution value of the reference profile and T_t is the reference value of the test batch. Table 9 shows the results of f_2 using the averaged dissolution profiles of the destructive and nondestructive method. If the value of f_2 is greater than or equal to 50, the profiles are considered similar [3, 65]. Results showed that the dissolution profiles obtained from both methods could be considered similar. An analysis of variance (ANOVA) was performed to evaluate whether the two methods are statistically different [66]. The null hypothesis is that the two method are similar for both spectral ranges. Result shows that F calculated is less than the F_{crit} for all shear condition using the entire spectral range and the 7000 to 5500 cm^{-1} region (Table 3). Since the F calculated is less than F_{crit} the null hypothesis is retained. These results are indicative that both methods are statistically similar at 95% of confidence level.

3.3.6. Method implementation

The validation results demonstrated the feasibility of prediction of dissolution profiles based on NIR diffuse reflectance spectra. This method can be implemented in industry as outlined in Figure 24. The implementation strategy follows recent European Medicines Agency (EMA) guidelines that state: "The NIRS method should, as a pre-condition, be able to reject samples that are outside of its defined scope (e.g. out of range, compositionally incorrect)"[67]. The strategy was

implemented by first using PCA to determine whether the spectra were within the defined scope of the model. Thus, PCA was used to determine whether the NIR spectra were similar to those obtained from tablets compressed at 305 MPa. The second step was to determine whether tablets had the expected drug concentration, and PCA and PLS was used in this evaluation. The third step predicted the dissolution behavior using PLS NIR calibration model. The fourth step took onto consideration the similarity between the NIR predicted dissolution profiles with those obtained from the USP Apparatus 2 dissolution tests. If tablets meet these requirements, the batch can be released.

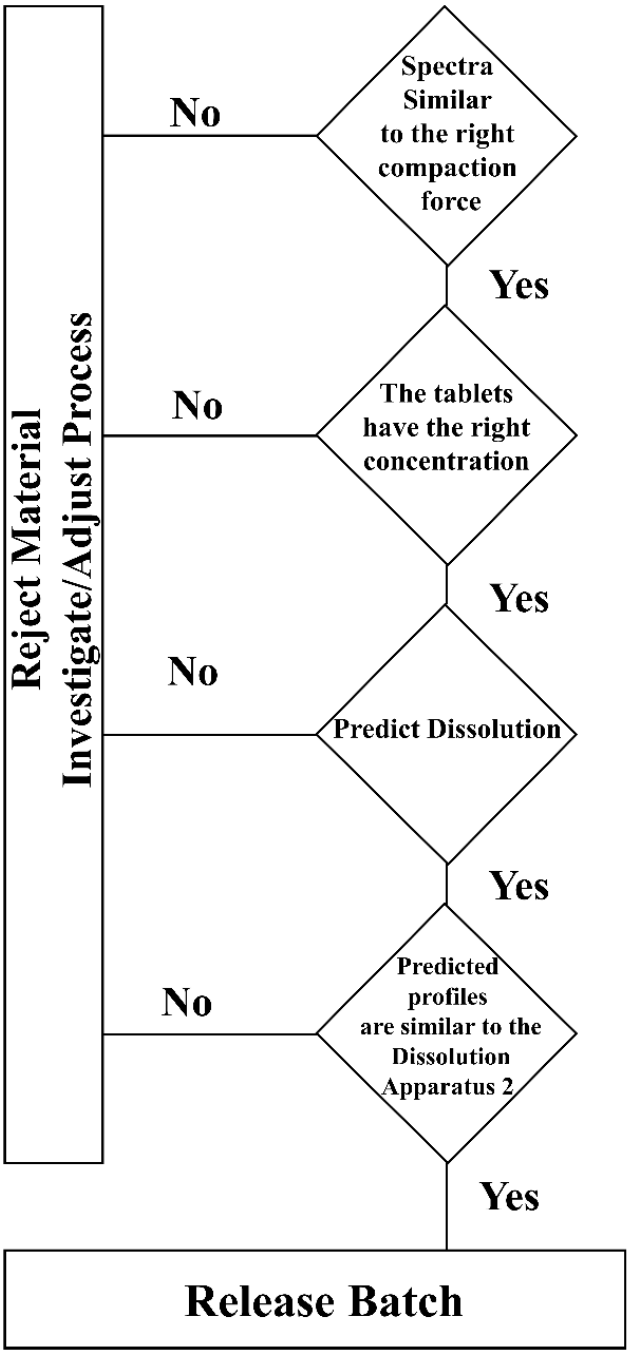

Figure 24. Proposed implementation strategy for continuous manufacturing processes.

3.4. CONCLUSION OF CHAPTER 3

This study shows that the applied shear affects the dissolution behavior of tablets with similar chemical composition and compaction force. Shear effects lead to changes in NIR diffuse reflectance spectra. Based on these results NIRS can be used in combination with multivariate data analysis to predict dissolution behavior with variation in process conditions. These results show a high correlation between the destructive test (USP Apparatus 2) and the nondestructive test (NIRS). NIR accurately predicts dissolution using a single PLS model instead of multiple PLS models at each time point. Validation of this methodology can be used for implementation in the quality by design strategy (QbD) and real time release testing (RTRT) in the pharmaceutical industry ensuring product quality.

CHAPTER 4

Characterization of resonant acoustic mixing using near-infrared chemical imaging

Based on work Published in: *Powder Technology 297 (2016) 349–356.*

4.1 LITERATURE REVIEW

Chemical imaging is the acquisition of images over a larger, usually contiguous, series of narrow spectral bands comparable to traditional spectroscopic techniques. This is the fundamental concept of chemical imaging – a rapid analytical method that simultaneously delivers spatial, analytical, spatial information. Chemical image data are visualized as a tridimensional hypercube, one wavelength and two spatial dimensions. Each spectra in the spatial map is represented as a pixel and contains all the spectral variability on the image plane[68]. Nondestructive destructive spectroscopic techniques do not provide the spatial information that can be key in resolving process issues based on process understanding. This need is addressed in part by NIRCI that offers spatially resolved chemical images of the sample. NIRCI can be used to determine content uniformity, particle sizes and distributions of all the sample components, polymorph distributions, moisture content and location, contaminations, coating and layer thickness, and a host of other structural details[69]. One factor influencing the physical attributes of solid dosage forms is compound distribution. For example, heterogeneous compound distribution can decrease the rate of tablet dissolution[70].

Several studies have shown that NIR-CI is suitable for determining the micro-mixing properties of pharmaceutical powders blends. NIRCI was used to study and compare the macro-mixing dynamics of pharmaceutical powder blending and the micro-mixing properties of final blends[20, 71-73]. Šaŝić et al. investigated the effects of processing on the micro-mixing properties of powder blends and tablets[71]. The effect of milling a powder mixture after bin blending on the micro-mixing performance (API agglomerate size) was investigated and results showed significant agglomeration in blends and tablets from the un-milled process. These previous studies demonstrated that in-line NIR-CI can be used to measure several micro-mixing properties during powder blending while distinguishing among three different cohesive APIs. In this study, powder blends from a new resonant acoustic mixer (RAM) are characterized using NIR-CI for the first time. NIR-CI was chosen for this study because many samples could be easily analyzed fast with higher spatial resolution. The RAM is a new type of mixer that works on the application of low frequency, high intensity acoustic field facilitating the movement of the loose powder mass to induce mixing. The acoustic mixing principle works on the creation of micro-mixing zones throughout the entire vessel while facilitating bulk movement of the materials. It was found that the RAM is capable of mixing cohesive APIs in as low as 30 s while the amount of energy input can be used to control the materials properties of lubricated blends as well as the properties of final product (i.e. tablets). However, API in low concentrations are typically highly potent and formulations must be developed without drug agglomerates, which could have a serious effect on patients. Therefore, the main objective of this study was to investigate the effects of process parameters, acceleration (mixing intensity) and blending time, on the agglomeration and dispersion of the API and lubricant in a common pharmaceutical powder blend produced in a laboratory resonant acoustic mixer (RAM). Qualitative NIR chemical imaging (i.e. chemical images) and

quantitative analyses (e.g. mean diameter of aggregates) were obtained. The information obtained through NIR chemical imaging strengthened the understanding of mixing mechanisms necessary to reduce aggregation of APIs in lubricated pharmaceutical powder blends and to develop safer formulations without drug aggregates that could affect patients.

4.2 MATERIAL AND METHODS

4.2.1 Near Infrared Chemical Imaging

Near Infrared Chemical Imaging (NIR-CI) was used to study the micro-mixing properties (spatial information) of the components in the powder blends obtained. A Spectral Dimension SyNIRgy chemical imaging spectrometer equipped with a Stirling cooled InGaAs focal plane array detector, a liquid crystal tunable filter, a microscope stage and computer-controlled illumination was used (Malvern Instruments, Worcestershire, UK). The chemical image data were collected in the diffuse reflectance mode and consisted of 320 × 256 pixels, with a spectral range of 1300 to 2300 nm (10-nm spectral spacing), forming the spectral hypercube. A 40-μm objective (field of view) measuring an area of 10 mm × 13 mm was used.

Chemical image pre-processing, pretreatment and analysis were performed with the "ISys 5.0" cross-platform chemical imaging analysis software (Malvern Instruments, Worcestershire, UK). The first step was to background-correct each chemical image. Dark and background references were obtained using identical settings as for the chemical images. The background correction converted the spectral data into absorbance units, normalizing the signal from the spectra obtained. The spectral data for each chemical image was then smoothed using a low pass triangle squared

spectral Fourier filter. Another step in the pre-processing was a “bad pixel” correction, which used the white reference to determine the few spatial and spectral pixels that were outliers (bad pixels) due to camera imperfections. These bad pixels were removed and replaced with the average pixel number of their non-outlier neighbors for each chemical image collected[74].

4.2.2 Chemical Image analysis

Near infrared (NIR) spectra of acetaminophen (APAP), magnesium stearate (MgSt) and silicified microcrystalline cellulose (Prosolv) were obtained to develop the method. The spectra were pre-treated using the standard normal variate (SNV) and a Savitzky–Golay second derivative with a filter length of 11 and filter order of 3. The second derivative spectra of the APAP, MgSt and a sample blend are shown in figure 25. The pre-treatments minimized the spectra differences obtained from physical differences, such as particle size and density, creating images that show the distribution of the components of interest. The wavelengths that showed the greatest differences in the spectra were observed at 1660 nm for APAP and 1730 nm for MgSt (figure 25), and these wavelengths were used to create the images for this study.

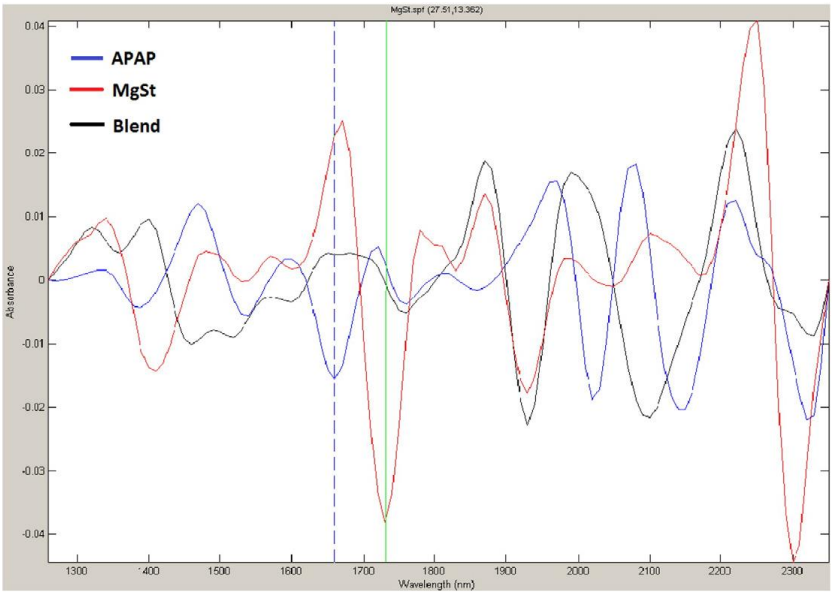

Figure 25. Second derivative spectra of API (APAP), lubricant (MgSt) and blend. The spectra here showed large differences at 1660 nm for APAP and 1730 for MgSt.

Measured intensity images were obtained for APAP at 1660 nm and MgSt at 1730 nm after pre-treatment. These images show the second derivative intensity (change in absorbance) of all the pixels used in analyzing each sample blend. This analysis is qualitative and is useful when large aggregates of the ingredient of interest are present. To obtain quantitative results for this type of experiments, binary images within a predefined threshold were analyzed. Binary images show the largest aggregates while the color (intensity) images show the dispersion of the API in the sample (blend).

Since the wavelengths that showed the most difference for APAP and MgSt had negative second derivative intensity values, the thresholds used to obtain the binary images and identify aggregates were chosen as follows: the minimum intensity value was used as lower threshold and the value of the [mean−2*Std Dev] as the upper threshold, as shown in figure 26. The mean and standard deviation (Std Dev) were the values obtained from the second derivative intensity pixel distribution

of the chemical image at each specified wavelength, depending on the ingredient under investigation. A binary image was created by assigning 1 to all pixels between the upper and lower thresholds and 0 to all other pixels. Once a binary image was obtained, it was treated with morphological filters to reduce threshold noise artifacts and artificial features. The morphological filters used were “clean” and “majority” as referred to in the chemical image analysis software. The clean filter removed isolated pixels in the binary image. The majority filter set a pixel to 1 in the binary image if a majority of pixels in its 3-by-3 neighborhood were 1′s. After the morphological filtering, the aggregate statistical analysis was performed. An aggregate was defined as a group of 9 (3-by-3) or more adjacent pixels, all within the predetermined intensity thresholds. Aggregate statistical analysis was performed on the binary images obtained. The metrics obtained from the binary image statistics shown in this article were the API mean aggregate area, the standard deviation of the aggregate area and the percentage of area covered in each binary image by the API aggregates.

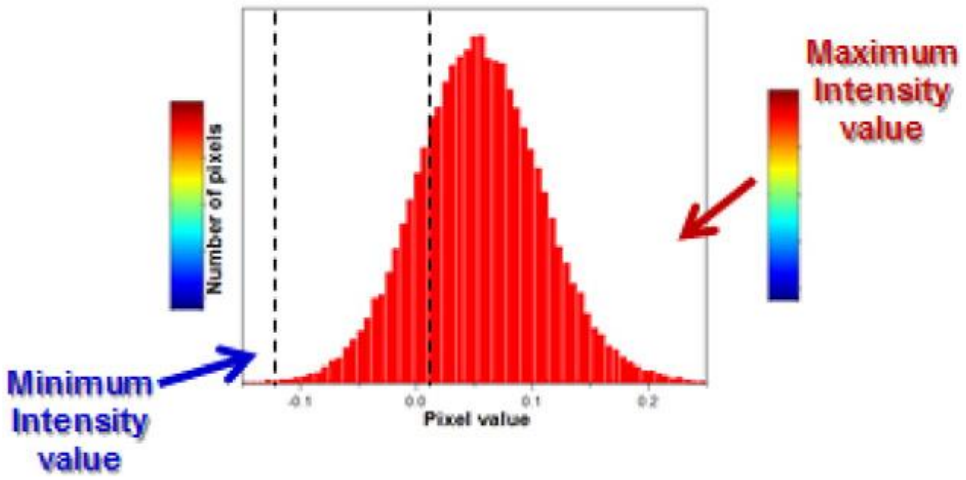

Figure 26. Minimum intensity value (lower threshold) and the [mean−2*Std Dev] (upper threshold) used to obtain binary images from the intensity images.

The API mean aggregate area and the standard deviation of the aggregate area were calculated by approximating the area of each aggregate as a circle and averaging the area of all aggregates in each binary image. The percentage of area covered is the portion of each whole binary image covered by API aggregates. The area of each binary image obtained was approximately 10 mm by 13 mm. For the second set of experiments, in which more than one sample per blend was measured and analyzed, the intensity images were concatenated. This was done so that the standard deviation is not relative to just one figure. If not concatenated, there will be the same number of particles outside the threshold always. The effect of mixing time and acceleration on each of the metrics described are summarized and explained in this article.

4.3 RESULTS AND DISCUSSION

4.3.1 Preliminary study

The intensity and binary images for APAP for the preliminary studies are shown in Fig. 27. Blends at lower acceleration (20g) and shorter mixing time (2 min) contained large aggregates of APAP indicating the API is poorly distributed throughout the blend (sample). The aggregates of APAP in the intensity images are composed of pixels with the lowest intensities (blue) and in the binary images are the pixels in black. These APAP aggregates are larger than those found in blends processed at higher acceleration (70g) and longer mixing time (4 min). Although, the final aggregate mean area for all four experiments is similar, the aggregate standard deviation of the area is larger for the blends mixed for only 2 min (Table 10). A higher standard deviation indicates that variability in aggregate area is larger and representative of poor mixing. These results were as

expected since a higher acceleration and longer mixing time provide higher energy input into the blend[75], decreasing the degree of aggregation of acetaminophen.

Blend	APAP	MgSt	Blending Parameter	"Mixing Extent"	Aggregate mean area (mm^2)	Aggregate Std Dev Area (mm^2)
1	10	0.75	20g-2 min	Poorly	0.279	0.536
2	10	0.00	20g-2 min	Poorly	0.219	0.688
3	10	0.75	70g-4 min	Well	0.211	0.299
4	10	0.00	70g-4 min	Well	0.199	0.267

Table 10. Preliminary study to determine the feasibility of the near-infrared chemical imaging analytical method. A higher concentration of acetaminophen (10% w/w) was used.

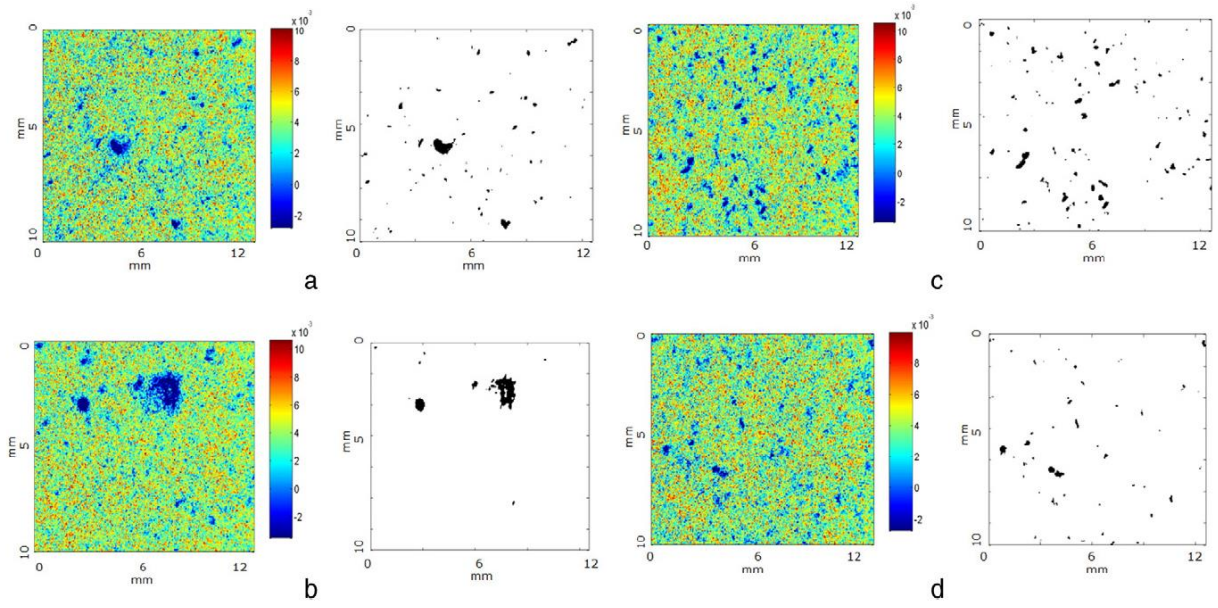

Figure 27. Intensity images at 1660 nm (left) and binary images (right) of APAP for (a) blend 1 (b) blend 2 (c) blend 3 and (d) blend 4. Blends are described in Table 10.

This preliminary study was also performed to determine whether the NIR-CI technique detected MgSt at the wavelength specified (1730 nm) and whether MgSt agglomerates and/or dispersion

could be detected using the described threshold. Intensity and binary images for MgSt are shown in Fig. 28. There was no noticeable difference in the results obtained for MgSt for the different mixing parameters. No large aggregates were detected using the lower and upper thresholds described. This means that the MgSt was well dispersed throughout the blend, confirming previous studies where MgSt mixed rapidly[75]. In all experiments here, a 40-μm objective (field of view) measuring an area of 10mm× 13mm was used.

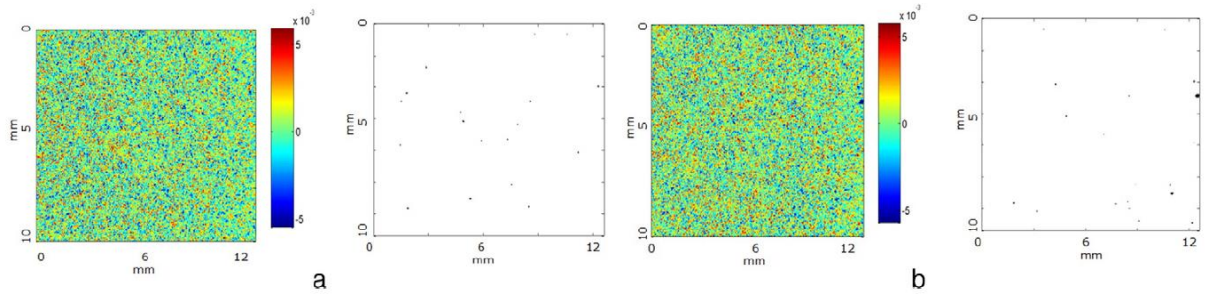

Figure 28. Intensity images at 1730 nm (left) and binary images (right) of MgSt for (a) blend 1 and (b) blend 3. Blends are described in Table 10.

Although MgSt is considered a cohesive material, it is known to coat other particles within a blend and its final particle size after blending is well below 40 μm[76]. To detect MgSt using this technique, either the field of view or the threshold would have to be changed. However, even if the radiation is collected from a very small field of view, the radiation collected scatters and the spectra will not be from a few magnesium stearate particles but also from neighboring particles[77]. These initial results indicate that the NIR-CI is not a good technique to identify single or a few particles of MgSt.

4.3.2 Micro-mixing performance

A second set of conditions with a common blend was examined to describe the effect of the process parameters on the micro-mixing performance in the RAM. The aggregation and dispersion of APAP (3% w/w) and MgSt (1% w/w) in a common excipient (Prosolv) was studied. The acceleration and total blending time were varied. Sample intensity and binary images of the API for this second set of experiments are shown in Figures 29 and 30. Blends mixed for 0.5 min at 20g (Figure 29) and 40g (Figure 30) are shown to describe the evident effect of acceleration on aggregation of the API used. In this case, five images areas of 10 mm × 13 mm were concatenated to compare several samples side-by-side. Large APAP aggregates were detected using this technique at lower acceleration (20g — Figure 29) when compared to blends at higher acceleration (40g — Figure 30) for the same amount of mixing time. These results show that APAP is better mixed, showing less aggregation and better dispersion, at 40g than at 20g. These results are in accordance with the results presented in the previous subsection. Similar qualitative results to the 40g blended for 0.5 min were obtained for all other intensities as well as binary images for the rest of the conditions studied. The chemical images in Figure 29 show that at higher energy inputs the agglomeration of the API is reduced. Such results cannot be objectively interpreted just by visual examination; thus, aggregate statistical analysis was performed on the binary images.

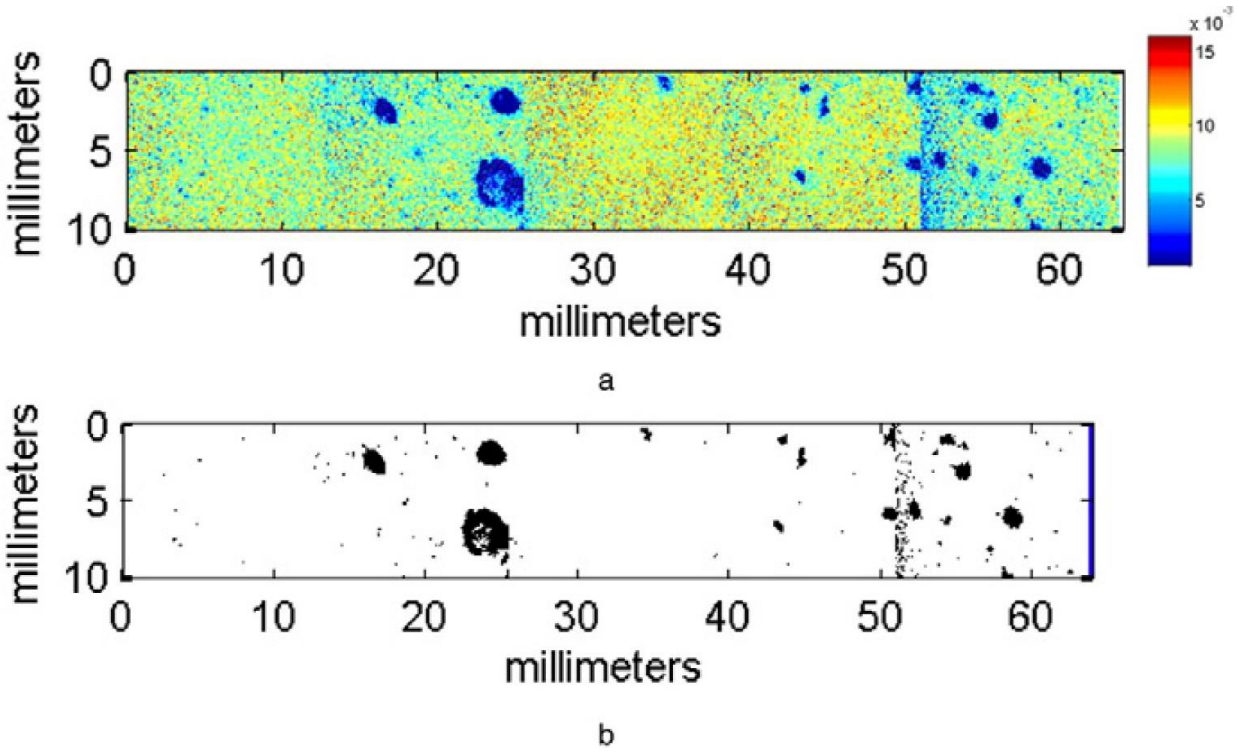

Figure 29. (a) Intensity and (b) binary images for APAP blended at 20g for 0.5 min.

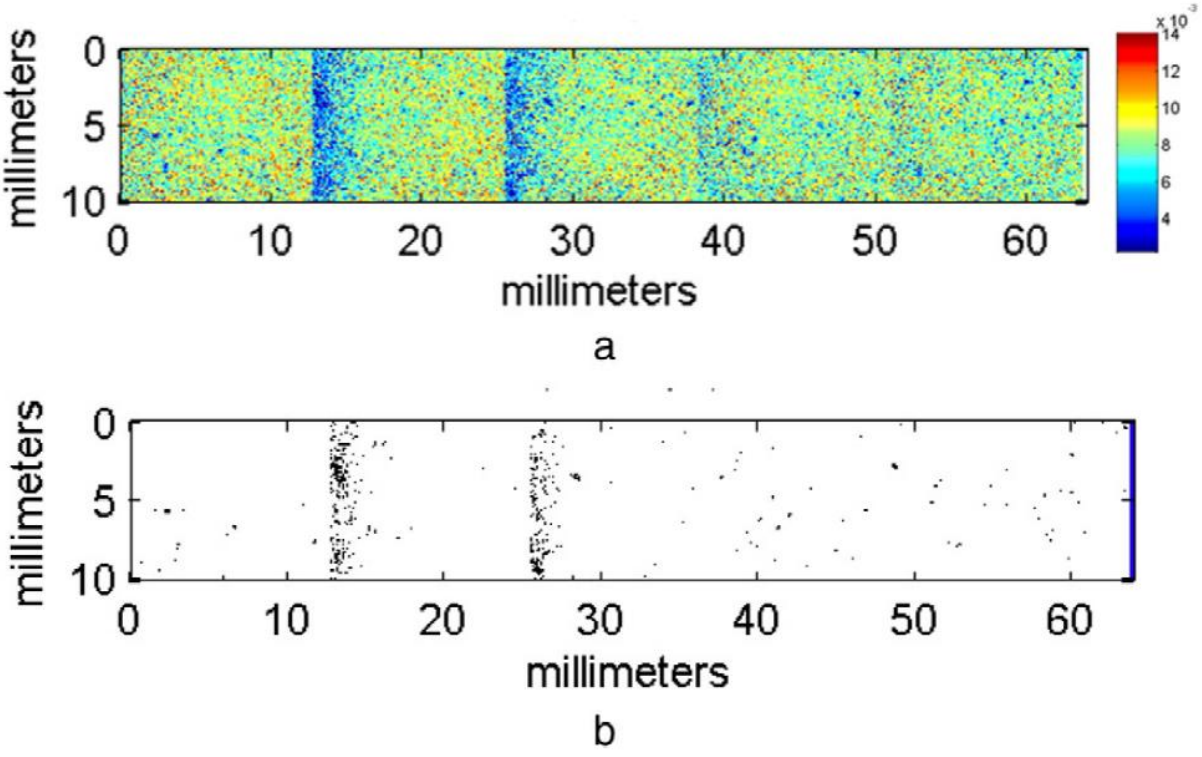

Figure 30. (a) Intensity image and (b) binary image for APAP at 40g for 0.5 min.

4.3.3 Statistical analysis of chemical images.

The main effects of the acceleration and total blending time on the API mean aggregate area, the standard deviation of the API aggregate area, and the percentage of area covered by API aggregates were considered as part of the study. The analysis examined the dependence of the global mean of each metric on acceleration and blending time. The API mean aggregate area decreased with increasing acceleration and blending time. The overall API mean aggregate area was much larger for blends after 0.5 min of blending when compared to those mixed after 1 and 4min. This indicates that most of the reduction in aggregate size occurs after 0.5min of mixing in the RAM. A similar trend is seen when the effect of acceleration on the mean aggregate size is considered. The API mean aggregate area is much larger at 20g when compared to those blends mixed at 40 and 70g. These phenomena can be explained by the large amount of energy input that goes into the blend at 40 and 70g when compared to the amount of energy at 20g[75]. The standard deviation of the API aggregate area decreased with increasing acceleration and total blending time. This shows that the variability in the aggregate area is reduced with an increase in the acceleration and total blending time. This means that the API aggregates found at higher accelerations and longer mixing times are more similar in size to one another than those aggregates obtained at lower accelerations and shorter mixing times. The standard deviation of the API aggregate area seems to decrease beyond the accelerations and blending times considered. This is an indication that the variability in the size of the API aggregates can be further reduced by blending for longer and/ or increasing the acceleration. The percentage of area covered by the API aggregates decreased with increasing acceleration and blending time. This means that there is a reduction in the mass fraction and size of the API aggregates with increasing acceleration and blending time. This indirectly confirms the

results obtained those obtained for the blending times used. With this illustration, we are able to conclude that the number of API particles in the aggregates was reduced with increasing blending time and acceleration.

4.4 CONCLUSION CHAPTER 4

The micro-mixing state of powder blends produced in a resonant acoustic mixer (RAM) was studied using near-infrared chemical imaging (NIR-CI). Both qualitatively (chemical images) and quantitative analysis (e.g. mean API aggregate area) were considered. It was found that APAP showed less aggregation (higher dispersion) at higher accelerations and longer blending times. These results were in accordance with the previous characterization of the RAM mixing performance. The RAM was shown to efficiently reduced API agglomeration without the need of any mechanical shearing. Such results are commonly obtained by using intensifier bars in mixers or by milling the blend after blending.. It was concluded that due to the smearing and coating nature of MgSt (soft material) and its nominal particle size, NIR-CI is not suitable to measure and quantify its dispersion in pharmaceutical blends produced in the RAM. This study proved that the resonant acoustic mixer is a good candidate for a variety of applications in which cohesive APIs, or powders in general, must be homogenized. The RAM could potentially be used in the early stages of formulation development where the API quantity is limited.

CHAPTER 5

Near-infrared chemical imaging and its correlation with the mechanical properties of chitosan–gelatin edible films

Published in: *Carbohydrate Polymers 136 (2016) 409-417*

5.1 LITERATURE REVIEW

Edible films are thin layers of a polymer material that control the solute exchange between the matrix and the environment, thus extending the shelf life of a food[78]. To achieve this, the films' polymer matrix should have the necessary physical-chemical properties for the specific food with which it will be used. Edible films can be created to have the necessary mechanical and structural properties with the use of hydrocolloid molecules, which are hydrophobic biopolymers with high molecular weight and long polymeric chains[79]. The most used compound for the manufacturing of edible films is gelatin, mainly due to its ability to form films at low temperatures[80] and chitosan, for being antibacterial, biodegradable, biocompatible, non-toxic and renewable[81].

With the NIR-CI, together with the use of chemometric tools, a characterization can be created with the distribution of the samples' compound of interest[82], obtaining the histogram parameters of the compounds' intensities: mean, standard deviation, kurtosis and skew. The mean of the distribution values corresponds to the abundance of the compounds on the surface of the sample[83]. The standard deviation of the distribution is defined as the variability of the abundance of the

samples' compounds[84]. Kurtosis measures the symmetrical tailing or 'peakedness' of the distribution, where zero indicates a normal distribution. Finally, skew is the measurement of the asymmetry of the distribution, with zero corresponding to a symmetric distribution[69, 85]. Viewed together, the variability of abundance, the degree of unimodal distribution and the asymmetry of the distribution are descriptors of the homogeneity of the sample. Moreover, these parameters depend on the spectral information of the sample, which changes in response to the interaction between the components[86]. NIR-CI was used to characterize the spatial distribution and abundance of the film-forming polymer and the drug contained in the film used in a pharmaceutical application. Both parameters were correlated with the size of the particle and the agglomeration of the drug, allowing them to determine the dissolution speed and drug uniformity obtained with the film[87]. This suggests that the abundance and distribution of the polymeric film compounds obtained by NIR-CI may be related to the films' physico-chemical properties. Since the mechanical properties of edible films are determined by the interaction between the plasticizers and the film-forming polymers[88], these properties could be analyzed with NIR-CI. This second study investigates the relationship between the abundance of the compounds and their variability, as obtained with NIR-CI, and the mechanical properties of the gelatin and chitosan edible films.

5.2 MATERIAL AND METHODS

5.2.1 Materials

The film forming solutions were fabricated using gelatin from cold water fish skin (Sigma-Aldrich Lot# SLBG7701V, average molecular mass 60 kDa; bloom number: 225–325; viscosity at 24°C, 31,500 cps), and chitosan from Pandalus borealis (Sigma-Aldrich Lot# MKBD4275V;

medium molecular weight;77% deacetylation, viscosity 450 mPa s at 1% concentration in 1% acetic acid). The plasticizers used were glycerol (≥99%, Sigma-Aldrich), sorbitol (≥99.5%, Sigma-Aldrich), polyethylene glycol-400 (PEG400) (EMD Millipore), and triacetin (99%, Acros Organics).

5.2.2 Near Infrared chemical images (NIRCI)

A Malvern Instrument Spectral Dimension SyNIRgi spectrometer chemical imaging system (Malvern, UK) was used. The Malvern system includes a focal plan array (FPA) mode with a tunable liquid-crystal filter that allowed full field analysis. The edible films were placed over a white ceramic disk with a 28 mm diameter, which was used as a reference for the acquisition system. Spectra and images were obtained in transflectance mode. In this mode, the radiation passes through the bulk of the film, bounces back in the highly reflective ceramic, passes through the bulk of the film again and then to the detector[89]. Therefore, the transflectance mode evaluates not only the surface but also part of the bulk of the film. The images were analyzed with a 40X objective and composed of 320 × 256 continuous pixels with a spectral range from 1200 to 2400 nm (81,920 pixels in a spectral area). The image analysis was performed using the Malvern ISys 5.0 software for cross-platform chemical imaging analysis[90]. The data obtained was arranged in a hyperspectral three-dimensional cube: X and Y with spatial information and Z with spectral information. For this analysis, the information contained in the hypercube was subjected to a baseline correction and a normalization to correct the scattering effects[82]. The pre-treatments used to normalize all of the spectral pixels included a standard normal variable (SNV) and second derivative Savitzky–Golay with a length of 11 and third order. The spectral quantitative treatments

that allowed the prediction of the compounds' abundances were obtained by Malvern ISys5.0 software with cross-platform chemical imaging analysis, using Matlab code routines. The software allows the construction of algorithms to determine the distribution of the film compounds and their abundance through partial least square discriminant analysis (PLS-DA). The term abundance is used to indicate that the signal related to an individual compound is analyzed at a specific sampling area on the surface of the film[83]. The abundance refers to the presence of a compound in a certain area, and differs from the term concentration that is based on volume instead of area. Pure compound spectra were used to create a library so as to quantify the abundance of each of the edible film's compounds[83]. The spectrum of pure chitosan was acquired from a film made with chitosan dissolved in acetic acid, the spectrum of pure gelatin from a film made with gelatin in solution, and the spectrum of pure plasticizers from the plasticizers in liquid state. In these models, each new factor or latent variable added to the model (variables that are not correlated with each other) indicates a lower systematic variation of the spectra but higher random variation. Each library was composed of the same number of elements that are in the film being analyzed, which allowed setting the optimal number of factors used in the calibration of the models.

The threshold for adjusting the limits to distinguish between the different compounds of the film is based on the similarity between the spectra of the pure compounds and the spectra of the film, along with the number of factors previously selected[91]. The application of the resulting model normalizes the spectral data with an image based on a scale from 0 to 1. This scale represents abundance from 0 to 100% for each compound for each pixel of the image. As result of this methodology, the chemical distribution image of the film components, their abundance and

histograms are obtained. The standard deviation of the component's abundance, skew (measure of the distribution asymmetry) and kurtosis (measure of the shape of the distribution) were reported.

5.3 RESULT AND DISSCUSION

5.3.1 Method Calibration

Partial Least Squares-Discriminant Analysis (PLS-DA) calibration models were developed to study the abundance of film forming compounds in the films prepared. The first step in this process consisted in a careful evaluation of the NIR spectra obtained. Figure. 31a shows the spectra of the pure compounds, whereas Figure. 31b shows spectra pre-treated with standard normal variable (SNV) and the Savitzky–Golay second derivative with a length of 11 third order.

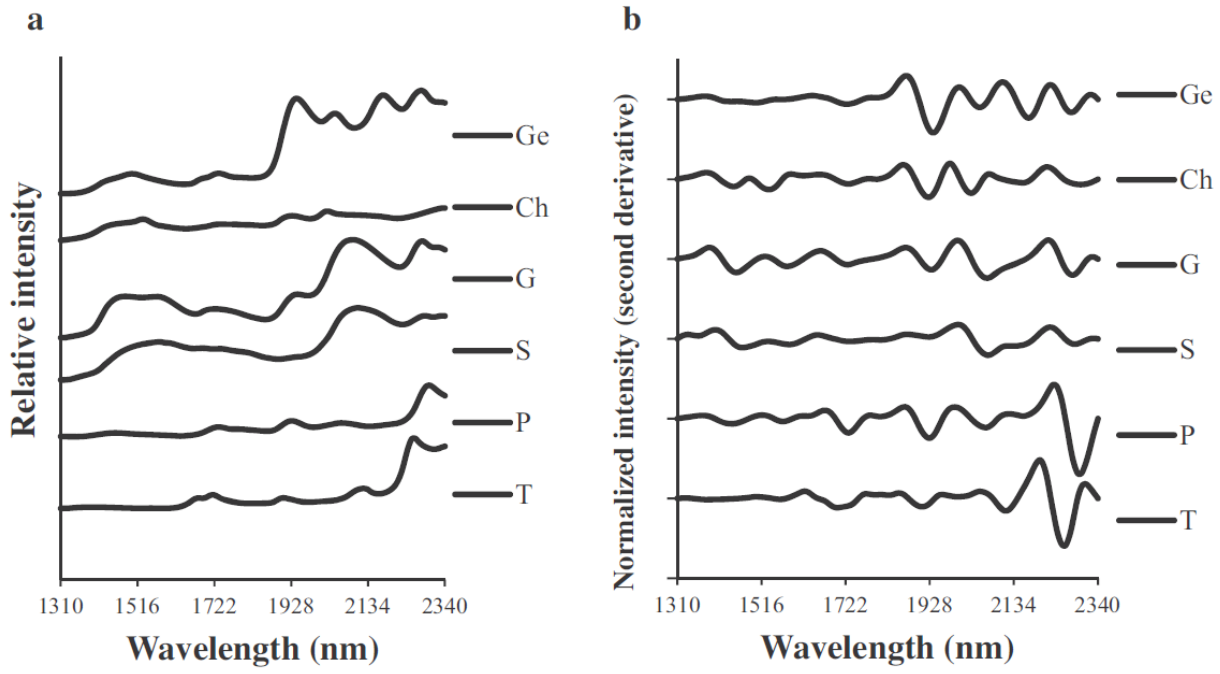

Figure 31. (. a) NIR spectra of pure compounds used to fabricate edible films. (b) NIR spectra of pure compounds with the average of the second derivative after normalization. NIR spectra were acquired by averaging the spectra of each pixel in an area of the hyperspectral image. Ge: gelatin, Ch: chitosan, G: glycerol, S: sorbitol, P: PEG400, T: triacetin.

There was a marked difference between the pure spectra of gelatin and chitosan, a necessary condition to predict the edible films' abundance (Figure 1a). In general, NIR spectra of proteins in ranges below 2200 nm are associated with NH stretching and bond; however, ranges below 2200 nm correspond to CH stretching and bond types[92]. Gelatin showed three bands: 1720 nm, associated with the first overtone of the stretching vibrations of the CH group[92]; 2160 nm corresponding to NH stretching of the amide-B groups plus the amide II group; and 2260 nm from the stretching of groups CH_2 and CH_3 [93]. Moreover, chitosan showed relative intensity bands at 1520, 1720, and 2020 nm. All of these bands are related since chitosan possesses three bonds that contribute to the NIR spectrum: the hydroxyl group, the amino group and the end of the polymeric chain[94]. The difference between the spectra was corroborated with the low correlation coefficient between the second derivatives of the spectra. Thus, it was possible to generate scores of images related to the abundance of gelatin and chitosan using calibration models[95]. Glycerol and sorbitol are both added and have very similar spectra (Figure 31a). The OH groups are responsible for the intense ranges of overtones between 1400–1450 nm and combination ranges between 1900–1940 nm of wavelength of the NIR spectra[96]. These ranges are mainly attributed to the symmetrical and asymmetrical stretching of the OH groups[97]. The structures of glycerol and sorbitol are formed by a carbon's skeleton with three and six OH groups, respectively; these groups are also found in the structure of chitosan. The similarity between glycerol and sorbitol could influence the determination of the abundance values of chitosan. This challenge was overcome through spectral pretreatment with the standard normal variable (SNV) and second derivative transformations, to diminish the correlation coefficient between both spectra. Table 11 shows that it was possible to

obtain values of abundance of chitosan, overcoming the similarity of the glycerol and sorbitol spectra.

Film	Total Abundance un-corrected		Abundance Corrected				Total Abundance corrected	
			Gelatin		Chitosan			
	(%)	STD	(%)	STD	(%)	STD	(%)	STD
Control	86.9	5.3	74.9	3.9	12.1	3.6	103.0	3.6
G	106.6	5.6	73.5	3.1	5.9	3.8	97.1	3.0
S	111.9	6.1	76.2	3.5	12.3	4.2	105.7	3.6
P	107.1	7.2	78.3	4.9	10.0	4.5	98.7	4.7
T	95.0	3.4	62.7	2.0	18.9	2.4	100.5	2.0
G+S	92.6	10.2	66.6	3.7	4.1	4.3	84.9	3.5
G+P	112.1	6.4	78.6	3.2	4.7	3.8	103.1	3.2
G+T	106.8	4.6	64.1	2.8	16.3	2.7	106.8	2.6
S+P	115.0	6.0	79.4	3.3	9.0	3.5	99.0	3.3
S+T	107.3	4.9	66.7	3.1	18.4	2.8	107.3	2.9
P+T	103.6	4.2	65.4	2.4	20.5	2.1	103.6	2.3
Total Average	105.2	5.2					100.9	3.2

Table 11. Values of total component abundance corrected and un-corrected for water content in edible films.

5.3.2 Abundance Distribution

After using PLS-DA models to obtain the total abundance of the films, this was then corrected for water content as shown in Table 11. As a result, the abundance of these plasticizers was quantified including the water present in the film. When the total abundance values of the edible films are corrected for water content, abundance values close to 100% are obtained. However, the glycerol, sorbitol, PEG 400 and the water molecules already have OH groups in their chemical structures, therefore the abundance of those plasticizers were calculated including the water contained in the film.

The standard deviations shown in Table 11 describe the spread of abundance values about the mean. However, the mean and the standard deviation do not show how the components are distributed throughout the film. This important information is provided by the chemical images and the histograms of film components shown in Figure 32. The strong red color in the images is indicative of areas of high abundance of components. These color images are an important first step to visualize the distribution of film components, and are based on the abundance values of the 81,920 pixel. Histograms were then used to evaluate the abundance distribution obtained, providing an estimate of the heterogeneity of each sample. The kurtosis and skew values describe the deviation from a normal distribution. The gelatin and chitosan in films without plasticizers showed negative values of kurtosis and skew but they are close to zero (Figure 32a), which shows that both compounds have a distribution near to a normal distribution. The gelatin and chitosan in films without plasticizers showed negative values of kurtosis and skew but they are close to zero (Figure 32a), which shows that both compounds have a distribution near to a normal distribution. The skew values indicate that gelatin presents more low abundance distribution. The gelatin and chitosan in films without plasticizers showed negative values of kurtosis and skew but they are close to zero (Figure 32a), which shows that both compounds have a distribution near to a normal distribution. The skew values indicate that gelatin presents more low abundance domains than chitosan. In addition, the standard deviation value of gelatin is slightly higher than the standard deviation value of chitosan; hence, gelatin had a less homogeneous distribution.

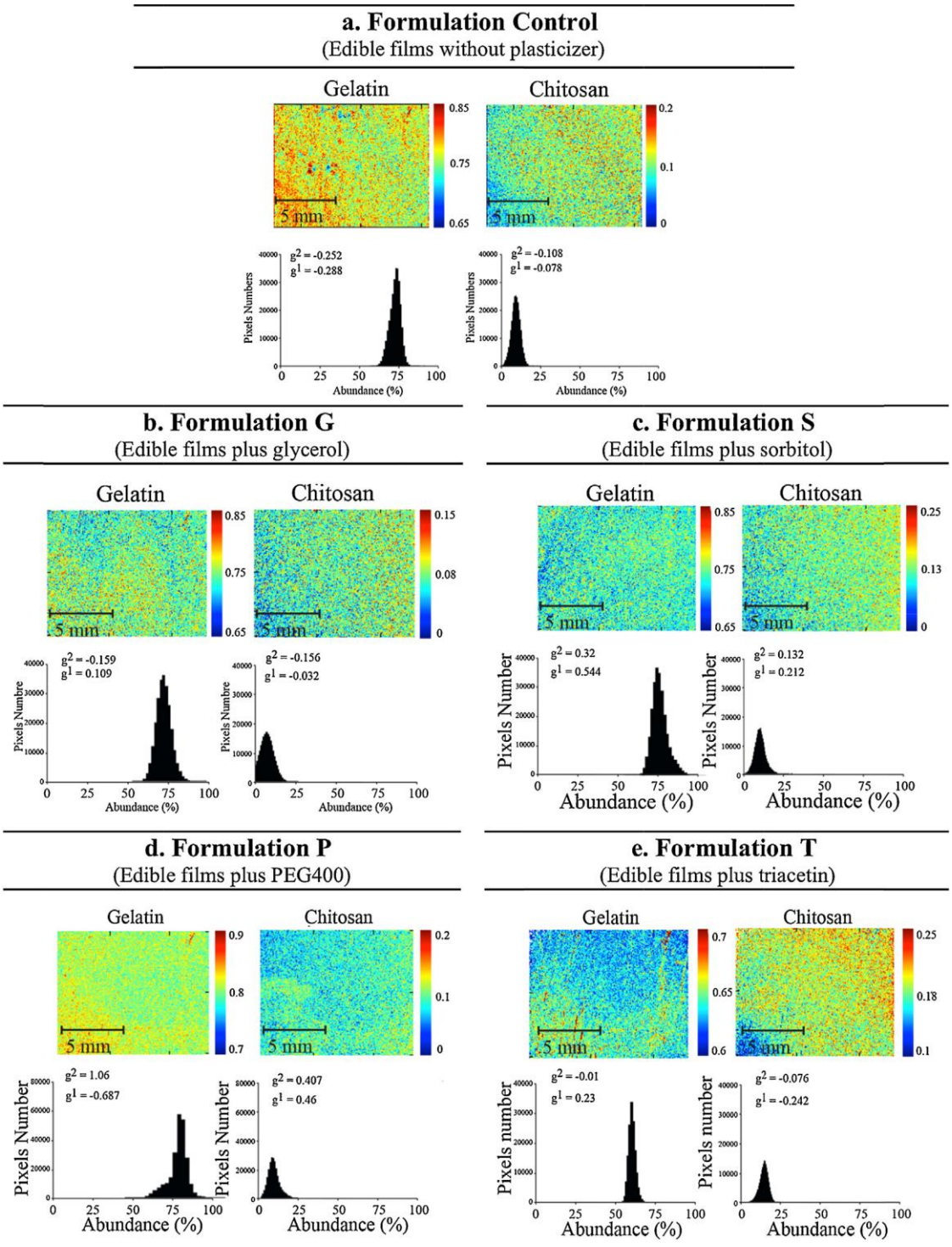

Figure 32. Chemical images of abundance distribution and histograms for film-forming polymers and plasticizers of edible films studied. Kurtosis (g2) and skew (g1) values of the histograms were used to study the distribution of the film's compounds. The side bar in each image shows the intensity of the compounds of each pixel, where red indicates higher intensity of the image. Each image corresponds to an edible film of triplicate per condition studied.

The spectra and chemical images were obtained by NIR-CI in transflectance mode. Thus, if a film presents phase separation due to overspplasticization, this will not necessarily interfere with the abundance measurements because they give information of the components throughout the film, not only of its surface. By adding glycerol to the film, the gelatin and chitosan kurtosis values varied slightly, maintaining their negative sign and therefore their homogeneity (Figure 32b). Moreover, the skew value of gelatin increased, implying a change of sign, while the skew of chitosan was maintained with a negative sign. In the presence of glycerol, the abundance variability increases for gelatin, however it decreases for chitosan (Table 11). Therefore, the addition of glycerol increases the number of areas with high abundance values of gelatin and varies slightly the number of these areas of chitosan. In the films where sorbitol was added, the kurtosis and skew values of gelatin and chitosan were greater than zero; however, the greatest changes were in the gelatin (Figure 32c). Specifically, the changes in the skew values indicate that the polymers showed an increase in the high abundance domains, particularly in gelatin. The changes in the kurtosis of both polymers showed that the addition of sorbitol are more heterogeneous than the control film. The homogeneity reduction in the distribution of the polymers suggests that sorbitol interacts with both polymers. The gelatin histograms of the films that included PEG400 showed the most negative skew values and greatest kurtosis values (Figure 32d). This indicates that the gelatin exhibits low presence of high concentration domains, generating less uniformity in the component's distribution[98]. Specifically, the negative skew indicates a reduction of high content fields of gelatin. The positive kurtosis of the film shows that the gelatin has a heterogeneous distribution with respect to the chitosan on the same film, while the positive skew value of chitosan indicates an increase of high abundance domains of chitosan. This information suggests that PEG 400 presents a high interaction with chitosan and a low interaction with gelatin. Compared with

the other films analyzed in this study, the kurtosis of gelatin and chitosan of the films treated with triacetin show the closest to zero values (Figure 32e). This implies that these films presented the most symmetrical and narrow distribution of their compounds[98]. Triacetin films show the lowest variability in total abundance (Table 11). Moreover, films with triacetin show the lowest variability of the total abundance. Triacetin is a molecule with low polarity, whereas gelatin and chitosan are polar polymers; which implies that triacetin will have a low interaction with gelatin and chitosan. The abundance of gelatin and chitosan varied according to the plasticizer added, even though films contained the same plasticizer concentration (Figure 33). The NIR-CI method uses the similarity of the spectrum of the pure compounds to identify (quantitatively and qualitatively) each compound in each sample[91]. This implies that when there is a conformational change of the compound, triggered by the interaction with another compound, a change in the spectrum is produced. It was observed the reductions of the abundance of gelatin in the films that were treated with triacetin, suggesting that triacetin interacts with gelatin. It was observed that glycerol interacts mainly with chitosan.

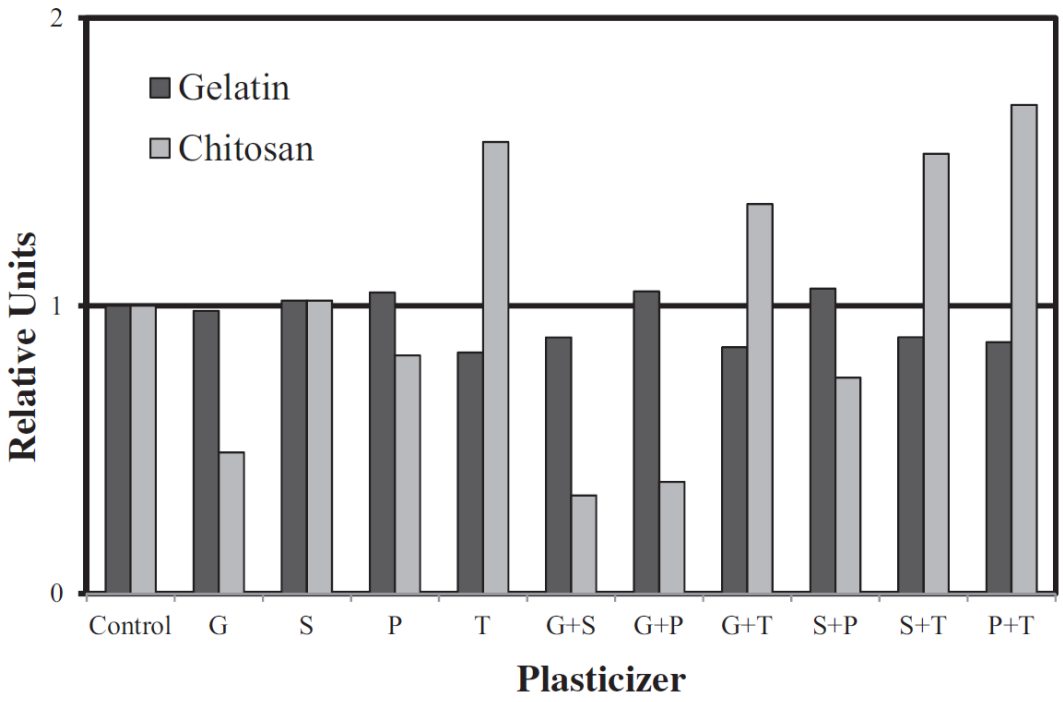

Figure 33. Normalized abundance values of chitosan and gelatin, corrected to the abundance values of both polymers present in the control film.

5.3.3 Mechanical properties

Films with triacetin showed the lowest variability of the total abundance value obtained by NIR-CI (Table 11). Additionally, the kurtosis value of gelatin and chitosan was closest to zero (Figure 32e). Triacetin has three double links, and these are responsible for the formation of rigid bonds with other molecules. These bonds would cause the formation of films with similar characteristics to the control film or low interaction. Tensile Strength values obtained for edible films with different plasticizers were within the range of edible gelatin and chitosan films where no phase separation in the system was observed.

5.4 CONCLUSION CHAPTER 5

This study is the first to report the use of NIR-CI to characterize gelatin and chitosan edible films, with the goal of understanding their mechanical properties and improving their design. NIR-CI reveals that the abundance of gelatin and chitosan varies in relation to the added plasticizer. Based mechanical properties and NIR-CI analysis, it was possible to show that chitosan interacts with glycerol and gelatin with triacetin. Even though the edible films showed uniform distribution of their compounds, the distribution of gelatin and chitosan change in response to the plasticizer that was added. PEG400 is the plasticizer that modifies the distribution of gelatin and chitosan the most, when compared to the control, whereas triacetin is the one that has the least impact on the distribution. Chitosan interacts mainly with the polar compounds (glycerol and sorbitol) that affect the mechanical properties of the films and relax their tridimensional structure. This indicates that the structural conformation of the edible film consists of a polymeric network of gelatin, while chitosan fulfills an anchoring role, interacting with plasticizers to diminish the rigidity and fragility of the film. The variability of the abundance of gelatin and chitosan showed a significant statistical correlation with the tensile strength of the films, showing that it is possible to determine the mechanical resistance of films with a rapid and non-invasive analysis.

CHAPTER 6

CONCLUSION AND FUTURE WORK

It has been demonstrated that shear stress on the powder mixtures can influence near infrared diffuse reflectance spectra on tablets. The effect od differences in c~~C~~ompaction forces ~~differences~~ on NIR ~~in~~ the spectra was well known previously by other researchers. The use~~d~~ of principal component analysis helps to identify small variabilities related on powder stress on diffuse reflectance spectra. This results ~~was~~ were confirmed using Angle resolved elastic light scattering with a 15 mW He–Ne linearly polarized laser with wavelength λ=632.8 nm to illuminate samples. This can be used understand how the process dynamics influence the NIR measurements to develop more robust modeling for continuous manufacturing.

The applied shear affects the dissolution behavior of tablets with similar chemical composition and compaction force. Shear effects lead to changes in NIR diffuse reflectance spectra. Based on these results NIRS can be used in combination with multivariate data analysis to predict dissolution behavior with variation in process conditions. These results show a high correlation between the destructive test (USP Apparatus 2) and the nondestructive test (NIRS). Implementation of this type of methodology can be used for implementation in the quality by design strategy (QbD) and real time release testing (RTRT) in the pharmaceutical industry. This type of work was developed using NIR spectroscopy and PLS modeling, but is not limited to other spectroscopy and modeling methods.

The forces applied on the resonant acoustic mixer were characterized using a cohesive active pharmaceutical ingredient. The use of the NIR-CI shows that the distribution of the API is less heterogeneous as higher forces were applied during mixing. For magnesium stearate, it was found that NIR-CI is not capable to quantify the dispersion across the surface of the sample.

NIRCI was use to characterize edible films of chitosan and gelatin it shows that the abundance of chitosan and gelatin varies according the plasticizers used. The variability of the abundance of gelatin and chitosan showed a significant statistical correlation with the tensile strength of the films, showing that it is possible to determine the mechanical resistance of films with a rapid and non-invasive analysis.

Future works on this subject will explore the use of manufacturing process data and ~~his~~ to correlation with dissolution properties on the formulation. Additionally, different spectroscopic techniques such as Terahertz spectroscopy in combination with multivariate techniques ~~can~~ could be used to predict dissolution nondestructively.

REFERENCES

1. Kukura, J.; Baxter, J. L.; Muzzio, F. J., Shear distribution and variability in the USP Apparatus 2 under turbulent conditions. *Int. J. Pharm.* **2004,** *279* (1-2), 9-17.
2. Röst, M.; Quist, P. O., Dissolution of USP prednisone calibrator tablets. *J. Pharm. Biomed. Anal.* **2003,** *31* (6), 1129-1143.
3. Guidance for Industry Dissolution Testing of Immediate Release Solid Oral Dosage Forms. S., H. H.; F.D.A; R., C. D. E., Eds. Rockville, MD, 1997.
4. Guidance for Industry PAT — A Framework for Innovative Pharmaceutical Development, Manufacturing, and Quality Assurance. U.S.D.H.H.S.; F.D.A; C.D.E.R.; C.V.M.; O.R.A., Eds. Rockville, MD, 2004.
5. Burns, D. A.; Ciurczak, E. W., *Handbook of Near-Infrared Analysis, Third Edition*. CRC Press: 2007.
6. Chemical Principles of Near-Infrared Technology. In *Near-Infrared Technology in the Agricultural and Food Industry*, Williams, P.; Norris, K., Eds. 2001.
7. Barajas, M. J.; Cassiani, A. R.; Vargas, W.; Conde, C.; Ropero, J.; Figueroa, J.; Romanach, R. J., Near-Infrared Spectroscopic Method for Real-Time Monitoring of Pharmaceutical Powders During Voiding. *Appl. Spectrosc.* **2007,** *61* (5), 496.
8. Næs, T.; Isaksson, T.; Fearn, T.; Davies, T., *A User-friendly Guide to Multivariate Calibration and Classification*. NIR Publications: Chichester, Uk, 2002.
9. Kramer, R., *Chemometric Techniques for Quantitative Analysis*. CRC Press: 1998.
10. Gray, V.; Kelly, G.; Xia, M.; Butler, C.; Thomas, S.; Mayock, S., The science of USP 1 and 2 dissolution: present challenges and future relevance. *Pharm. Res.* **2009,** *26* (6), 1289-302.
11. Dissolution. In *U.S. Pharmacopeia National Formulary 2011: USP 34 NF 29*, United States Pharmacopeial: 2011.
12. Near-Infrared Spectroscopy in Laboratory and Process Analysis. In *Encyclopedia of Analytical Chemistry*, Meyers, R. A., Ed. John Wiley & Sons, Ltd: Online, 2012.
13. Vanarase, A. U.; Alcalà, M.; Jerez Rozo, J. I.; Muzzio, F. J.; Romañach, R. J., Real-Time Monitoring of Drug Concentration in a Continuous Powder Mixing Process Using NIR Spectroscopy. *Chem. Eng. Sci.* **2010,** *65* (21), 5733.
14. Ward, H. W.; Blackwood, D. O.; Polizzi, M.; Clarke, H., Monitoring Blend Potency in a Tablet Press Feed Frame Using near Infrared Spectroscopy. *J. Pharm. Biomed. Anal.* **2013,** *80* (2013), 23.
15. Shi, Z.; Cogdill, R. P.; Short, S. M.; Anderson, C. A., Process Characterization of Powder Blending by Near-Infrared Spectroscopy: Blend End-Points and Beyond. *J. Pharm. Biomed. Anal.* **2008,** *47* (4-5), 745.
16. Igne, B.; Zacour, B. M.; Shi, Z.; Talwar, S.; Anderson, C. A.; Drennen, J. K., Online Monitoring of Pharmaceutical Materials Using Multiple NIR Sensors—Part I: Blend Homogeneity. *J. Pharm. Innov.* **2011,** *6* (1), 59.
17. Green, R. L.; Thurau, G.; Pixley, N. C.; Mateos, A.; Reed, R. A.; Higgins, J. P., In-Line Monitoring of Moisture Content in Fluid Bed Dryers Using Near-IR Spectroscopy with Consideration of Sampling Effects on Method Accuracy. *Anal. Chem.* **2005,** *77* (14), 4522.
18. Kaye, B. H., *Powder Mixing*. Springer: 1997.
19. Lacey, P. M. C., Developments in the Theory of Particle Mixing. *J. Appl. Chem.* **1954,** *4* (5), 268.

20. Osorio, J. G.; Stuessy, G.; Kemeny, G. J.; Muzzio, F. J., Characterization of Pharmaceutical Powder Blends Using in Situ Near-Infrared Chemical Imaging. *Chem. Eng. Sci.* **2014,** *108* (2014), 257.
21. Hogg, R., Mixing and Segregation in Powders: Evaluation, Mechanisms and Processes. *KONA Powder Part. J.* **2009,** *27* (2009), 17.
22. Pingali, K.; Mendez, R.; Lewis, D.; Michniak-Kohn, B.; Cuitino, A.; Muzzio, F., Evaluation of Strain-Induced Hydrophobicity of Pharmaceutical Blends and its Effect on Drug Release Rate Under Multiple Compression Conditions. *Drug. Dev. Ind. Pharm.* **2011,** *37* (4), 428-435.
23. Fukui, E.; Miyamura, N.; Kobayashi, M., Effect of Magnesium Stearate or Calcium Stearate as Additives on Dissolution Profiles of Diltiazem Hydrochloride from Press-Coated Tablets with Hydroxypropylmethylcellulose Acetate Succinate in the Outer Shell. *Int. J. Pharm.* **2001,** *216* (1-2), 146.
24. Aoshima, H.; Miyagisnima, A.; Nozawa, Y.; Sadzuka, Y.; Sonobe, T., Glycerin Fatty Acid Esters as a New Lubricant of Tablets. *Int. J. Pharm.* **2005,** *293* (1-2), 34.
25. Willetts, J. P.; Robbins, P. T.; Roche, T. C.; Bowley, M.; Bridson, R. H., Exploring the Effects of High Shear Blending on Lactose and Drug Using Fluidised Bed Elutriation. *Int. J. Pharm.* **2012,** *434* (1-2), 279.
26. Hussain, M. S. H.; York, P.; Timmins, P., A Study of the Formation of Magnesium Stearate Film on Sodium Chloride Using Energy-Dispersive X-Ray Analysis. *Int. J. Pharm.* **1988,** *42* (1–3), 95.
27. Short, S. M.; Cogdill, R. P.; Wildfong, P. L.; Drennen, J. K.; Anderson, C. A., A Near-Infrared Spectroscopic Investigation of Relative Density and Crushing Strength in Four-Component Compacts. *J. Pharm. Sci.* **2009,** *98* (3), 1109.
28. Otsuka, M.; Tanabe, H.; Osaki, K.; Otsuka, K.; Ozaki, Y., Chemoinformetrical Evaluation of Dissolution Property of Indomethacin Tablets by Near-Infrared Spectroscopy. *J. Pharm. Sci.* **2007,** *96* (4), 788-801.
29. Ropero, J.; Colon, Y.; Johnson-Restrepo, B.; Romanach, R. J., Near-Infrared Chemical Imaging Slope as a new Method to Study Tablet Compaction and Tablet Relaxation. *Appl. Spectrosc.* **2011,** *65* (4), 465.
30. Ellison, C. D.; Ennis, B. J.; Hamad, M. L.; Lyon, R. C., Measuring the Distribution of Density and Tabletting Force in Pharmaceutical Tablets by Chemical Imaging. *J. Pharm. Biomed. Anal.* **2008,** *48* (1), 7.
31. Blanco, M.; Alcalá, M., Content Uniformity and Tablet Hardness Testing of Intact Pharmaceutical Tablets by Near Infrared Spectroscopy. *Anal. Chim. Acta* **2006,** *557* (1-2), 359.
32. Alcala, M.; Ropero, J.; Vazquez, R.; Romanach, R. J., Deconvolution of Chemical and Physical Information from Intact Tablets NIR Spectra: Two- and Three-way Multivariate Calibration Strategies for Drug Quantitation. *J. Pharm. Sci.* **2009,** *98* (8), 2758.
33. Mehrotra, A.; Llusa, M.; Faqih, A.; Levin, M.; Muzzio, F. J., Influence of Shear Intensity and Total Shear on Properties of Blends and Tablets of Lactose and Cellulose Lubricated with Magnesium Stearate. *Int. J. Pharm.* **2007,** *336* (2), 291.
34. Hernandez, E.; Pawar, P.; Rodriguez, S.; Lysenko, S.; Muzzio, F. J.; Romanach, R. J., Effect of Shear Applied During a Pharmaceutical Process on Near Infrared Spectra. *Applied spectroscopy* **2016,** *70* (3), 455-66.
35. Stover, J. C., *Optical scattering : measurement and analysis / John C. Stover*. SPIE Optical Engineering Press: Bellingham, Wash., USA, 1995.

36. Continuum and Discontinuum Theories of Diffuse Reflection. In *Handbook of Near-Infrared Analysis*, 3 Ed. ed.; Burns, D. A.; Ciurczak, E. W., Eds. CRC Press: 2007; pp 21-64.
37. Born, M.; Wolf, E.; Bhatia, A. B.; Gabor, D.; Stokes, A. R.; Taylor, A. M.; Wayman, P. A.; Wilcock, W. L., *Principles of Optics: Electromagnetic Theory of Propagation, Interference and Diffraction of Light*. Cambridge University Press: 2000.
38. Llusa, M.; Levin, M.; Snee, R. D.; Muzzio, F. J., Shear-Induced APAP De-Agglomeration. *Drug Dev. Ind. Pharm.* **2009,** *35* (12), 1495.
39. Watanabe, A.; Morita, S.; Ozaki, Y., Temperature-Dependent Structural Changes in Hydrogen Bonds in Microcrystalline Cellulose Studied by Infrared and Near-Infrared Spectroscopy with Perturbation-Correlation Moving-Window Two-Dimensional Correlation Analysis. *Appl. Spectrosc.* **2006,** *60* (6), 618.
40. Awa, K.; Shinzawa, H.; Ozaki, Y., Monitoring of recrystallisation of microcrystalline cellulose inside pharmaceutical tablets during storage using near infrared diffuse reflectance spectroscopy. *J. Near Infrared Spectrosc.* **2014,** *22* (2014), 210.
41. Thoorens, G.; Krier, F.; Leclercq, B.; Carlin, B.; Evrard, B., Microcrystalline cellulose, a direct compression binder in a quality by design environment--a review. *Int. J. Pharm.* **2014,** *473* (1-2), 72.
42. Bohren, C. F.; Huffman, D. R., *Absorption and Scattering of Light by Small Particles*. Wiley: 1983.
43. Dressman, J. B.; Amidon, G. L.; Reppas, C.; Shah, V. P., Dissolution testing as a prognostic tool for oral drug absorption: immediate release dosage forms. *Pharm. Res.* **1998,** *15* (1), 11-22.
44. In Vitro Dissolution Testing for Solid Oral Dosage Forms. Sciences, P., Ed. 2010; Vol. 5.
45. FIP Guidelines for Dissolution Testing of Solid Oral Products. DISSOLUT. TECHNOL., 1997; pp 5-14.
46. Kukura, J.; Arratia, P. E.; Szalai, E. S.; Muzzio, F. J., Engineering tools for understanding the hydrodynamics of dissolution tests. *Drug. Dev. Ind. Pharm.* **2003,** *29* (2), 231-9.
47. Gao, Z.; Moore, T. W.; Smith, A. P.; Doub, W. H.; Westenberger, B. J., Studies of variability in dissolution testing with USP apparatus 2. *J. Pharm. Sci.* **2007,** *96* (7), 1794-801.
48. Guidance for Industry: Q8(R2) Pharmaceutical Development. USDHHS; FDA; CDER; CBER; ICH, Eds. Rockville, MD, US, 2009; pp 1 - 25.
49. Murthy, K. S.; Samyn, J. C., Effect of shear mixing on in vitro drug release of capsule formulations containing lubricants. *J. Pharm. Sci.* **1977,** *66* (9), 1215-1219.
50. Vanarase, A. U.; Muzzio, F. J., Effect of operating conditions and design parameters in a continuous powder mixer. *Powder Technol.* **2011,** *208* (1), 26-36.
51. Mendez, R.; Muzzio, F. J.; Velazquez, C., Powder hydrophobicity and flow properties: Effect of feed frame design and operating parameters. *AIChE J.* **2012,** *58* (3), 697-706.
52. Zannikos, P. N.; Li, W. I.; Drennen, J. K.; Lodder, R. A., Spectrophotometric prediction of the dissolution rate of carbamazepine tablets. *Pharm. Res.* **1991,** *8* (8), 974-8.
53. Donoso, M.; Ghaly, E. S., Prediction of drug dissolution from tablets using near-infrared diffuse reflectance spectroscopy as a nondestructive method. *Pharm. Dev. Technol.* **2004,** *9* (3), 247-63.
54. Freitas, M. P.; Sabadin, A.; Silva, L. M.; Giannotti, F. M.; do Couto, D. A.; Tonhi, E.; Medeiros, R. S.; Coco, G. L.; Russo, V. F.; Martins, J. A., Prediction of drug dissolution profiles from tablets using NIR diffuse reflectance spectroscopy: a rapid and nondestructive method. *J. Pharm. Biomed. Anal.* **2005,** *39* (1-2), 17-21.

55. Blanco, M.; Alcala, M.; Gonzalez, J. M.; Torras, H., Determination of dissolution profiles in intact pharmaceutical tablets by NIR spectroscopy. *PAT - J. Process Anal. Technol.* **2006,** *3* (5), 25-29.
56. Lozano, V. A.; Camina, J. M.; Boeris, M. S.; Marchevsky, E. J., Simultaneous determination of sorbic and benzoic acids in commercial juices using the PLS-2 multivariate calibration method and validation by high performance liquid chromatography. *Talanta* **2007,** *73* (2), 282-6.
57. Tabasi, S. H.; Moolchandani, V.; Fahmy, R.; Hoag, S. W., Sustained release dosage forms dissolution behavior prediction: a study of matrix tablets using NIR spectroscopy. *Int. J. Pharm.* **2009,** *382* (1-2), 1-6.
58. Żarów, A.; Zhou, B.; Wang, X.; Pinal, R.; Iqbal, Z., Spectroscopic and X-ray Diffraction Study of Structural Disorder in Cryomilled and Amorphous Griseofulvin. *Appl. Spectrosc.* **2011,** *65* (2), 135-143.
59. Strachan, C. J.; Taday, P. F.; Newnham, D. A.; Gordon, K. C.; Zeitler, J. A.; Pepper, M.; Rades, T., Using terahertz pulsed spectroscopy to quantify pharmaceutical polymorphism and crystallinity. *J. Pharm. Sci.* **2005,** *94* (4), 837-46.
60. *USP 30 - NF 25*. United States Pharmacopeial Convention: Rockville, MD, 2007.
61. Wang, J.; Wen, H.; Desai, D., Lubrication in tablet formulations. In *Eur. J. Pharm. Biopharm.*, 2010; Vol. 75, pp 1-15.
62. Martens, H.; Martens, M., *Multivariate Analysis of Quality: An Introduction*. John Wiley & Sons, Ltd: Chichester, England, 2001.
63. Maggio, R. M.; Castellano, P. M.; Kaufman, T. S., A new principal component analysis-based approach for testing "similarity" of drug dissolution profiles. *Eur. J. Pharm. Sci.* **2008,** *34* (1), 66-77.
64. Maggio, R. M.; Castellano, P. M.; Kaufman, T. S., PCA-CR analysis of dissolution profiles. A chemometric approach to probe the polymorphic form of the active pharmaceutical ingredient in a drug product. *Int. J. Pharm.* **2009,** *378* (1-2), 187-93.
65. Shah, V.; Tsong, Y.; Sathe, P.; Liu, J.-P., In Vitro Dissolution Profile Comparison—Statistics and Analysis of the Similarity Factor, f2. *Pharm. Res.* **1998,** *15* (6), 889-896.
66. Miller, J. N.; Miller, J. C., *Statistics and Chemometrics for Analytical Chemistry*. Prentice Hall/Pearson: 2010.
67. Guideline on the use of near infrared spectroscopy by the pharmaceutical industry and the data requirements for new submissions and variations. EMEA; CHMP; CVMP; QWP, Eds. European Medicines Agency: London, U.K., 2014; pp 1-28.
68. Ravn, C.; Skibsted, E.; Bro, R., Near-infrared chemical imaging (NIR-CI) on pharmaceutical solid dosage forms-comparing common calibration approaches. *J Pharm Biomed Anal* **2008,** *48* (3), 554-61.
69. Near-Infrared Chemical Imaging for Product and Process Understanding. In *Process Analytical Technology*, John Wiley & Sons, Ltd: 2010; pp 245-279.
70. Gendrin, C.; Roggo, Y.; Collet, C., Pharmaceutical applications of vibrational chemical imaging and chemometrics: a review. *J Pharm Biomed Anal* **2008,** *48* (3), 533-53.
71. Sasic, S.; Kong, A.; Kaul, G., Determining API domain sizes in pharmaceutical tablets and blends upon varying milling conditions by near-infrared chemical imaging. *Analytical Methods* **2013,** *5* (9), 2360-2368.
72. Li, W.; Woldu, A.; Kelly, R.; McCool, J.; Bruce, R.; Rasmussen, H.; Cunningham, J.; Winstead, D., Measurement of drug agglomerates in powder blending simulation samples by

near infrared chemical imaging. *International journal of pharmaceutics* **2008,** *350* (1–2), 369-373.
73. Ma, H.; Anderson, C. A., Characterization of Pharmaceutical Powder Blends by NIR Chemical Imaging. *Journal of pharmaceutical sciences* **2008,** *97* (8), 3305-3320.
74. Burger, J., Bad pixel detection in hyperspectral staring camera systems. *NIR news* **2009,** *20* (1), 9-12.
75. Osorio, J. G.; Muzzio, F. J., Evaluation of resonant acoustic mixing performance. *Powder Technology* **2015,** *278*, 46-56.
76. Pingali, K.; Mendez, R.; Lewis, D.; Michniak-Kohn, B.; Cuitino, A.; Muzzio, F., Mixing order of glidant and lubricant – Influence on powder and tablet properties. *International journal of pharmaceutics* **2011,** *409* (1), 269-277.
77. Hudak, S. J.; Haber, K.; Sando, G.; Kidder, L. H.; Lewis, E. N., Practical Limits of Spatial Resolution in Diffuse Reflectance NIR Chemical Imaging. *NIR news* **2007,** *18* (6), 6-8.
78. Edible Films and Coatings: Why, What, and How? In *Edible Films and Coatings for Food Applications*, Huber, K. C.; Embuscado, M. E., Eds. Springer New York: New York, NY, 2009; pp 1-23.
79. Falguera, V.; Quintero, J. P.; Jiménez, A.; Muñoz, J. A.; Ibarz, A., Edible films and coatings: Structures, active functions and trends in their use. *Trends in Food Science & Technology* **2011,** *22* (6), 292-303.
80. Gómez-Estaca, J.; Gómez-Guillén, M. C.; Fernández-Martín, F.; Montero, P., Effects of gelatin origin, bovine-hide and tuna-skin, on the properties of compound gelatin–chitosan films. *Food Hydrocolloids* **2011,** *25* (6), 1461-1469.
81. van den Broek, L. A. M.; Knoop, R. J. I.; Kappen, F. H. J.; Boeriu, C. G., Chitosan films and blends for packaging material. *Carbohydrate Polymers* **2015,** *116*, 237-242.
82. Sacré, P. Y.; De Bleye, C.; Chavez, P. F.; Netchacovitch, L.; Hubert, P.; Ziemons, E., Data processing of vibrational chemical imaging for pharmaceutical applications. *Journal of Pharmaceutical and Biomedical Analysis* **2014,** *101*, 123-140.
83. Juan, A. d.; Tauler, R.; Dyson, R.; Marcolli, C.; Rault, M.; Maeder, M., Spectroscopic imaging and chemometrics: a powerful combination for global and local sample analysis. *TrAC Trends in Analytical Chemistry* **2004,** *23* (1), 70-79.
84. Puchert, T.; Lochmann, D.; Menezes, J. C.; Reich, G., Near-infrared chemical imaging (NIR-CI) for counterfeit drug identification—A four-stage concept with a novel approach of data processing (Linear Image Signature). *Journal of Pharmaceutical and Biomedical Analysis* **2010,** *51* (1), 138-145.
85. Montgomery, D. C.; Runger, G. C., *Applied Statistics and Probability for Engineers*. John Wiley & Sons: 2010.
86. Lefèvre, T.; Subirade, M., Molecular structure and interaction of biopolymers as viewed by Fourier transform infrared spectroscopy: model studies on β-lactoglobulin. *Food Hydrocolloids* **2001,** *15* (4), 365-376.
87. Jérez Rozo, J. I.; Zarow, A.; Zhou, B.; Pinal, R.; Iqbal, Z.; Romañach, R. J., Complementary Near Infrared and Raman Chemical Imaging of Pharmaceutical Thin Films. *Journal of pharmaceutical sciences* **2011,** *100* (11), 4888-4895.
88. Bergo, P.; Sobral, P. J. A., Effects of plasticizer on physical properties of pigskin gelatin films. *Food Hydrocolloids* **2007,** *21* (8), 1285-1289.

89. Li Yoon, W.; D. Jee, R.; C. Moffat, A.; D. Blackler, P.; Yeung, K.; C. Lee, D., Construction and transferability of a spectral library for the identification of common solvents by near-infrared transflectance spectroscopy. *Analyst* **1999,** *124* (8), 1197-1203.
90. Susarla, R.; Sievens-Figueroa, L.; Bhakay, A.; Shen, Y.; Jerez-Rozo, J. I.; Engen, W.; Khusid, B.; Bilgili, E.; Romanach, R. J.; Morris, K. R.; Michniak-Kohn, B.; Dave, R. N., Fast drying of biocompatible polymer films loaded with poorly water-soluble drug nano-particles via low temperature forced convection. *International journal of pharmaceutics* **2013,** *455* (1-2), 93-103.
91. Palou, A.; Cruz, J.; Blanco, M.; Tomàs, J.; de los Ríos, J.; Alcalà, M., Determination of drug, excipients and coating distribution in pharmaceutical tablets using NIR-CI. *Journal of Pharmaceutical Analysis* **2012,** *2* (2), 90-97.
92. Segtnan, V. H.; Isaksson, T., Temperature, sample and time dependent structural characteristics of gelatine gels studied by near infrared spectroscopy. *Food Hydrocolloids* **2004,** *18* (1), 1-11.
93. Wang, J.; Sowa, M. G.; Ahmed, M. K.; Mantsch, H. H., Photoacoustic Near-Infrared Investigation of Homo-Polypeptides. *The Journal of Physical Chemistry* **1994,** *98* (17), 4748-4755.
94. Cervera, M. F.; Heinämäki, J.; de la Paz, N.; López, O.; Maunu, S. L.; Virtanen, T.; Hatanpää, T.; Antikainen, O.; Nogueira, A.; Fundora, J.; Yliruusi, J., Effects of Spray Drying on Physicochemical Properties of Chitosan Acid Salts. *AAPS PharmSciTech* **2011,** *12* (2), 637-649.
95. Technologies and practical considerations for implementing near-infrared chemical imaging. In *Raman, infrared, and near-infraredchemical imaging*, John Wiley & Sons Inc.: Hoboken, NJ, USA, 2010; pp 75-91.
96. Chen, D.; Hu, B.; Shao, X.; Su, Q., Removal of major interference sources in aqueous near-infrared spectroscopy techniques. *Analytical and bioanalytical chemistry* **2004,** *379* (1), 143-148.
97. Boada-Lopez, J.; DeJesus-Maldonado, I.; Jerez, J.; Romañach, R.; Diffoot-Carlo, N.; Sundaram, P., Collagen abundance in mechanically stimulated osteoblast cultures using near infrared microscopy. *Journal of Biomechanics 46* (14), 2442-2450.
98. Near-Infrared Chemical Imaging as a Process Analytical Tool. In *Process Analytical Technology*, Blackwell Publishing Ltd: 2007; pp 187-225.